MARTIN MARIETTA ENERGY SYSTEMS LIBRARIES
3 4456 0251687 3

CENTRAL RESEARCH LIBRARY
DOCUMENT COLLECTION

cy 63

ORNL-3534
C-93a – Advanced Concepts for Future Application – Reactor Experiments
M-3679 (31st ed., Rev.)

AEC RESEARCH AND DEVELOPMENT REPORT

DECLASSIFIED
CLASSIFICATION CHANGED TO:
By Authority of: 11.20.69
By: 11.20.69

MEDIUM-POWER REACTOR EXPERIMENT

PROGRESS REPORT

FOR THE PERIOD JULY 1, 1963

TO SEPTEMBER 30, 1963

(Title Unclassified)

CENTRAL RESEARCH LIBRARY
DOCUMENT COLLECTION
LIBRARY LOAN COPY
DO NOT TRANSFER TO ANOTHER PERSON
If you wish someone else to see this document, send in name with document and the library will arrange a loan.

OAK RIDGE NATIONAL LABORATORY
operated by
UNION CARBIDE CORPORATION
for the
U.S. ATOMIC ENERGY COMMISSION

[redacted]

[redacted]

LEGAL NOTICE

This report was prepared as an account of Government sponsored work. Neither the United States, nor the Commission, nor any person acting on behalf of the Commission:

A. Makes any warranty or representation, expressed or implied, with respect to the accuracy, completeness, or usefulness of the information contained in this report, or that the use of any information, apparatus, method, or process disclosed in this report may not infringe privately owned rights; or

B. Assumes any liabilities with respect to the use of, or for damages resulting from the use of any information, apparatus, method, or process disclosed in this report.

As used in the above, "person acting on behalf of the Commission" includes any employee or contractor of the Commission, or employee of such contractor, to the extent that such employee or contractor of the Commission, or employee of such contractor prepares, disseminates, or provides access to, any information pursuant to his employment or contract with the Commission, or his employment with such contractor.

[redacted]

ORNL-3534

Contract No. W-7405-eng-26

MEDIUM-POWER REACTOR EXPERIMENT
PROGRESS REPORT

for the Period July 1, 1963
to September 30, 1963

A. P. Fraas, Project Manager

Date Issued

JAN 2 - 1964

OAK RIDGE NATIONAL LABORATORY
Oak Ridge, Tennessee
operated by
UNION CARBIDE CORPORATION
for the
U.S. ATOMIC ENERGY COMMISSION

[redacted]

MARTIN MARIETTA ENERGY SYSTEMS LIBRARIES

3 4456 0251687 3

[redacted]

FOREWORD

Because of urgent requests for more frequent reporting of progress on the design and development of the boiling-potassium reactor than has been provided by the Space Power Program Semiannual Progress Reports for the periods ending in June and December, a decision was made to issue additional quarterly progress reports on the reactor development portion of the space power program for the periods ending in March and September. Thus, this report covers the progress during the past quarter on the design, research, and development work under way on the stainless steel, boiling-potassium reactor system and the medium-power reactor experiment to which it will lead. Much of this work is basic and is likely to be beneficial to the SNAP-2, -8, -10, and -50 Programs.

[redacted]

[redacted]

CONTENTS

	Page
FOREWORD	iii
SUMMARY	vii
1. MPRE DESIGN	1
Studies of Configurations for Flight Systems	1
Radiator Design to Meet Launch Requirements	7
Structural Design	8
Meteoroid Protection	9
Radiator Weight Estimates	11
System Flow Distribution, Stability, and Control	13
Digital Computer Code	13
Electrical Analog	17
2. REACTOR PHYSICS	18
Analyses of the Third and Fourth Critical Experiments	18
Reactor Control Studies	21
Iris Diaphragm	23
Rotating Drums	24
Movable Plug	29
Alteration of Reference Reactor	30
Conclusions	31
3. DEVELOPMENT TESTS	33
Jet-Pump Cavitation Tests	33
Vapor-Separator Tests	40
Single-Rod Capsule Tests with Water	43
Single-Rod Capsule Tests with Potassium	46
Nucleation Sites	46
Endurance Tests	47
Protective Devices for Rod Heaters	48
Seven-Rod Boiler System Tests with Water	51
Development of Seven-Rod Boiler System for Tests with Potassium	53
System Construction	54
Turbine-Driven Pump Development	54

[redacted]

[redacted]

Instrumentation 58
Endurance Test Conditions 60
Tests of a 91-Rod Boiler System with Water 60
Phase I Tests 61
Correlation with Literature Data 65
Phase II System 67
Design of a 91-Rod Boiler System for Tests with Potassium ... 72
Design of a Regenerative Feed Heater 75
Preparations for Tests of a Small Vapor Separator with an Air-Water Mixture Under Zero-Gravity Conditions 81

[redacted]

SUMMARY

1. MPRE Design

Studies of Configurations for Flight Systems. Many questions regarding the details of the arrangements of the various components of a flight system arose in connection with the design of the electrically heated mockups. To provide some guidance in coping with these problems, a conceptual design was worked out for a launch package. In preparing this design, considerable attention was given to the accommodation of high-acceleration loads and severe vibration and noise during launching, together with orbital startup problems. The design is sufficiently complete to permit a preliminary estimate of the weights of both the principal components and the complete package.

System Flow Distribution, Stability, and Control. The analytical work on the control concept discussed in previous reports was extended, and a digital computer code was prepared. This code will be used to investigate the effects of changes in the amount of flow restriction in the various segments of the circuits, as well as changes in the characteristics of the pumps and turbines. To supplement the digital computer-analysis work on the flow-distribution characteristics of the system, development of an electrical analog is continuing to provide a tool for investigating the dynamic characteristics of the system.

2. Reactor Physics

Analyses of the Third and Fourth Critical Experiments. The critical experiments that were completed during the previous reporting period were analyzed. Results are presented for reactivity effects as determined in both the experiments and the machine calculations, and the disparities between them (which are relatively small) are discussed. The material covered includes the radial and axial power distributions, values for k_{eff}, and reactivity coefficients for various materials inserted in the core.

Reactor Control Studies. Three types of control device were examined analytically for use in the MPRE. These include rotating drums

in the reflector, a poisoned-plate iris that could be opened or closed between the bottom of the core and the reflector, and movable end plugs in the bottom of the reflector. Either the rotating drums or the movable end plugs should provide sufficient $\Delta k/k$ to satisfy the control requirements, but the poisoned-plate iris does not. The movable end plugs have an advantage in that they give a mechanically simpler and more reliable design than the rotating cylindrical drums, which would be subject to warping and bowing.

3. Development Tests

Jet Pump Cavitation Tests. A new test stand was designed and built for carrying out cavitation tests with jet pumps operating in water, and preliminary tests were completed. These tests showed that the rig provides an effective tool for investigating performance of jet pumps and that it is important to use a rounded rather than a sharp edge at the junction between the conical inlet and the mixing section of the jet pump.

Vapor Separator Tests. Tests were conducted with full-size parts of the vapor separators for both the 91-rod boiling-water system and the 91-rod boiling-potassium system. Configurations were worked out that provide vapor qualities of 99% or better with air-water mixture flow rates corresponding to the full design output of the system.

Single-Rod Capsule Tests with Water. Tests for investigating liquid superheating and nucleation site effectiveness have shown that even with porous materials in a ring shrunk around the base of a firerod, the principal source of bubbles in the water is the fissure between the ring and the firerod. This is consistent with the results of similar tests in potassium.

Single-Rod Capsule Tests with Potassium. Endurance tests are continuing satisfactorily. Two rods have completed over 2000 hr at 2.5 and 3.75 kw per rod, respectively (i.e., 60 and 90% of design power).

Seven-Rod Boiler System Tests with Water. Tests of the seven-rod boiler system were continued using a rod bundle with a 5/8-in. centerline spacing in place of the 9/16-in. spacing used previously. Tests also included the investigation of the effects of changes in the turbine driving

the feed pump. These tests validate the use of a 5/8-in. centerline spacing for the heater rods used in the seven-rod boiling-potassium system in which the wider spacing was used to facilitate welding the headers required to provide a leaktight potassium system.

Development of Seven-Rod Boiler System for Tests with Potassium. The potassium system was assembled, checked out, and found to be leaktight. The installation of heaters, thermocouples, instruments, and accessory equipment is under way. Barring unusual interruptions or difficulties, the test rigs should be ready to start up early in November.

Test of a 91-Rod Boiler System with Water. The Phase I tests on the system were completed, and preliminary values were established for burnout limitations on boiler-exit vapor quality. Equipment for the Phase II system is largely installed, including the tapered-tube radiator, the free turbine-driven pump unit, and the radiator scavenging jet pumps. Preliminary shakedown tests of the revised system are under way at the time of this writing.

Design of a 91-Rod Boiler System for Tests with Potassium. The greater part of the design work on the system and its components was completed, and procurement was initiated for most of the components. Designs for both the air-cooled box that surrounds the radiator and absorbs the heat emitted by thermal radiation and for the regenerative feed heater were completed, along with analyses to show the adequacy of these components over a wide range of system operating conditions.

Zero-Gravity System Test. The design of a small air-water system to test the vapor separator for a seven-rod boiling-water system was completed, and the parts were fabricated. The system will be small enough to be readily portable so that, when bench tests have been completed, flight tests in the KC-135 can be readily carried out.

[redacted]

1. MPRE DESIGN

A. P. Fraas

The bulk of the design effort on the MPRE program is currently being devoted to component development. However, a limited design effort is continuing, and a reference design has been laid out to provide preliminary answers to questions that have arisen with respect to possible flight configurations, particularly with respect to the radiator structure and shielding requirements. These questions are discussed below, and progress on the stability and control problem is cited.

Studies of Configurations for Flight Systems

A. P. Fraas J. J. Tudor

Many questions that can be answered only on the basis of a particular system configuration have arisen with respect to the radiator, the jet pumps, and the shield of a flight version of the MPRE. In an effort to answer these, several layouts were prepared to provide a basis for estimating the weight and other penalties associated with favoring one aspect of the system design at the expense of another. The most promising of these layouts is shown in Fig. 1.1. This was based on the system flow sheet and the reactor layout shown previously.[1,2] The payload would be located in the nose cone above the assembly shown. While the configuration of Fig. 1.1 was worked out for the installation of the MPRE in something like the Atlas-Centaur vehicle, the basic arrangement and structure are applicable to much larger vehicles and power plants. This configuration provides a point of departure for evaluating the effects of design perturbations to the proposed layout and the relative merits of other configurations.

---

[1]J. Foster, System Flowsheet and Instrumentation Diagram, p. 7, Fig. 1.1, "Space Power Program Semiann. Prog. Rep. June 30, 1963," USAEC Report ORNL-3489, Oak Ridge National Laboratory.

[2]A. P. Fraas, MPRE Design, p. 4, Fig. 1.1, "Space Power Program Semiann. Prog. Rep. Dec. 31, 1962," USAEC Report ORNL-3420, Oak Ridge National Laboratory.

[redacted]

[redacted]

ORNL-LR-DWG. 63-6104

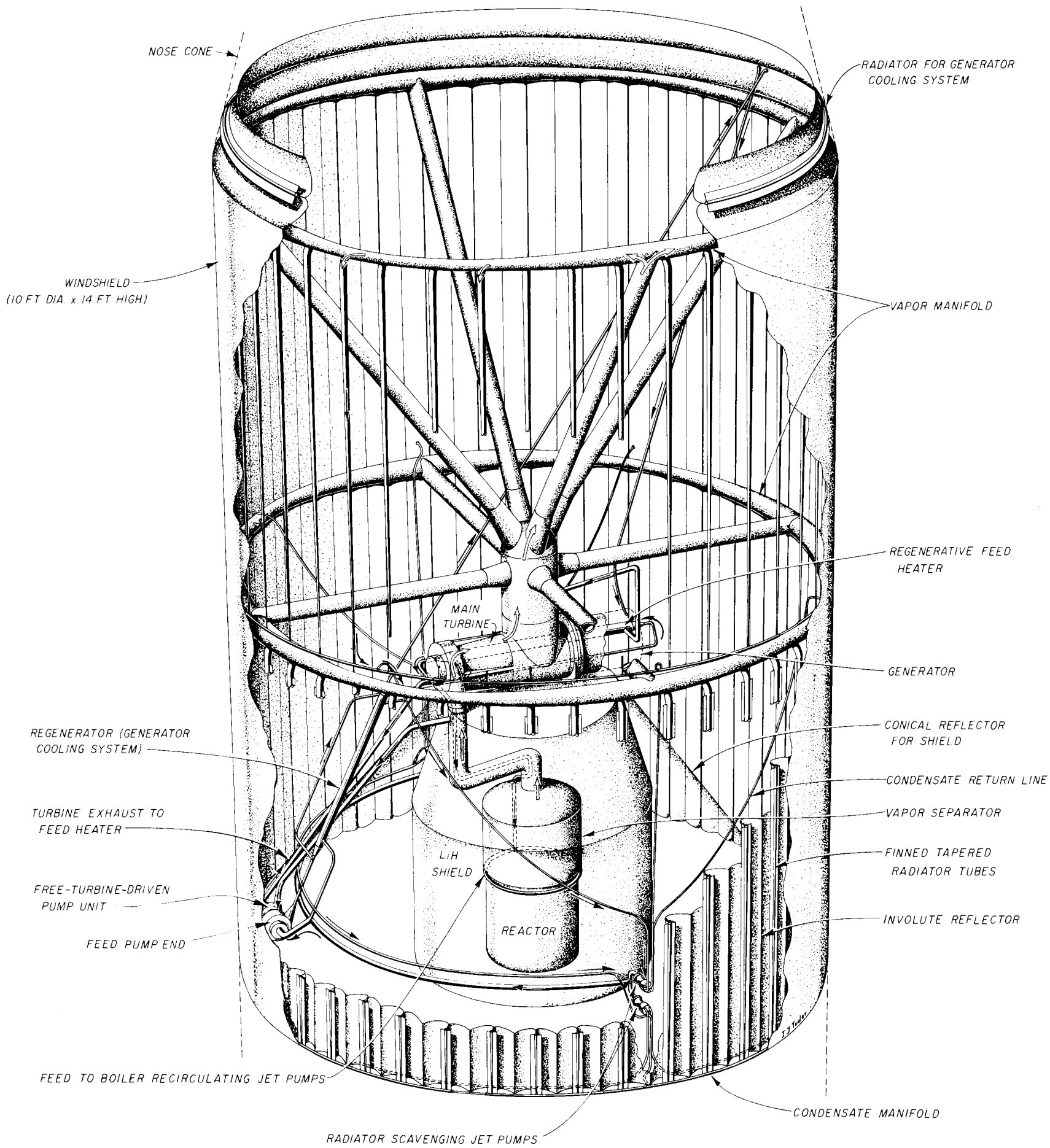

Fig. 1.1. Preliminary Reference Design for a Launch Package Based on the MPRE System.

[redacted]

The layout of Fig. 1.1 differs markedly from the launch configurations that have been proposed for SNAP-2, -8, and -10 and for SPUR. In the latter the reactor is placed at the top of the nose cone, and the radiator lies within the slender shadow cone of a minimal shadow-disk shield. These system configurations serve to minimize the shield weight at the expense of major structural problems and their attendant weight penalties. They also give a high center of gravity for the payload, and this leads to serious dynamic stability problems in the launch vehicle. It has been apparent for some time that it might be better to make use of a radiator and system configuration such as that of Fig. 1.1 for which fast-neutron scattering from the radiator may constitute the principal dose at the payload unless shielding is employed around the sides of the reactor. The biggest uncertainty in this connection is the permissible dose at the payload, and this in turn depends on the type of electronic equipment employed. The problem is complicated by such matters as the fact that one of the electronic properties of a transistor may be as much as 100 times more sensitive to fast-neutron radiation than others. Thus a given transistor employed in one way may be satisfactory at a much higher dose level than if used in another way in another circuit. It happens that the uncertainty in this respect currently is such that if electronic equipment can be built to tolerate as high a radiation dose level as many solid-state physicists believe, no side shielding around the MPRE reactor will be required. If, on the other hand, allowable dose levels must be kept to values that have been demonstrated to be acceptable with more conventional electronic equipment, the fast-neutron radiation from the side of the reactor may have to be reduced by a factor of as much as 100 to keep the dose of fast neutrons scattered from the radiator to the payload within acceptable limits.

Rough preliminary estimates of the weights of the major components of the configuration in Fig. 1.1 are presented in Table 1.1. Two sets of data for the shield weight are given, one for a total integrated fast-neutron dose at the payload of 10^{12} neutrons/cm^2 in 10,000 hr and one for a total neutron dose of 10^{14} neutrons/cm^2. If, as shown for the system configuration of Fig. 1.1, shielding is required around the sides of the

Table 1.1. Weight of Major Components of Power Plant Launch Package of Fig. 1.1

System electrical output, kw	140	140	300	300
Material of construction	Stainless steel	Stainless steel	Niobium	Niobium
Reactor outlet temperature, °F	1540	1540	2000	2000
Dose at payload 30 ft from reactor in 10,000 hr, neutrons/cm^2	10^{12}	10^{14}	10^{12}	10^{14}
Weights of components, lb				
Shield	1200	400	1600	500
Reactor	750	750	850	850
Radiator and manifolds	1080	1080	950	950
Turbine-generator unit	300	300	500	500
Free-turbine-driven pump unit	30	30	30	50
Regenerative feed heater	20	20	40	40
Generator cooling system	30	30	60	60
Connecting piping	70	70	120	120
Potassium	50	50	50	50
Controls and instrumentation	100	100	100	100
Burner and fuel for 1 hr	150	150	150	150
Total weight, lb	3780	2980	4450	3350
Total weight per unit of electrical output, lb/kw	27	21	15	11
Weight after jettisoning windshield and Lox-kerosene heating system, lb	3470	2670	4140	3040
Total weight per unit of electrical output after jettisoning, lb/kw	25	19	14	10

reactor to reduce the neutron dose scattered from the radiator to the payload, a preliminary estimate indicates that the weight penalty will be about 800 lb. This does not seem to be a large penalty in view of the compactness of the package, its sturdy structure, and its low center of gravity.

It should be pointed out that a factor that helps to keep the weight penalty to a reasonable value is that, since the payload would be in the tip of the nose cone, its diameter would be small - a value of 5 ft was

assumed - while its vertical height would be large. This contrasts with the large-diameter (10 ft), relatively thin disk envisioned for SNAP-8 and reduces the size of the shielding required for the shadow cone.

The neutron shielding material was assumed to consist of lithium hydride operated at a temperature of about 400°F at the outer surface and a maximum temperature in the interior of 1000°F. The gamma heating in the inner portion of the lithium hydride shielding over the top of the reactor appeared from preliminary estimates to be too great to meet the 1000°F maximum temperature requirement, hence it will be necessary to employ beryllium rods about 1/4 in. in diameter extending radially outward horizontally from the inner hot zone at the top of the shield to the surface. By using enough of these so that there will be 5 vol % beryllium, the thermal conductivity will be doubled, and the heat can be dissipated to space by thermal radiation from the outer surface without giving internal temperatures above 1000°F. A thin, conical, aluminum reflector is employed around the shield to help dissipate the thermal radiation from the shield surface to space. With this arrangement it appears that no cooling coils within the shield material will be required.

The free-turbine-driven pump unit is mounted at a level close to that of the liquid in the expansion tank so that vapor can flow to the turbine. This is close to the level of the lower of the two radiator liquid manifolds so that the pump will prime for starting without accumulating a large liquid inventory in the radiator tubes. The reactor assembly is mounted so that, prior to starting, the level of the liquid metal in the system can be raised to about the midpoint of the expansion tank immediately beneath the vapor separator. Heat from a Lox-kerosene burner with a strong admixture of recirculating combustion gases would be applied to the bottom of the reactor pressure vessel in the region left open by withdrawal of the control rod plugs. (The nuclear problems of the control devices shown in Fig. 1.1 are discussed in Chap. 2, this report.) The system pressure and temperature would increase gradually, with thermal convection serving to circulate vapor up through the reactor, through the turbines, and to the radiator manifold. Condensate would return under the action of gravity until a sufficient power was reached so that the

free-turbine-driven pump unit would start. The system would then be checked out and launched at this heat addition rate. The system would be kept hot, and the free-turbine-driven pump unit would be operating throughout the launch and the initial orbit until the nuclear startup was accomplished. This approach greatly reduces the number of steps required to complete the startup in orbit. Even more important, it gives promise of avoiding difficulties with free-liquid surfaces during the zero and near-zero power portion of a startup in orbit, since it appears that the power and flow rate can be kept high enough with the Lox-kerosene burner so that fluid dynamic forces will be effective in controlling the free liquid surfaces. The consumption of Lox and kerosene would be about 100 lb/hr.

The problem of warming up the system for a start from the cold condition was discussed in the previous report,[3] where it was shown that it would be quite reasonable to carry out such an operation with no auxiliary heat except at the reactor and around the liquid return lines from the radiator.

If the high-temperature portion of the system of Fig. 1.1 were constructed of a refractory alloy, such as columbium, so that it could be operated with a reactor outlet temperature of 2000°F, the optimum radiator temperature would be about 1350°F. This would permit the power output to be increased by a factor of 2.12 without any increase in the size of the main radiator. The radiator for the generator cooling system would have to be doubled in size, but it is small. This is such an interesting possibility that two additional columns were added to Table 1.1 to give a rough indication of the weight of such a system. The radiator weight, if changed, would be reduced somewhat, since the higher vapor density would actually reduce the volume flow. Thus the flow passage area in the tubes and manifolds could be reduced some. The shield weight would be increased because of the higher source strength and because of the greater amount of beryllium that would have to be used to remove the heat by thermal conduction from the inner portions of the lithium hydride

[3]R. B. Korsmeyer, Preheating Requirements for Radiator, pp. 25-29, "Space Power Program Semiann. Prog. Rep. June 30, 1963," USAEC Report ORNL-3489, Oak Ridge National Laboratory.

shield. The turbine weight would not be increased appreciably, since the turbine size would remain substantially the same - again because the increase in vapor density would more than offset the increase in power. The generator size and weight would have to be increased approximately in proportion to the power output. Similarly, the size and weight of the feed heater and the generator cooling system would increase in proportion to the power, as would the size and weight of the jet pumps and the liquid lines. The free turbine pump should weigh essentially the same for the two systems, as would the startup and control equipment.

Radiator Design To Meet Launch Requirements

A. P. Fraas

The difficulties of designing a radiator for a space power plant are considerably increased by the launch requirements. Not only must an acceleration of 10 g be accommodated, but the radiator structure must be sufficiently stiff and rugged to withstand severe vibration arising from combustion roughness. Shaking forces are transmitted throughout the structure of the launch vehicle that give accelerations of from 10 to 20 g over the frequency range from 40 to 400 cps. A second serious source of shaking forces is the noise from the rocket exhaust, which gives sound pressure levels of the order of 160 decibels.

The radiator layout shown in Fig. 1.1 was evolved in searching for a structure well suited to stowage in a launch vehicle and yet designed to give a high degree of vacuum tightness, sufficient sturdiness to withstand launch loads and vibration, sufficient protection from meteoroids to keep the probability of a puncture below 1% per year, and a fluid passage arrangement that will give good control of the free-liquid surfaces for both prelaunch checkouts and low-power operation throughout the launch. The thermal radiation surfaces consist of 7-ft-long tapered tubes arranged around the perimeter of a 10-ft-diam cylinder with the tube axes parallel to the axis of the vehicle. Two cylindrical banks, each 7 ft high, form a 14-ft-high, 10-ft-diam assembly. To minimize the area vulnerable to meteoroid penetration, an involute reflector is used so that the rear

surfaces of the tubes and fins also emit thermal radiation to space. Tests have indicated that the involute reflector will be about 87% effective. This arrangement makes it possible to get close to the maximum heat output from a given size of launch package envelope without excessive fin weights. (For any given fin efficiency the fin weight per unit of surface area varies as the square of the fin height.) Further, the rear sides of the radiator tubes require no armor, since the involute reflector on the opposite side of the radiator should act as a bumper to disperse any meteoroid particles that penetrate it. The extra weight of the involute reflector is much more than justified by the saving in fin weight. The tube wall thickness is greater on the outside to increase the resistance of the tube wall to penetration by meteoroids, as indicated in Fig. 1.2. While this configuration has the disadvantage that the radial pipes from the turbine outlet to the circumferential manifolds would interfere with retraction of equipment to be stowed inside the radiator drum for launching, the installation as a whole has a low center of gravity.

Structural Design

The tube, fin, and reflector structure, by itself, is rather flimsy and unsuitable both aerodynamically and structurally for launching. However, if an aluminum windshield about 0.010 in. thick is placed around the outer perimeter of the tubes, and the space between it and the aluminum involute reflector is filled with polyurethane foam, the resulting structure should be quite strong and stiff, since all the components would be bonded together by the polyurethane. Further, the internal damping in the polyurethane foam should be effective in restricting the amplitude of any resonant vibrations. Such a structure could be launched at a temperature of, say, 160°F with the potassium working fluid circulated by heat supplied by chemical fuel. After starting the reactor in orbit and increasing the power to give a radiator temperature of the order of 400°F, the polyurethane foam would be vaporized off to the high vacuum surrounding the vehicle, and the aluminum windshield could be stripped off so that the heat would be dissipated by direct thermal radiation from the radiator tubes and fins.

[redacted]
ORNL-DWG 63-6555

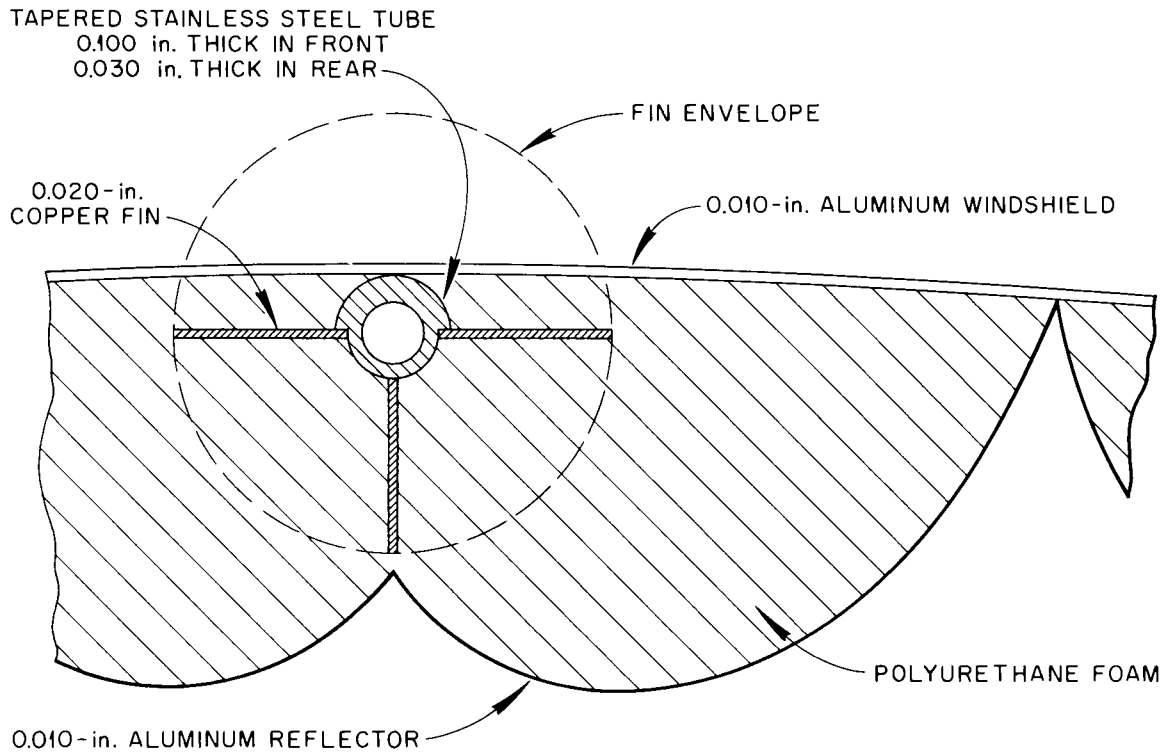

Fig. 1.2. Horizontal Cross-Section Through a Typical Radiator Tube Showing the Structure for Launching. (Full Scale.) The portion shown is an element of a cylindrical drum.

The weight and inertial loads of the reactor and shield assembly, turbine-generator unit, and related equipment would be carried upward through the 0.050-in.-thick radial vapor pipes to the upper manifold ring. This would distribute the load fairly well to the tubes, windshield, and involute reflector around the perimeter. The uniformity of the circumferential distribution of the load at the base of the package would be increased by an additional thickness of sheet aluminum, which would be used in the form of a band about 6 in. high around the perimeter in the region between the upper and lower tube banks to serve as reinforcing to accommodate the 10-g acceleration loads.

Meteoroid Protection

The projected area of the radiator tubes and manifolds that is exposed to meteoroids is 70 ft^2, or 7 m^2. For a 1% probability of a penetration

per year, the flux of penetrating particles must be

$$\frac{1}{(30 \times 10^6 \text{ sec/yr})} \frac{1}{(7 \text{ m})} \frac{1}{100} = 5 \times 10^{-11} \text{ particles/m}^2\cdot\text{sec} .$$

From Fig. 1 of Whipple's recent paper,[4] the meteoroid mass for this flux of penetrating particles is 1×10^{-3} g. The mean velocity is 22 km/sec, or 72,000 ft/sec.

From Fig. 27 of a paper by Gehring and Lieblein,[5] the thickness of niobium tubes required to resist penetration by 3/32-in.-OD glass particles weighing 0.016 g and moving at 25,000 ft/sec is 0.135 in. The Brinnell hardness of the niobium ranged from 120 to 135. The equivalent mass for the same incident kinetic energy as meteoroids would be 0.00192 g. The thickness for incipient penetration is given by

$$t = K \left(\frac{E}{B}\right)^{1/3} ,$$

where E is the energy of the incident particle and B is the Brinnell hardness. For stainless steel tubes having a Brinnell hardness of 160, the thickness for incipient penetration can be estimated from the data for niobium in ref. 5, as follows:

$$\frac{t}{0.135} = \left[\frac{127\ (1 \times 10^{-3})}{160\ (2 \times 10^{-3})}\right]^{1/3} = (0.397)^{1/3}$$

---

[4]F. L. Whipple, On Meteoroids and Penetration, presented at the American Astronautical Society Interplanetary Missions Conference, January 1963, Los Angeles, California.

[5]J. W. Gehring and S. Lieblein, Preliminary Results on Effects of Hypervelocity Impacts on Space Radiator Tubes, ARS Paper No. 2544-62, presented to the American Rocket Society Space Power Systems Conference, Santa Monica, California, September 25-28, 1962.

$$t = 0.135 \times 0.73 = 0.10 \text{ in.}$$

Thus tubes having a wall thickness of 0.10 in. can be employed, and the wall can be thinned to 0.030 in. over the rear half of the tube by machining or grinding to give an average wall thickness of 0.065 in.

Radiator Weight Estimates

Estimated performance, dimensional, and weight data for the proposed configuration are summarized in Table 1.2. The weight data are particularly interesting in that the weight of the tubes and fins represents only about one-half the total weight at launch. Another 16% is chargeable to the aluminum windshield and the polyurethane foam, which would be jettisoned after the unit had been placed in orbit if the structure were not to be called upon again to withstand severe loads, such as those associated with a lunar landing. Another 25% of the total weight is chargeable to the ducts and manifolds and about 10% to the involute reflector. For this case the overall weight before launch is approximately 7.5 lb/kw(e), while after jettisoning the windshield the weight would be reduced to approximately 6.5 lb/kw(e).

The high fin efficiency coupled with the large fin height lead to a somewhat greater taper ratio in the tubes than was employed in the ORNL test radiators built to date. The third fin at the back of the tube increases the heat rejection capacity of the tube by about 30% and further increases the taper ratio required to give a quasi uniform vapor velocity along the length of the tube. Thus, while the tubes are the same length, i.e., 7 ft, and the tube outlet diameter is the same, the tube inlet diameter for the design of Table 1.2 has been increased to 1.2 in. to accommodate the larger vapor inflow rate.

The fin weight might be cut approximately in half through the use of aluminum fins. This would present difficult differential expansion and brazing problems, but the potential weight saving makes this approach worth investigation. The efficiency of the involute reflector might be increased by using a highly polished surface. This would also reduce its operating temperature, which will be around 700°F at full power.

Table 1.2. Performance, Dimensional, and Weight Data for a Cylindrical-Drum Main Radiator Designed for Launching

Power to be dissipated	
kw	860
Btu/hr	2.93×10^6
Ideal dissipation to 500°R at 1500°R, Btu/hr·ft^2	8562
Emissivity of sandblasted and oxidized type 310 stainless steel	0.92
Fin efficiency	0.90
Involute reflector efficiency	0.87
Average heat flux, Btu/hr·ft^2	6730
Area required, ft^2	435
Height of cylinder for 21-ft-diam vehicle (Saturn C-2), ft	6.6
Height of cylinder for 10-ft-diam vehicle (Atlas-Centaur), ft	14
Weight of 0.020-in. copper fins (assuming $2.7/7.5 \times 435 = A$), lb	160
Weight of 0.050-in.-wall stainless steel tubes, lb	365
Weight of 0.010-in.-thick aluminum reflector, lb	85
Weight of stainless steel vapor ducts and manifolds, lb	300
Weight of 0.010-in.-thick aluminum windshield, lb	60
Weight of 1.5-lb/ft^3 polyurethane foam, lb	100
Weight of aluminum meteoroid bumper at top end, lb	10
Total launch weight, lb	1080
Net weight after jettisoning windshield, lb	920
Vulnerable surface area (total), ft^2	80

System Flow Distribution, Stability, and Control

M. E. LaVerne M. M. Yarosh
A. R. Barbin

As discussed in previous progress reports, particularly the preceding one,[6] one of the major features of the MPRE is a simple control system which, while simple, requires precise engineering to obtain proper matching of the characteristics of the various components. Work on these complex matching problems is continuing, with the current objective being a system that will have good control characteristics over the range from about 10 to 100% power. A computer code for investigating the effects on the system static characteristics of various component characteristics was prepared. In addition, an electrical analog was built and operated with the characteristics of all the components included, except the cavitation characteristics of the jet pumps and the feed pump. During the coming quarter it will be possible to compare the results obtained from both the digital computer and the electrical analog with experimental test data, since data will be obtained from the Phase II version of the 91-rod boiler system, which includes the free-turbine pump, jet pumps, and a tapered-tube condenser.

Digital Computer Code

The analysis outlined in the previous progress report was extended and reduced to a digital computer code. The free-turbine-pump units built for the 91-rod boiler systems have the same diameter pump and turbine wheels as planned for the MPRE. The characteristics of these units differ from the characteristics of those for the MPRE only because of the difference in capacity. Seven nozzles would be employed in the partial-admission turbine, as compared with only three in the units for the 91-rod boiler systems, and the feed pump impeller vanes for the MPRE will have an axial height double that for the 91-rod boiler system. Thus the

---

[6]A. P. Fraas, Effects of Power Output on Inventory and Flow Distribution Through MPRE System, pp. 12-25, "Space Power Program Semiann. Prog. Rep. June 30, 1963," USAEC Report ORNL-3489, Oak Ridge National Laboratory.

characteristic curves obtained experimentally for the units for the 91-rod boiler system will serve as an excellent point of departure for system analysis. The first step in preparing the computer code for the system was to prepare analytical expressions to match the curves obtained experimentally for these turbine-driven pump units. The analytical curve for the head coefficient plotted as a function of the flow coefficient is shown in Fig. 1.3. The experimental points obtained in testing the unit are also plotted. Similar comparisons of the analytical expressions for the overall efficiency and the ratio of the bearing lubricant flow to the total flow as functions of the flow coefficient are shown in Figs. 1.4 and 1.5. Analytical expressions were also prepared to describe the performance of the jet pumps in the noncavitating region that were based on

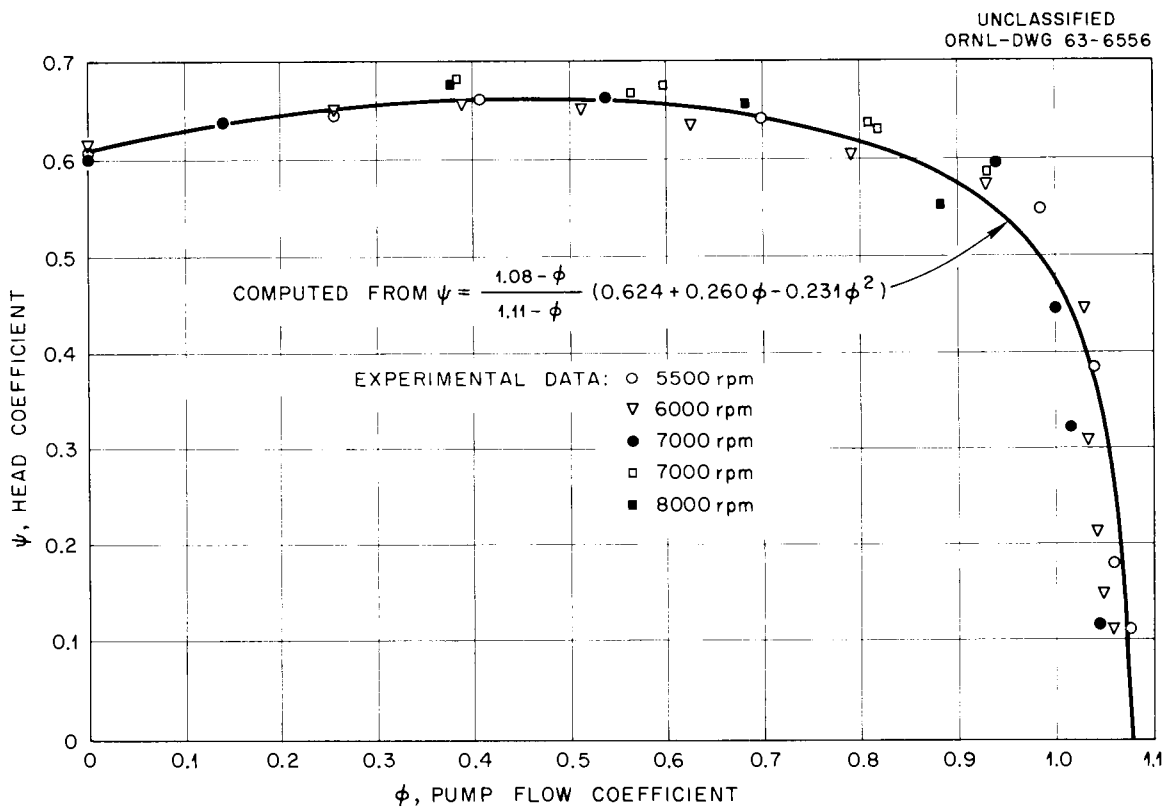

Fig. 1.3. Comparison of Test Data with the Analytical Curves Used to Define the Centrifugal Feed Pump Performance.

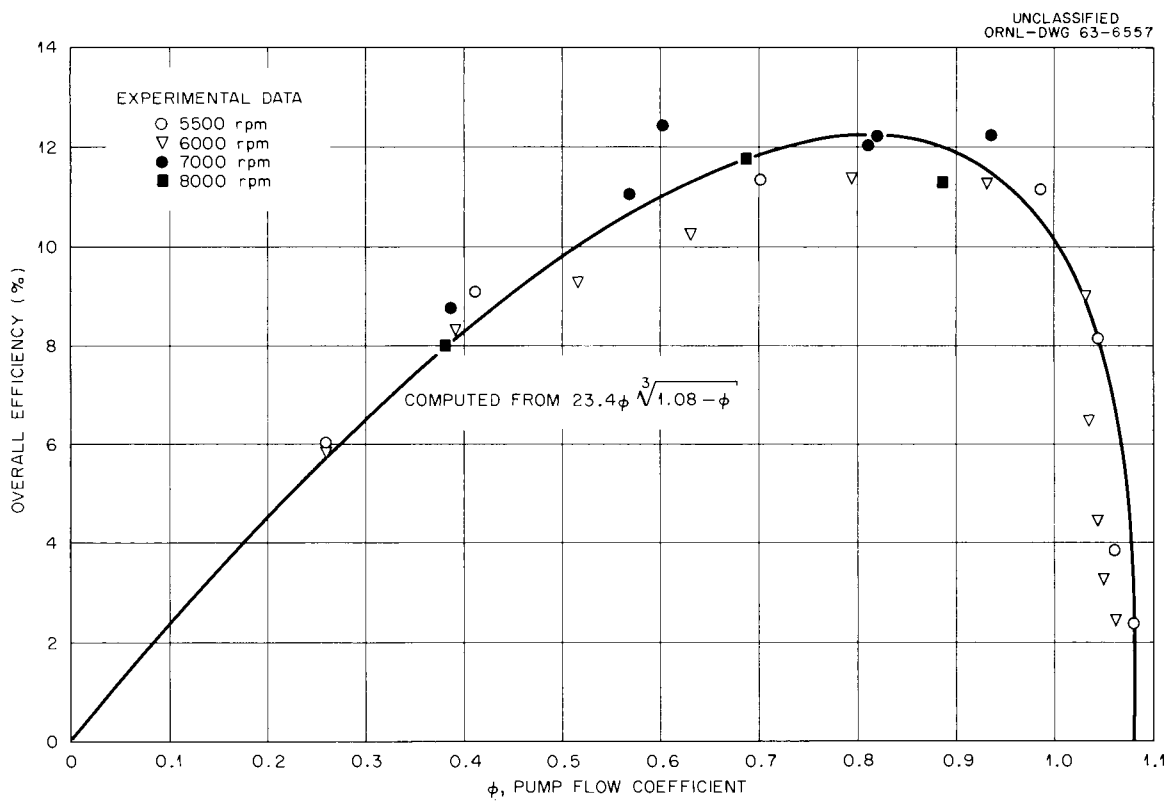

Fig. 1.4. Comparison of Test Data with the Analytical Curve for the Overall Efficiency of the Free-Turbine-Driven Pump Unit.

the experimental data given previously.[7] The two-phase pressure drop through the reactor core was calculated by following the procedure outlined previously.[8] The code also permits insertion of pressure loss coefficients for each of the major components in the system.

The code is designed to determine the speed of the free-turbine-driven pump unit and the system flow and pressure distribution for any given power input. It does this by a series of iterations in which the computer seeks for the flow distribution for which the characteristics of all the various components match. As indicated in ref. 6, the boiler

---

[7]L. W. Evers and A. G. Grindell, Tests of Jet Pumps, "Space Power Program Semiann. Prog. Rep. Dec. 31, 1962," USAEC Report ORNL-3420, Oak Ridge National Laboratory.

[8]M. E. LaVerne, Core Flow Stability, pp. 5-9, "Space Power Program Semiann. Prog. Rep. June 30, 1962," USAEC Report ORNL-3337, Oak Ridge National Laboratory.

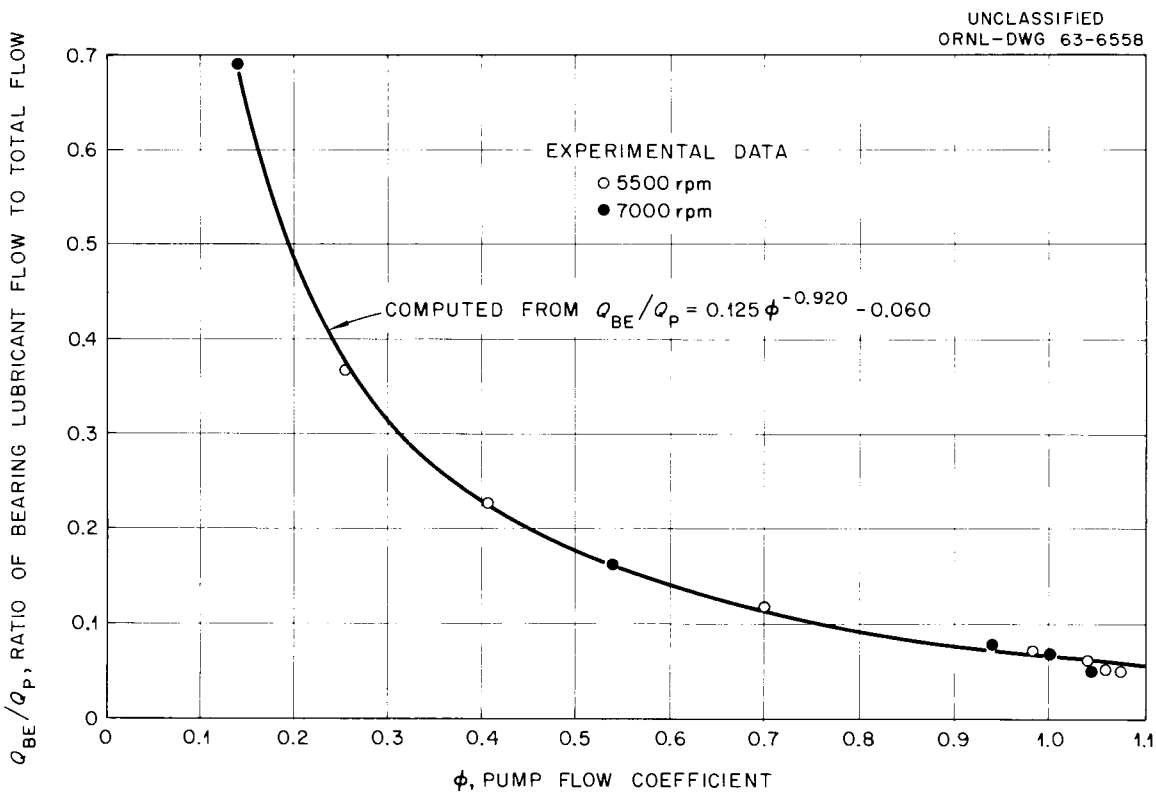

Fig. 1.5. Comparison of Test Data with the Analytical Curve for the Bearing Lubricant Flow for the Free-Turbine-Driven Pump Unit.

outlet pressure is proportional to the power input so that with a given set of system component pressure loss coefficients, the speed of the free-turbine-driven pump unit can be estimated, thus giving a point of departure for the iteration. Since the speed of the free-turbine-driven pump unit depends on the liquid flow through the feed pump, it is necessary to carry out a series of iterations to determine the flow to the various system components and converge on the speed of the free-turbine-driven pump unit that gives equilibrium conditions. The problem is complicated somewhat by variations in the boiler exit quality and pressure drop with the jet-pump driving head. The code does not include the cavitation characteristics of the jet pumps. Rather, it determines the amount of mismatch that must be accommodated by cavitation in either the condenser scavenging jet pumps or the centrifugal feed pump or both. With the code it will be possible to determine the amount of this mismatch at each of a series of loads from full power down to a very low power for each of a series of

jet-pump nozzle diameters and each of a variety of equivalent orifice areas for restrictions both in parallel and in series within the free-turbine-driven pump unit. Once these data are computed by machine it will be possible to carry out a hand analysis to determine the range over which the mismatch in system characteristics can be accommodated by cavitation in the centrifugal feed pump or the jet pumps or both. Thus the code will provide an excellent guide for carrying out experiments with the phase II 91-rod boiler system.

Simulation of the turbine-generator unit with a critical-pressure-drop orifice is an excellent approximation, since, as the turbine speed increases from a completely stalled rotor to a complete runaway condition, the vapor flow through the turbine at a given pressure ratio ordinarily varies only about ±15% from the mean.

Electrical Analog

Following the same basic approach as that described above, an electrical analog of the MPRE system was constructed and operated on the ORNL analog computer to investigate the dynamics of the system. The model was more complex than that used for the digital computer code, since it also included effects of the thermal inertia, the fluid velocities, and the free-turbine-driven pump rotor inertia. The cavitation performance of the centrifugal and jet pumps has not yet been included; however, in place of using the jet-pump cavitation characteristics, it was possible to operate the system by using some manual control devices to bring it into balance. The preliminary results indicate that the system responds well to transients and is stable with respect to small fluctuations.

2. REACTOR PHYSICS

O. L. Smith A. M. Perry
J. C. Robinson

Analyses of the Third and Fourth Critical Experiments

The beryllium-reflected critical experiments were described in the previous report[1] and in ref. 2. The techniques used in analyzing them were the same as those used for the first two experiments, which were also described in the previous report. The calculated values of k_{eff} for the third experiment were 1.036, using the regular solution of the transport equation,[3] and 1.026, using the adjoint solution. The two solutions would be expected to give the same value for k_{eff}; the source of the small difference has not been established.

A comparison of the experimental and calculated fission distributions along the axis of the system and in the core midplane is shown in Fig. 2.1. The experimental and calculated curves are normalized to each other at the center of the core. The agreement is seen to be good except in the outer half of the top reflector. A comparison of the experimental and calculated cadmium ratios (bare-foil rate divided by covered-foil rate) in the top reflector is shown in Fig. 2.2. The flux perturbation factors listed in the previous report were applied to the experimental results. The disagreement in Fig. 2.2 implies that the calculations underestimate the fraction of neutrons with energies below the cadmium cutoff. The disagreement in Fig. 2.1 may also be interpreted in this fashion, that is, the calculations appear to underestimate the thermal peaking in the reflector.

---

[1]A. M. Perry and O. L. Smith, Reactor Physics, pp. 36–51, "Space Power Program Semiann. Prog. Rep. June 30, 1963," USAEC Report ORNL-3489, Oak Ridge National Laboratory.

[2]J. T. Mihalczo, "A Small Beryllium-Reflected UO_2 Critical Assembly," USAEC Report ORNL-TM-655, Oak Ridge National Laboratory, July 23, 1963.

[3]B. Carlson, C. Lee, and J. Walton, "The DSN and TDC Neutron Transport Codes," USAEC Report LAMS-2346, Los Alamos Scientific Laboratory, Feb. 12, 1960.

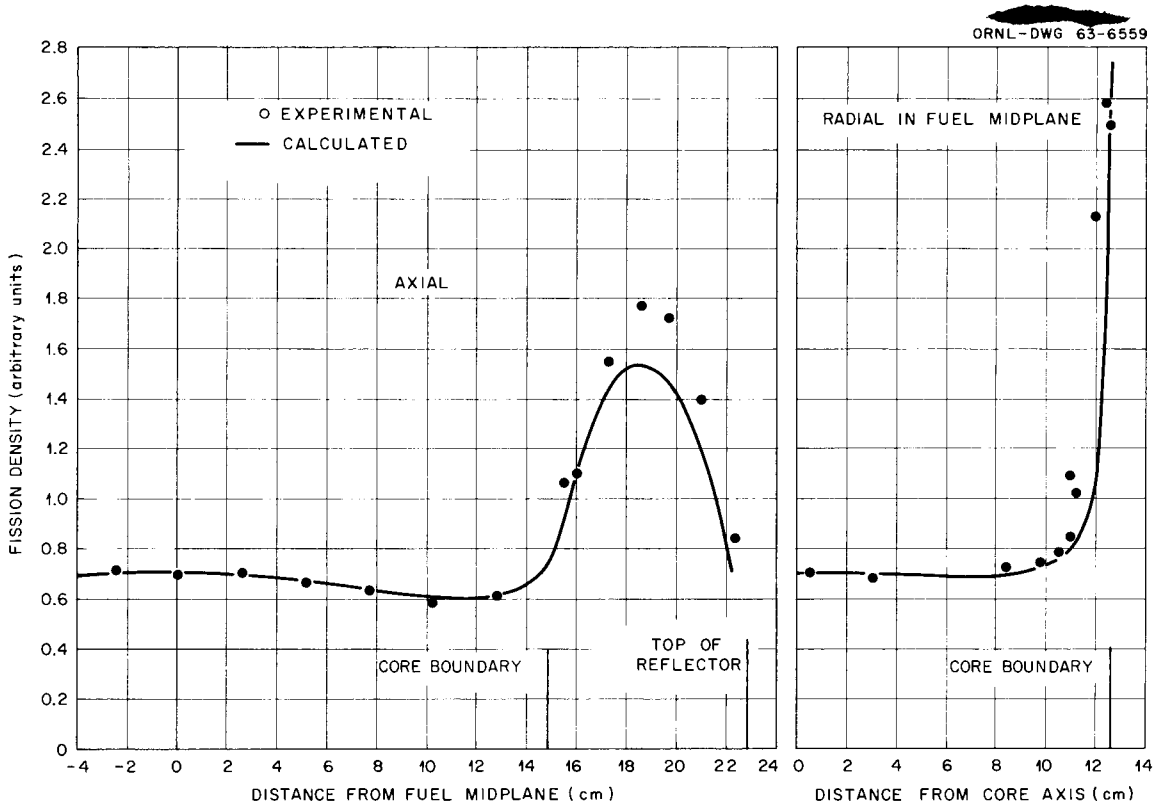

Fig. 2.1. Axial and Radial Fission Densities in the Third Critical Experiment.

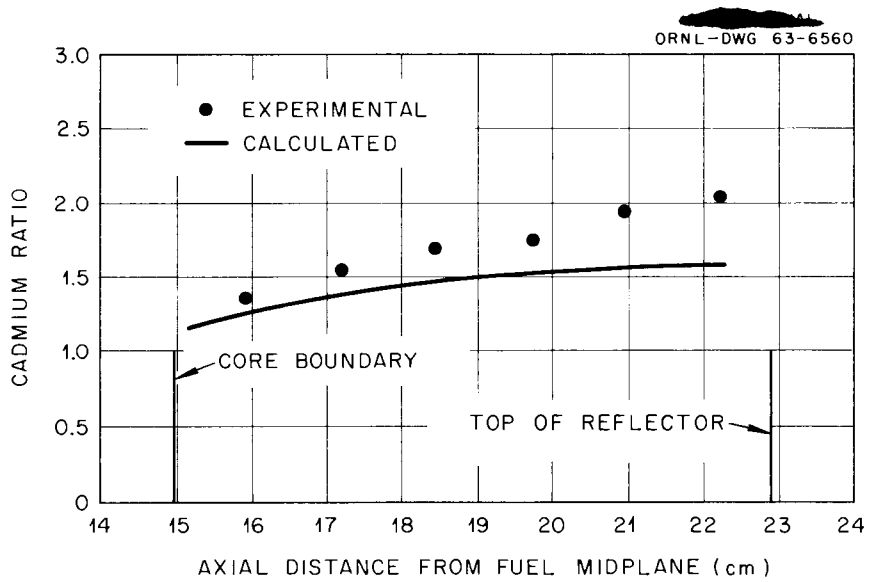

Fig. 2.2. Cadmium Ratio in Third Experiment.

[redacted] calculated values of k_{eff} for the fourth experiment were 1.032, using the regular transport solution, and 1.028, using the adjoint solution. No flux tranverses were made in the fourth experiment.

Reactivity coefficients were measured for several different materials in the beryllium-reflected experiments. The measurements were undertaken partly to obtain direct experimental information for materials of present or possible future interest in the MPRE program and partly to provide further evidence for assessing the reliability of the computations. The measured reactivity changes were subsequently calculated using perturbation analyses[4] based on the regular and adjoint solutions of the transport equation. The experimental and calculated results are listed in Table 2.1.

---

[4]W. E. Kinney and G. E. Whitesides, The TDC Perturbation Code, p. 258, "Neutron Phys. Prog. Rep. Sept. 1, 1961," USAEC Report ORNL-3193, Oak Ridge National Laboratory.

Table 2.1. Comparison of Experimental and Calculated Reactivity Coefficients

Critical Experiment	Material [redacted] Shape	Total Mass (g)	Δk_{eff} Measured[a]	Δk_{eff} Calculated	Ratio of Calculated Δk_{eff} to Experimental Δk_{eff}
3	CH_2 rod	18.42	0.00183	0.0025	1.37
3	Type 304 stainless steel rod	1704	0.00111	0.00145	1.31
3	Carbon rod	82	0.000563	0.00055	0.98
3	Niobium rod	1050	+0.00368	-0.000838	-2.28
3	B_4C tube	30.5	-0.000499	-0.00062	1.24
3	Stainless steel disk	1290	0.00060	0.000677	1.13
3	Aluminum disk	464	0.00125	0.00138	1.10
4	Potassium calandria	3403	0.00138	0.00415	3.01

[a]Assuming \$1.00 = 0.0075 Δk_{eff}.

In the third experiment the materials were in the form of either thin rods, approximately 1/8 in. in diameter and 12 in. long, located in a number of the interstices between fuel pins, or thin disks approximately 1/8 in. thick and 10 in. in diameter, located directly over the core. In one case, for B_4C, the material was in the form of powder packed into a hollow fuel tube located on the axis of the core. In the fourth experiment the material (potassium) was contained in a stainless steel calandria and distributed throughout the core. In each case, regular and ajoint solutions of the transport equation were obtained for the clean system and the reactivity change due to addition of the material was calculated using the perturbation code. Although the number of rods varied from case to case, they were distributed as nearly uniformly as possible over the volume associated with the 180 innermost fuel pins (effective radius, 10.43 cm). In the calculations the material masses were smeared over this volume. The geometry of the disks could be handled exactly, and no smearing was necessary.

Table 2.1 indicates various degrees of success in calculating the reactivity changes. The possible sources of the discrepancies include (1) failure of the TDC code to calculate the regular and adjoint fluxes correctly, (2) inaccuracies in the cross section data used in the TDC and perturbation codes, and (3) failure of the perturbation method. Efforts are being made to investigate each of these possibilities.

Reactor Control Studies

Three possible mechanisms for reactivity control of the MPRE were studied. The first device was an iris diaphragm of B_4C which could move across the inlet end of the core. The second was a set of rotating drums in the side reflector; a portion of the surface of each drum was covered with a thin layer of B_4C. The third was a movable plug of reflector at the inlet end of the core. The characteristics of most interest in these studies were (1) the total reactivity swing available, (2) the residual poison of the device in the operating configuration, and (3) the effect of the control device on the core power distribution during reactor operation.

In order to evaluate the control mechanisms, a reference reactor design was set up with the intention of approximating the MPRE design configuration as nearly as possible at the present time. The reference reactor is shown in Fig. 2.3. The core contains UO_2 with 93.2% enrichment enclosed in stainless steel tubes. The ratio of steel volume to fuel volume is 0.2. The core contains a 0.3 coolant void fraction and the lower one-fourth of the core has this void filled with liquid potassium. The reflector and core dimensions were selected to give flat power distributions in the axial and radial directions with $k_{eff} = 1.026$. The power distributions are shown in Figs. 2.4 and 2.5. The shapes of the curves are essentially independent of the positions selected for the traverses. When the core void is completely filled with potassium, $k_{eff} = 1.0305$. When the potassium is completely removed from the system, $k_{eff} = 1.0230$. The change in k_{eff} from full to empty is thus $\Delta k_{eff} = 0.0075$. The weight

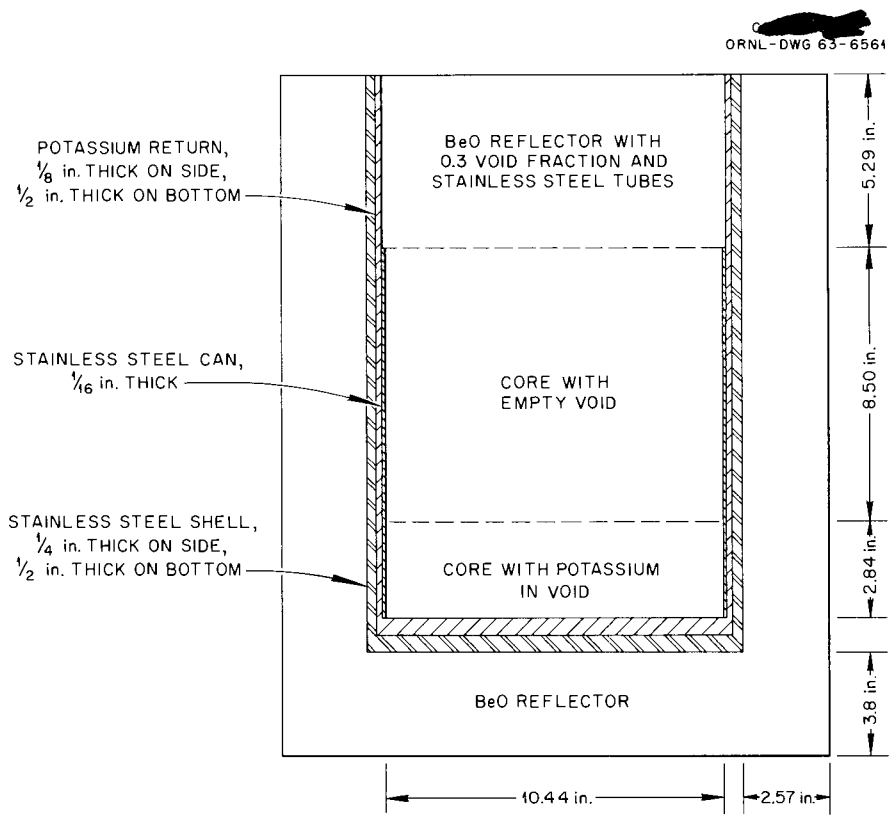

Fig. 2.3. Reference Reactor.

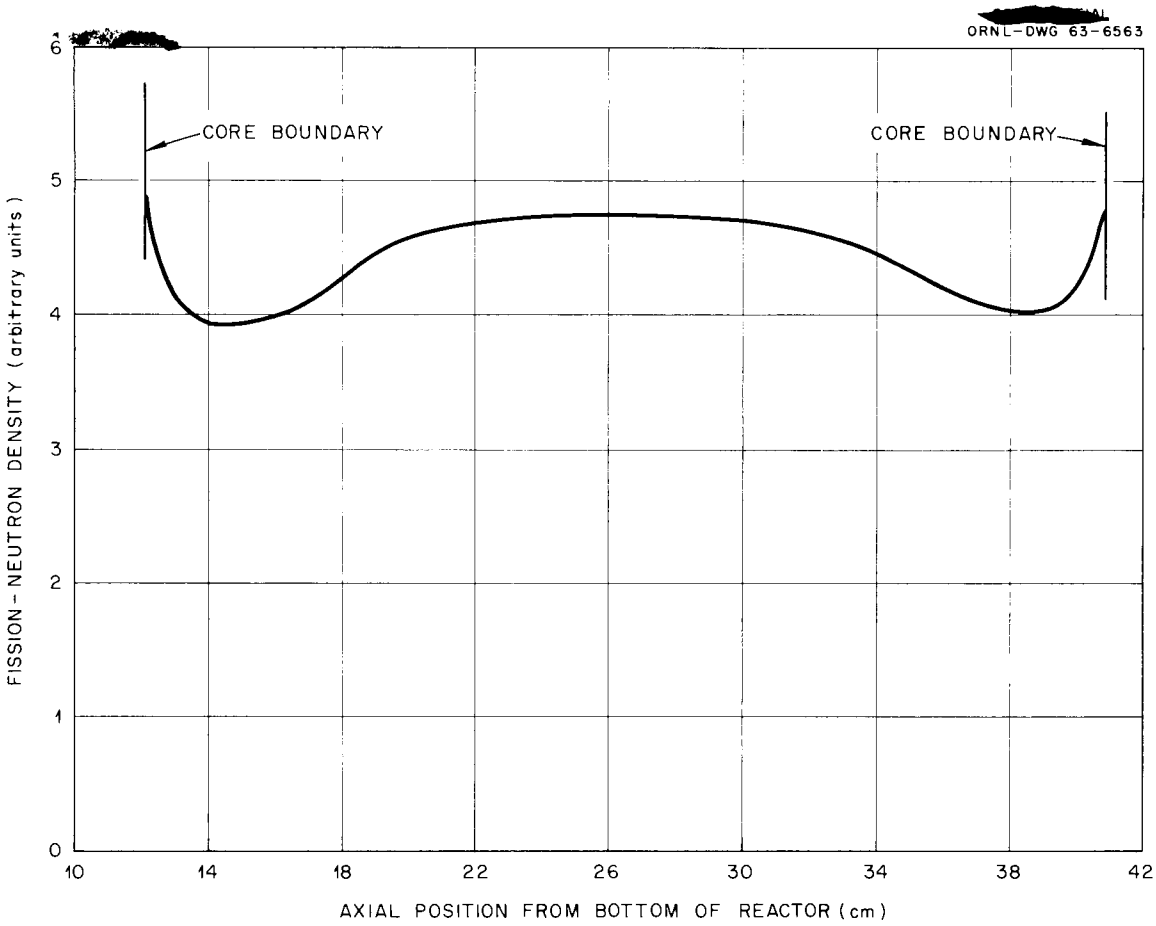

Fig. 2.4. Reference Reactor Axial Power Distribution.

of the configuration is 671 lb. The mean neutron energy in the core is 0.372 Mev.

Iris Diaphragm

In order to approximate the effect of closing an iris diaphragm of poison material across the inlet end of the core, a 1/2-in.-thick layer of natural-enrichment B_4C (ρ = 2.5 g/cm^3) was superimposed upon the layer of steel below the core. The calculated k_{eff} was 1.0138, giving Δk_{eff} = −0.0122. Since reactivity changes less than about 4% in k_{eff} are presently believed to be insufficient for good control, the iris diaphragm appears to be an unsatisfactory mechanism for total reactor control, although it could conceivably have some applicability as a shimming device.

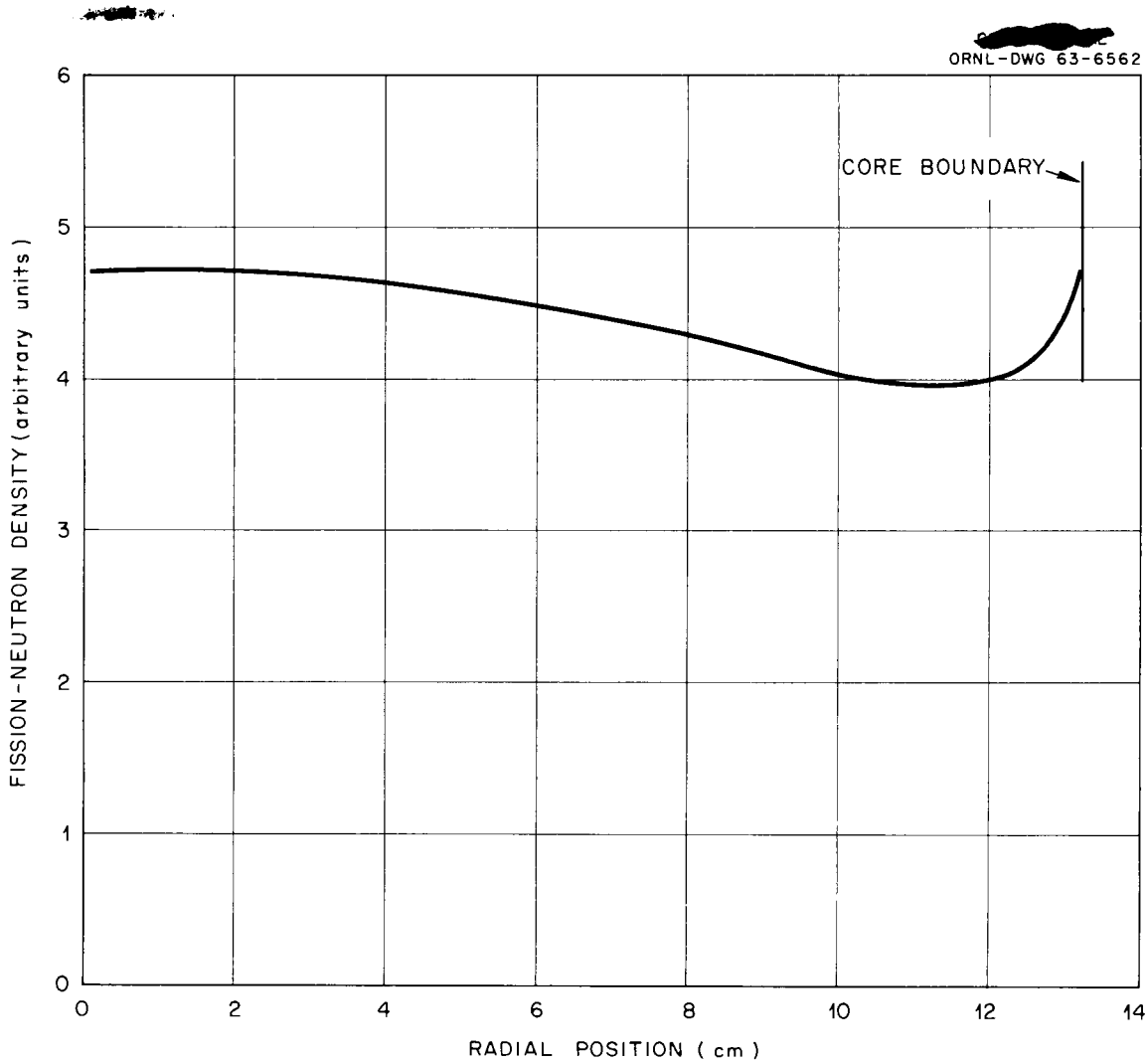

Fig. 2.5. Reference Reactor Radial Power Distribution (Traverse in Core Midplane).

Rotating Drums

The basic configuration of a rotatable drum control device is shown in Fig. 2.6. To approximate the effect of turning the drum, a series of neutronic calculations in x,y geometry[5] was performed. The calculations represented an infinitely long cylindrical reactor with cylinder boundaries approximated stepwise so that the total core area and total reflector area

[5] J. Bengston et al., "2DXY, Two-Dimensional Cartesian Coordinate S_n Transport Calculation," AGN TM-392, Aerojet Nuclear, June 1961.

[redacted]
ORNL-DWG 63-6564

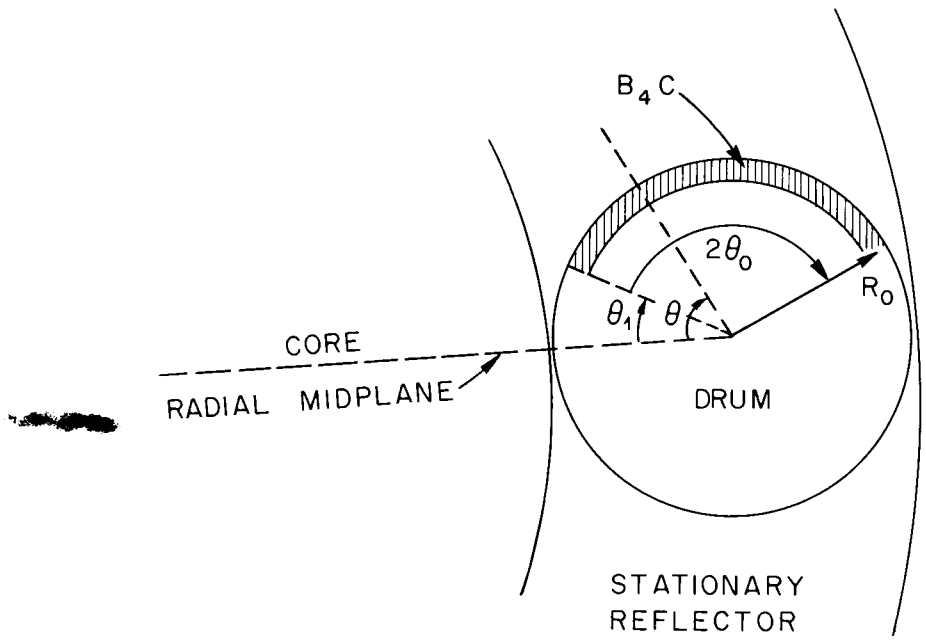

Fig. 2.6. Geometry of Rotating Drum Control Device.

in the x,y geometry were equal to the corresponding areas in the reference reactor midplane. The B_4C layer on a drum was approximated by a rectangular area 1/4 in. thick and 2 in. long. The length corresponded to the amount of material necessary to cover a 90-deg sector of the drum surface. Two-dimensional calculations were performed with the longest dimension of the B_4C (1) flush with the inner surface of the reflector, (2) normal to the reflector surfaces and half way between them, and (3) flush with the outer reflector surface. This sequence approximated motion of the poison from the "in" to the "out" position. Also a calculation was performed with the B_4C completely removed, that is, replaced with BeO. Table 2.2 shows the value of k_{eff} for each poison position. The results of Table 2.2 represent the effect of eight control drums in the reflector. When all eight B_4C rectangles are in the "in" position, 45% of the core surface is covered.

The power distribution in the core for each drum orientation is given in Fig. 2.7. The curves for the "out" position are nearly identical with

[redacted] Table 2.2. Effect of Placing B_4C in Various Reflector Locations

Poison Position	k_{eff}	Peaking Ratio (see text)
In	1.189	0.76
Intermediate	1.208	0.86
Out	1.224	0.99
Removed	1.224	0.99

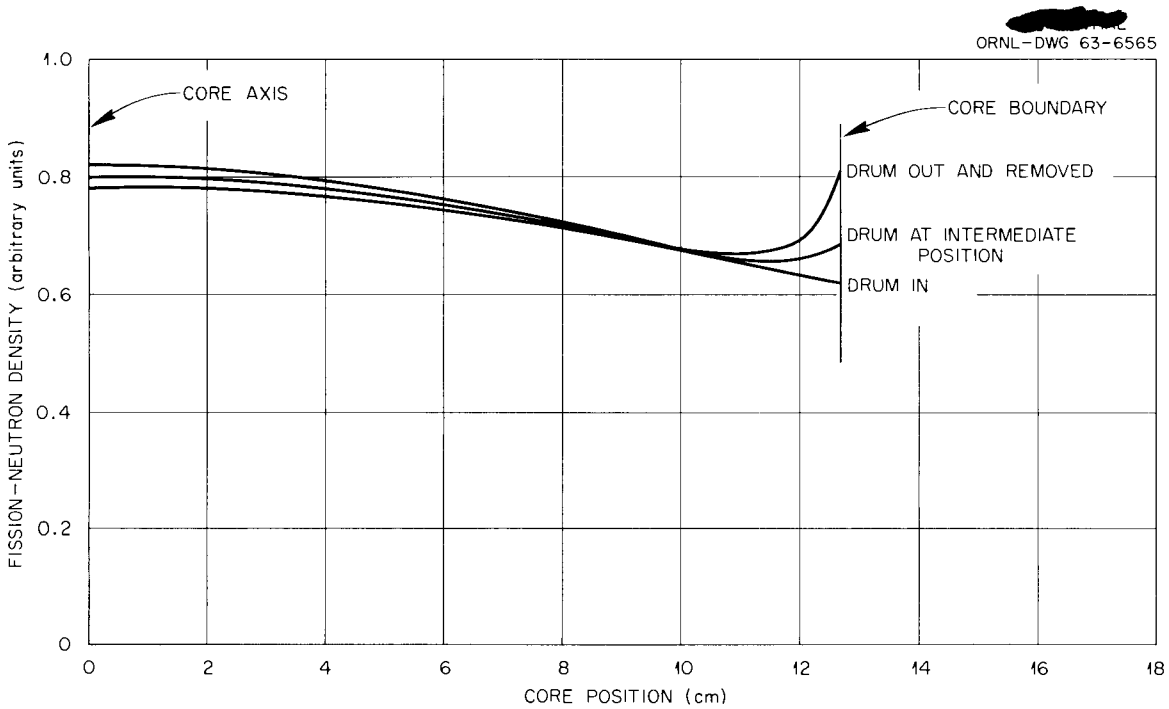

Fig. 2.7. Core Power Distribution for Three Control Drum Orientations (Traverses Taken Along a Line Bisecting the B_4C).

the case of poison removed. Table 2.2 shows the peaking ratio for each case, the peaking ratio being defined as the power density at the core surface divided by the power density at the core axis. When the B_4C is in the intermediate position, corresponding to an operating configuration, the power density along the core surface is flat, that is, it is not scalloped by the proximity of the poison.

An approximate expression was developed for the control worth of a drum in any orientation θ_1 (see Fig. 2.6) and with arbitrary B_4C sector $2\theta_0$. The relative worth of a drum at orientation θ_1 is defined as the magnitude of the change in reactivity produced by rotation of the drum from the "out" position to position θ_1. If the values of k_{eff} relative to k_{eff}(removed) are plotted as a function of average poison separation from the core surface, the result is a nearly straight line with slope $a = -0.0151$ and intercept $b = 0.035$. This line is defined as the absolute worth of the poison for the reason that it does not include residual poison effects.

The absolute worth of an angular section $2\theta_0$ in orientation θ_1 is given approximately by

$$\Delta k^{a}_{eff} = \frac{R_0}{0.45\pi d} \left\{ aR_0[\sin\theta_0 - \sin(\theta_1 + 2\theta_0)] + b\theta_0 \right\} , \qquad (1)$$

where d is the core diameter (d = 10.44 in.) and the other parameters are as previously defined (R_0 = 1.16 in.). The residual poison of a drum is obtained by evaluating this expression for θ_1 corresponding to the out position, and the relative worth of a drum in position θ_1 is then given by subtracting the residual poison from Eq. (1). The relative worth of the drum in the "in" position is given by

$$\Delta k^{r}_{eff}(\text{out-in}) = -\frac{4aR_0^2 \sin\theta_0}{0.45\pi d} = 0.00551 \sin\theta_0 . \qquad (2)$$

Thus the maximum reactivity swing available is $\Delta k_{eff} = 0.0055$ per drum with a 180-deg sector covered with B_4C.

The expressions given above were then generalized to include the effect of varying the B_4C thickness and the B^{10} enrichment. A series of one-dimensional calculations indicated that for a B_4C thickness between 1/8 and 1/2 in. and for any B^{10} enrichment the relative worth of a drum is approximately proportional to $(te)^{1/2}$, where t is the thickness of the B_4C relative to 1/4 in. and e is the B^{10} enrichment relative to the natural enrichment. This expression may be included as a multiplier in Eqs. (1)

and (2). In particular

$$\Delta k^{r}_{eff}\ (\text{out-in}) = 0.0055\ \eta(te)^{1/2}\ \sin\theta_0\ , \tag{3}$$

where η is also included to represent the number of drums in the total control system. Some representative values of Eq. (3) are listed in Table 2.3.

Table 2.3. Reactivity Worth of Representative Drum Configurations

η	t	e	$2\theta_0$	Δk^{r}_{eff} (out-in)	Residual Poison
12	1	5	π	0.145	0.0420
6	1	5	π	0.0725	0.0210
6	1	5	$\pi/2$	0.051	0.00287

If the drums and surfaces of the drum cavities are each covered with 40 mils of stainless steel, there is a small reactivity loss due to the displacement of the BeO. This loss is approximately 1/2% in k_{eff} for six drums and 1% for twelve drums.

Since the drums could, in practice, be isolated from the stationary reflector and could conceivably lead to large temperature differences between a drum and the stationary part, a study was made to establish the temperature change across a small void at the surface of a totally isolated drum. A one-dimensional model was used with a BeO cylinder located inside a BeO reflector. The reflector temperature was assumed to be 1300°F. The mechanism for heat transfer was assumed to be thermal radiation, and the heat balance equation was

$$\dot{Q} = C(T_s^4 - 1760^4)\ , \tag{4}$$

where $\dot{Q}$ is the heat generation rate in the cylinder, C is a composite constant involving properties of the BeO and the geometry of the model,

and T_s is the surface temperature of the cylinder. The source Q was assumed to consist of a gamma-heat term and a neutron-thermalization term. The volume-averaged gamma heat rate in the reflector of the reference reactor was calculated to lie between 0.098 and 0.147 w/cm^3 when the core power level was 1 Mw (thermal). The volume-averaged neutron heat was calculated to be 0.073 w/cm^3. Using these values in Eq. (4), it is found that $1326°F \leq T_s \leq 1340°F$. These temperature limits are based on average fluxes in the reflector and may underestimate the source term because of flux peaking effects in the interior of the reflector. However, it is to be noted that if the source term is increased by 350%, $T_s \sim 1390°F$, representing still a comparatively small temperature change across the gap. There thus appear to be no serious difficulties associated with heat buildup in the drum.

Movable Plug

The volume of bottom reflector below the shell was displaced downward 3.8 in. and then 7.6 in., and the reactivity and power distribution were calculated in each case. Table 2.4 gives the calculated k_{eff} for each case, including the reference (undisplaced) configuration.

Table 2.4. Reactivity and Peaking Ratio for a Series of Plug Locations

Plug Location	k_{eff}	Peaking Ratio
Undisplaced	1.026	1.0
Displaced 3.8 in.	0.993	0.58
Displaced 7.6 in.	0.980	0.43

The axial power distribution for each case is shown in Fig. 2.8. The peaking ratio at the inlet end of the core is given in Table 2.4. The peaking ratio at the outlet end is essentially unaffected by motion of the plug. The shape of the radial power distribution is also effectively unchanged by plug movement. The net neutron leakage from the system increases from 54 to 59% as the plug moves from the undisplaced

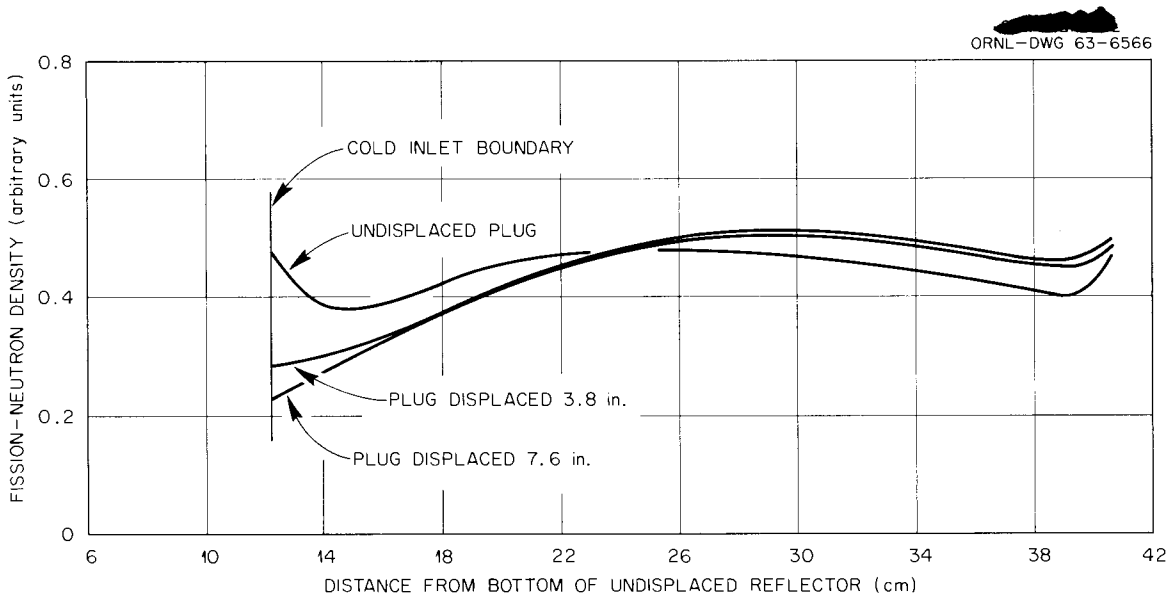

Fig. 2.8. Axial Power Distribution for Three Plug Locations.

position to the 7.6-in. position. While the peaking ratio is quite unfavorable with the plug withdrawn, this would correspond to the zero power condition. At any substantial power the peaking ratio would be close to unity.

Alteration of Reference Reactor

After completion of the reactor control studies presented above, the reference system was modified to include an axial-power distribution that decreases approximately 30% between the inlet end and the outlet end of the core. This modification is intended to compensate for superheating of the coolant as it passes through the core. The modification was achieved by cutting the top reflector thickness in half and adjusting the core dimensions to maintain $k_{eff} = 1.026$. The top reflector thickness is thus 2.63 in., the new core diameter is 10.72 in., and the height is 11.67 in. The thicknesses of the other regions of the reference system were unmodified. The axial and radial power distributions in the modified system are shown in Figs. 2.9 and 2.10. The shapes of the curves are essentially independent of the location of the traverses. It is believed that the results of the reactor control studies are not appreciably changed by this revision of the reference reactor.

[redacted] [redacted]

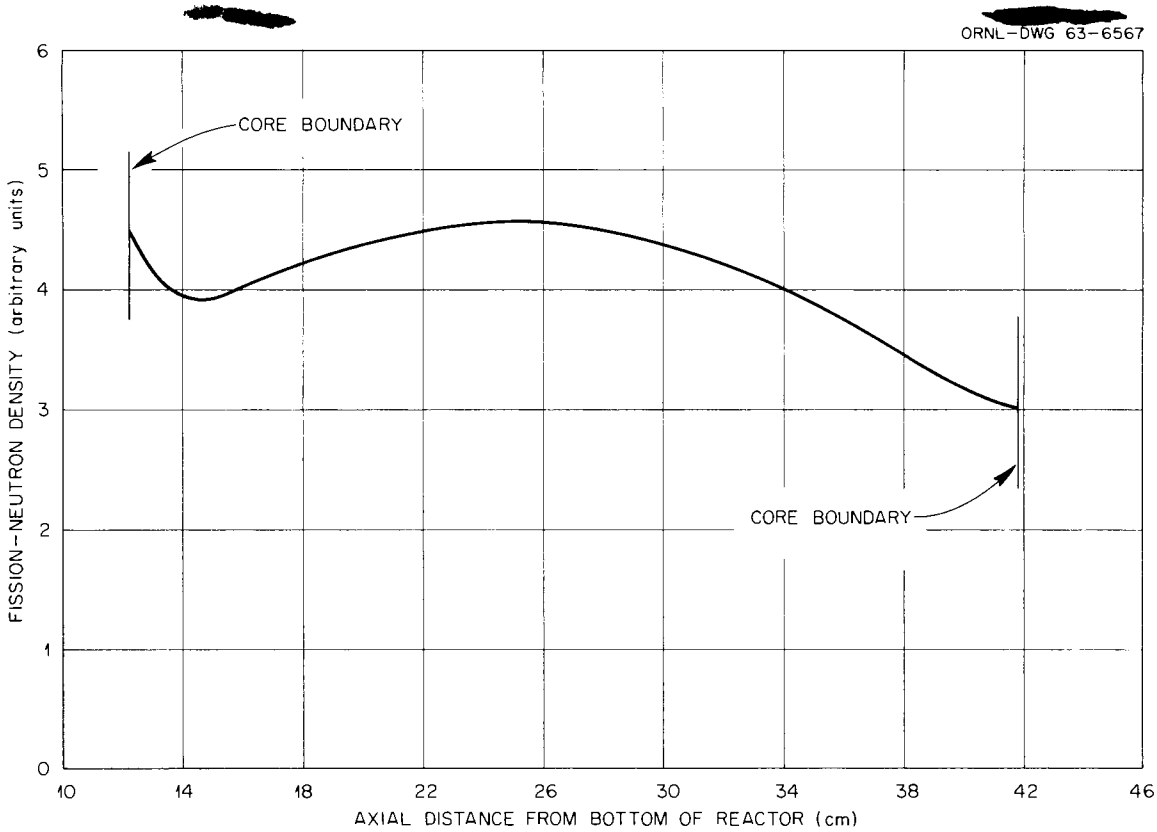

Fig. 2.9. Axial Power Distribution in Modified Reference Reactor.

Conclusions

In terms of the evaluation criteria established above, the iris diaphragm appears to be useful only as a reactor shimming control, while the rotating drums and movable plug appear to be satisfactory for total reactor control. The results indicate that for a reactivity swing of about 4% in k_{eff}, the power density at the core surface is changed about 25% for the drum mechanism and about 50% for the movable plugs, with smaller changes occurring at interior points. It is tentatively estimated that a 1 1/2% reactivity swing may be necessary for reactor control during full power operation over a three-year interval. Consequently it appears that the greatest power density fluctuation that would be sustained during high-temperature operation is approximately 10% for the drums and 20% for the movable plug. Although exact limits have not been established for the permissible range of power fluctuations, these changes are believed to lie well within the range of acceptability.

[redacted]

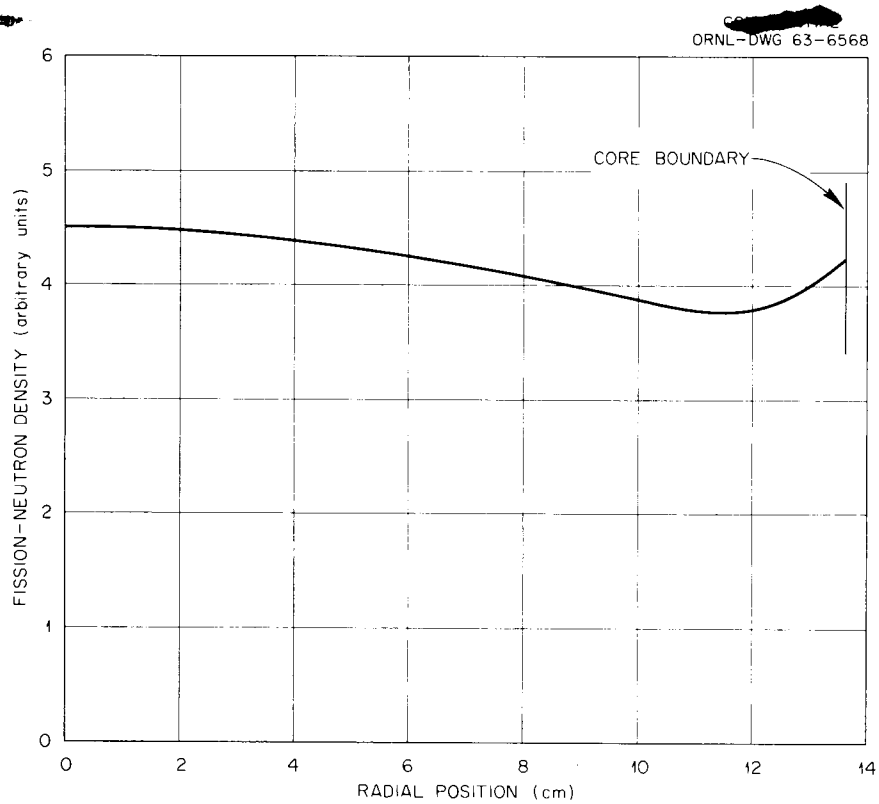

Fig. 2.10. Radial Power Distribution in Midplane of Modified Reference Reactor.

Pending further study of the control mechanisms, it appears that the rotating drum device has the advantage of producing no alteration in the geometric outline of the reactor. It represents a minimum volume configuration both in terms of the total space required for the reactor and control device and in terms of the size of the shield required for shadowing a given size of payload. The movable plug device lacks these advantages, although it has the substantial advantages of being mechanically simpler and less susceptible to temperature distortions.

3. DEVELOPMENT TESTS

A. P. Fraas R. E. MacPherson
A. G. Grindell H. W. Savage

A new test rig for investigating the cavitation characteristics of jet pumps operating with water was built and tested, and useful data were obtained. Tests of the liquid-vapor separator in the air-water test rigs continued. A vapor-separator and expansion-tank configuration for the 91-rod potassium boiler was improved to the point where the quality of the mixture leaving the vapor separator at design conditions is better than 99.9%. Single-rod heater tests with water indicated that a simple sleeve of solid metal fitting closely around the Firerod gave as effective a set of nucleation sites as any of the porous or perforated-metal devices tested. Similar results were obtained from tests in boiling potassium.

Endurance tests of the Firerods in the boiling-potassium reflux capsules indicated that reliable rod operation for 2000 hr can be obtained with nucleation sites at a power of 3 kw per rod and 1540°F. Tests were made with the seven-rod boiler water system using a 5/8-in. instead of a 9/16-in. centerline spacing for the Firerod heaters. Satisfactory control of the system was obtained. Some burnout data were taken with the 91-rod boiling-water system prior to damage of several rod heaters during the last few days of the Phase I tests. The construction portion of the Phase II program is essentially completed.

Jet-Pump Cavitation Tests

D. Canfield A. P. Fraas
M. E. LaVerne

The need for good cavitation performance data for jet pumps was pointed out in the previous report, and the basis for the design of a new rig that would yield this information was outlined. The detailed design has now been completed; the test rig has been built; and preliminary tests with water have been carried out. A schematic diagram of the flow circuit is shown in Fig. 3.1, and a detailed section through the test chamber, which indicates the methods for measuring the cavitation-suppression head

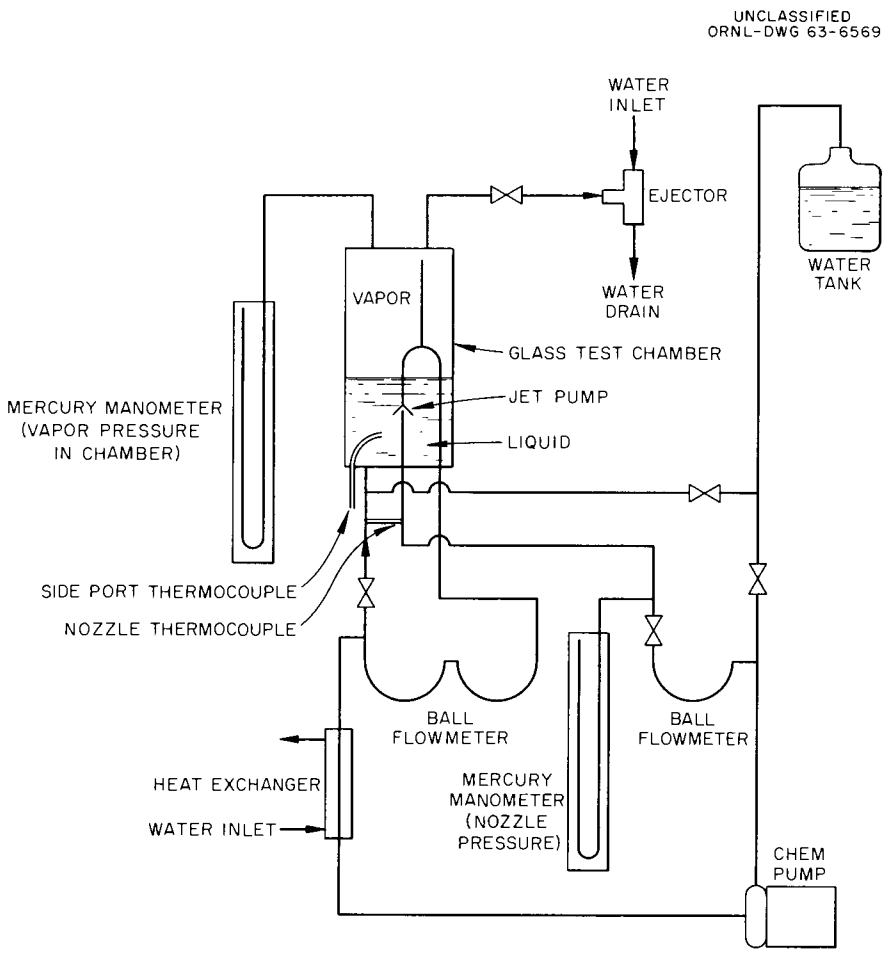

Fig. 3.1. Schematic Diagram of the Jet-Pump Cavitation-Performance Test Rig.

and the jet-pump delivery pressure, is shown in Fig. 3.2. Since the entire water bath in the test chamber is at a uniform temperature (about 100°F), with the free surface at the boiling point, the cavitation-suppression head is simply the vertical distance from the inlet to the jet pump up to the free-liquid surface in the test chamber. A similarly simple and direct measurement of the pump discharge pressure is obtained by taking the difference in elevation between the liquid level of the bath and the liquid level in the single-leg manometer in the pump discharge. Both pressure heads were measured in inches of water, and both provide simple, accurate, and unequivocal measures of the head in question, provided the bath in the test chamber is maintained at the boiling point. That this was in fact the case was determined by observing the evolution

UNCLASSIFIED
ORNL-DWG 63-6570

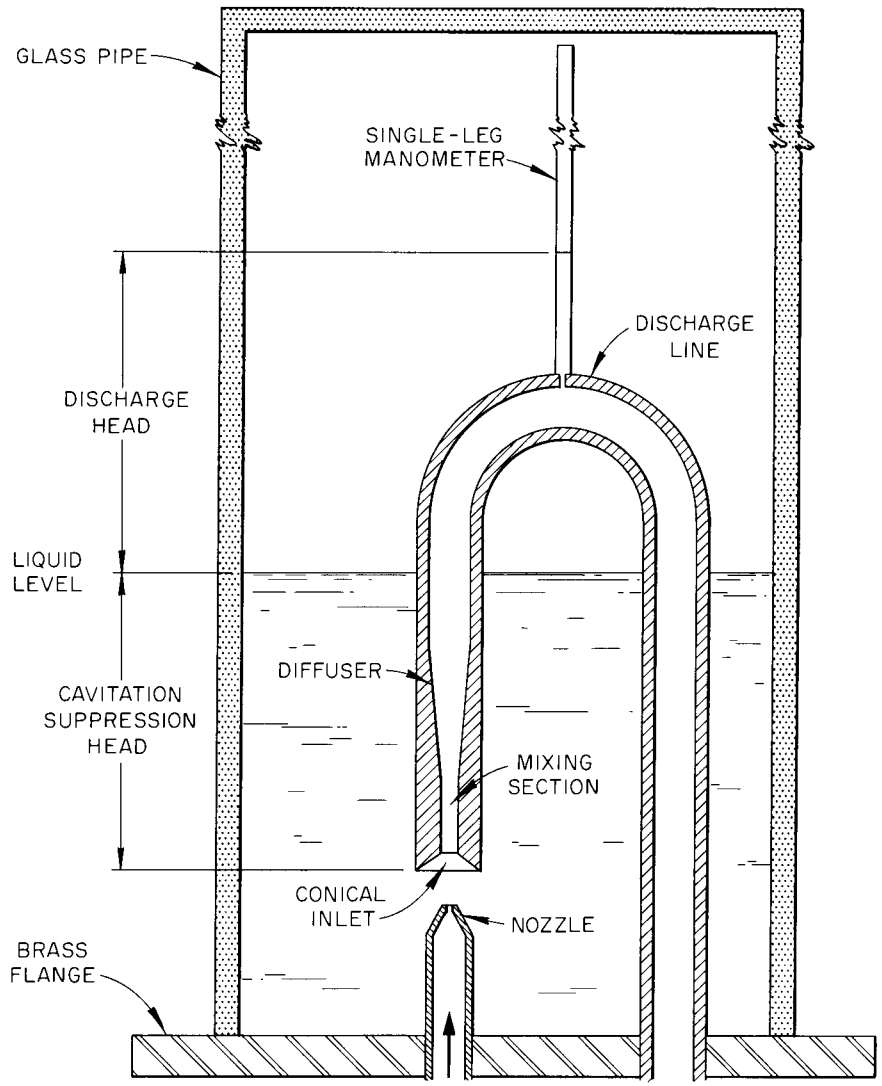

Fig. 3.2. Section Through Test Chamber Showing the Method Used for Measuring the Cavitation-Suppression Head and the Discharge Head.

of bubbles from nucleation sites just below the free-liquid surface. It is hoped that it will be possible to run tests with the bath in the test chamber so free of nucleation sites that superheating of the liquid can be obtained, but this has not been possible in the tests made to date.

The system flows were measured with an unusual device, a ball flowmeter.[1] This type of unit was chosen because it made possible a high

[1]H. L. Schulman and K. A. Van Wormer, "Flow Measurement with Ball Flowmeter," AICHE Journal, September 1958.

degree of system leaktightness with a low pressure drop in the flowmeter and no inverted traps in the system. Some difficulty was experienced in arriving at the proper proportions with the available ball sizes and materials, but, after several attempts, suitable flowmeter proportions were found. Two ball flowmeters were used in series to measure the total discharge flow, with one flowmeter intended for the low-flow range and the other for the high-flow range. Two balls of different size were used in the same 180° bend to cover the desired flow range for the jet driving stream.

One of the problems encountered in trying out ball flowmeters was excessive turbulence and irregular ball jumping when the radius of the bend was less than about six times the tube internal diameter. This was corrected by using larger bend radii in the tubes.

Dimensional data on the jet pumps tested are presented in Fig. 3.3. Two pump barrels were employed which differed in the radius between the

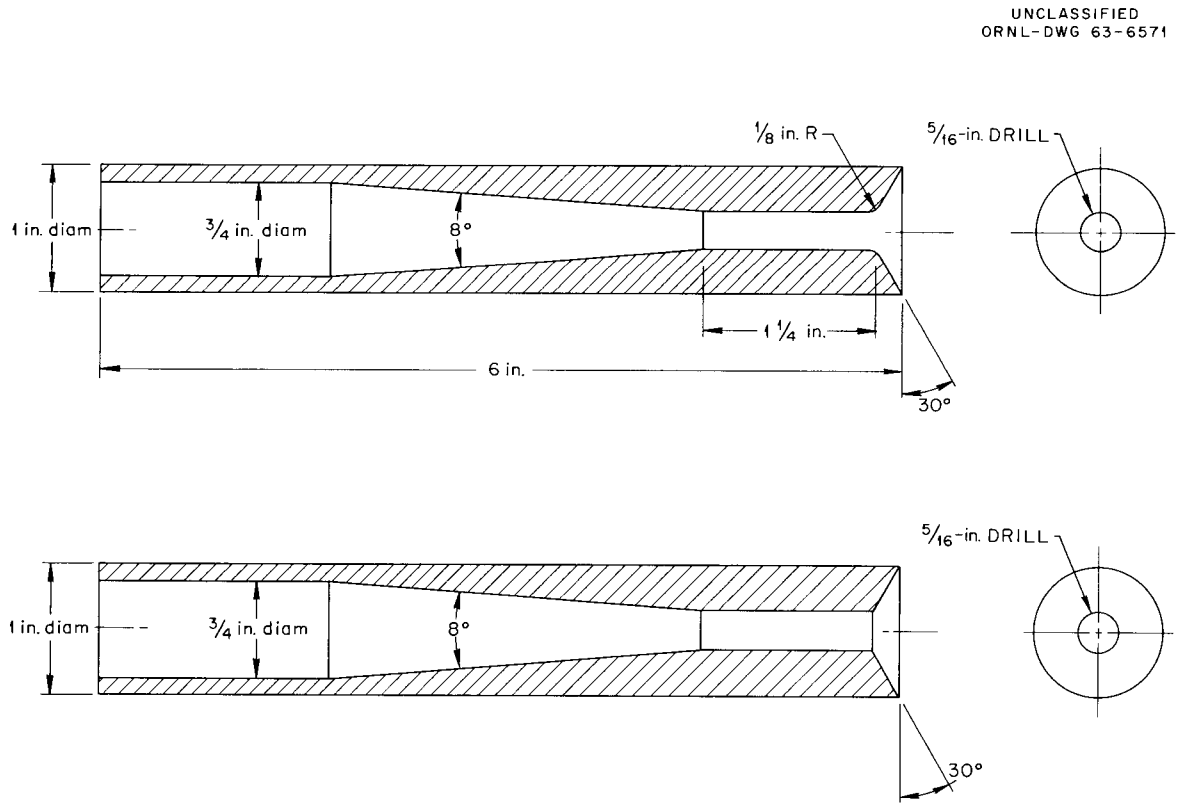

Fig. 3.3. Sections Through the Two Plexiglas Jet Pumps Tested.

conical inlet and the cylindrical mixing section, i.e., the first pump had a sharp corner at this point, while the second had a 1/8-in. radius. The pumps were made of Lucite to permit machining to close tolerances. Two additional pumps (made of glass) were procured, but they have not yet been tested. These will be used to investigate the possible effects of the differences in the wetting forces between water and the glass and Lucite surfaces; the well-cleaned glass wets well, while the Lucite, even when clean, is poorly wetted by water.

One of the principal objectives of operation of the test rig was direct observation of the vapor-bubble pattern that develops during cavitation. Two distinct types of pattern were found. The first took the form of a long, thin cone of very fine bubbles in the boundary between the free jet and the aspirated stream. This extended downstream from some point between the tip of the jet nozzle and the middle of the mixing section of the jet pump with the rounded inlet. The other type of cavitation was experienced with jet pumps in which there was a sharp corner at the juncture between the inlet cone and the cylindrical mixing section of the jet pump. In this case, the cavitation began with a higher cavitation suppression head and was evidenced by the formation of an annular film of very fine bubbles extending downstream from the sharp corner at the inlet to the mixing section. In either case, as the level of the boiling liquid in the chamber was lowered, a short section of the film of bubbles (from 1/2 to 1 in. long) appeared intermittently. When one end of a steel rod was held firmly against the glass wall of the test chamber while the other was held against the observer's ear, the appearance and disappearance of this vapor film was observed to accompany the appearance and disappearance of a slight rattling noise similar to that experienced with cavitation in centrifugal pumps and that accompanying "smooth" boiling in the single-rod boiling capsule experiments.

Further reductions in the liquid level in the test chamber maintained the vapor film continuously, with its length extending progressively farther downstream. The length of the vapor bubble region increased with further reductions in the cavitation suppression head until, under very severe cavitation, complete collapse of the output flow occurred and bubbles came up around the outside of the jet pump barrel.

Since cavitation tends to occur in high-velocity regions where the local static pressure drops below the vapor pressure of the liquid, the cavitation characteristics of jet pumps should depend on parameters similar to those that have been found to give good correlation for centrifugal pumps. Also, since the maximum velocity in the jet pump is that in the jet, and since this depends on the jet pressure drop, it appears that one of the best measures of the tendency toward cavitation is the ratio between the cavitation-suppression head and the jet pressure drop, or driving head. Thus, it was decided to investigate the jet-pump cavitation performance by obtaining experimental data in which the cavitation-suppression head was progressively reduced while holding the restrictions in the system constant. Figure 3.4 shows a set of curves of this sort. The parameter ϕ is commonly used as a measure of the pump flow performance; it is simply the ratio of the sidestream flow to the jet flow. Similarly, the parameter N is commonly used as a measure of the pump pressure rise; this is simply the ratio of the pump pressure rise to the jet driving head. It is to be noted that as the cavitation-suppression head was reduced, there was no change in either N or ϕ until the parameter H_{sv}/H_j was reduced to 0.04. The three sets of data presented in Fig. 3.4 are for three different jet driving-stream pressure drops. All three curves define much the same curve of ϕ vs H_{sv}/H_j, but there is a pronounced spread in the three sets of data plotted for N as a function of H_{sv}/H_j. The reasons for this are not apparent. However, in the first set of data taken (not included here), a disordered scattering of the data for N was found that led to the suspicion that air bubbles had formed in the discharge pipe from the jet pump. The data for the jet-pump pressure rise were then plotted against the pump discharge flow rate on log-log coordinates and the points were found to scatter badly. A similar plot for a second series of test runs was made and is shown in Fig. 3.5. The points in Fig. 3.5 fall reasonably close to a mean straight line, as they should, since the pressure drop from the discharge end of the jet pump through the flowmetering system and back into the test chamber should vary simply as the square of the flow through this portion of the circuit. The data of Fig. 3.5 were then used to prepare Fig. 3.4.

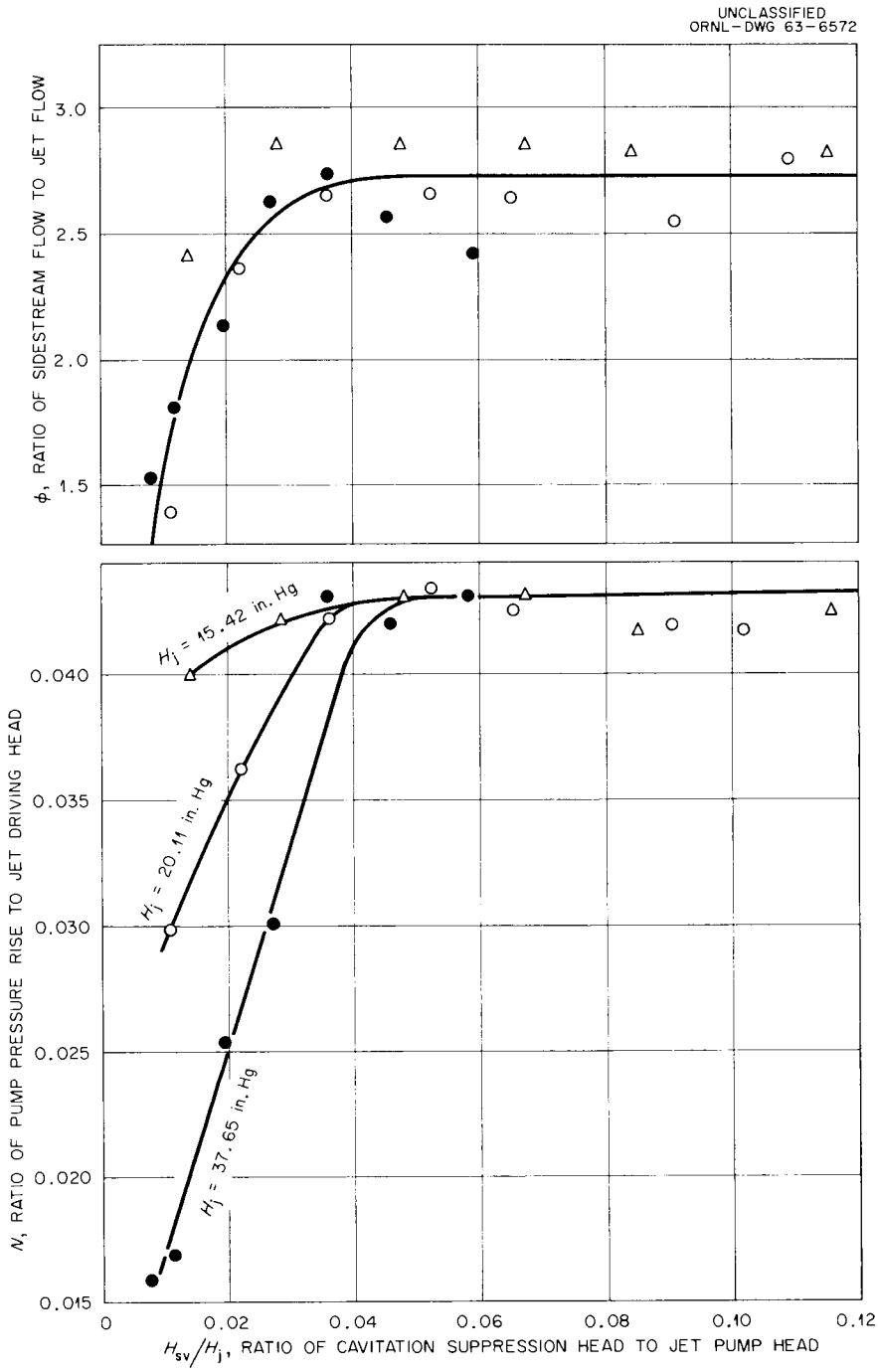

Fig. 3.4. Effects of Cavitation Suppression Head on the Head and Flow Parameters for the Jet Pump with a 1/8-in. Radius at the Inlet.

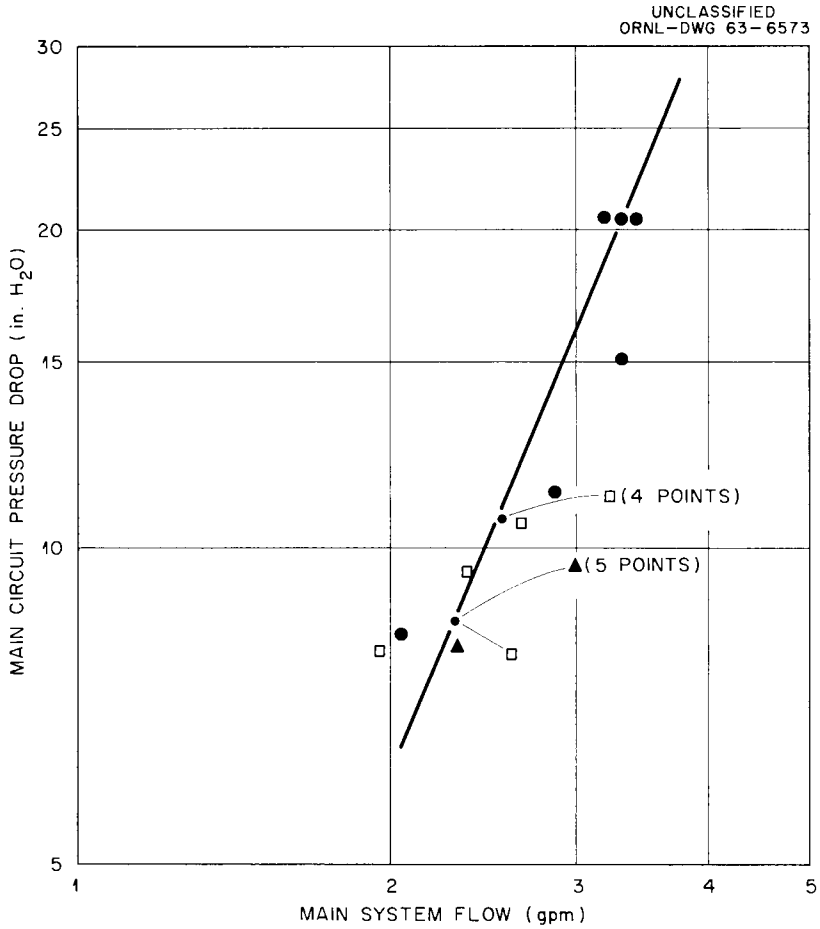

Fig. 3.5. Discharge Flow vs Pressure Drop in Jet Pump.

Further tests are planned with other jet pump proportions to determine to what extent the coordinates of Fig. 3.4 provide an adequate basis for correlating data. In addition, an attempt will be made to fill the system with extremely pure air-free water so that substantial amounts of liquid superheat can be obtained. Tests will then be made with this very pure water to determine whether it will reduce the cavitation-suppression head requirements.

Vapor-Separator Tests

J. Foster J. K. Jones

Tests continued on the evaluation of vapor-separator assemblies designed to remove liquid entrained in the vapor stream from the boiler.

Two separators [redacted] the type shown in Fig. 3.6 were built and tested. The most significant change in the design of these separators was the addition of the deflector ring at the trap entrance. Tests demonstrated that for proper trap entrance slot widths between the deflector ring and the trap entrance lip, separation performance was much improved over that realized with former arrangements. A typical set of curves is shown in Fig. 3.7.

The two test separators were made using Lucite, and tests were conducted with air-water mixtures. Since the 91-rod boiling-water test

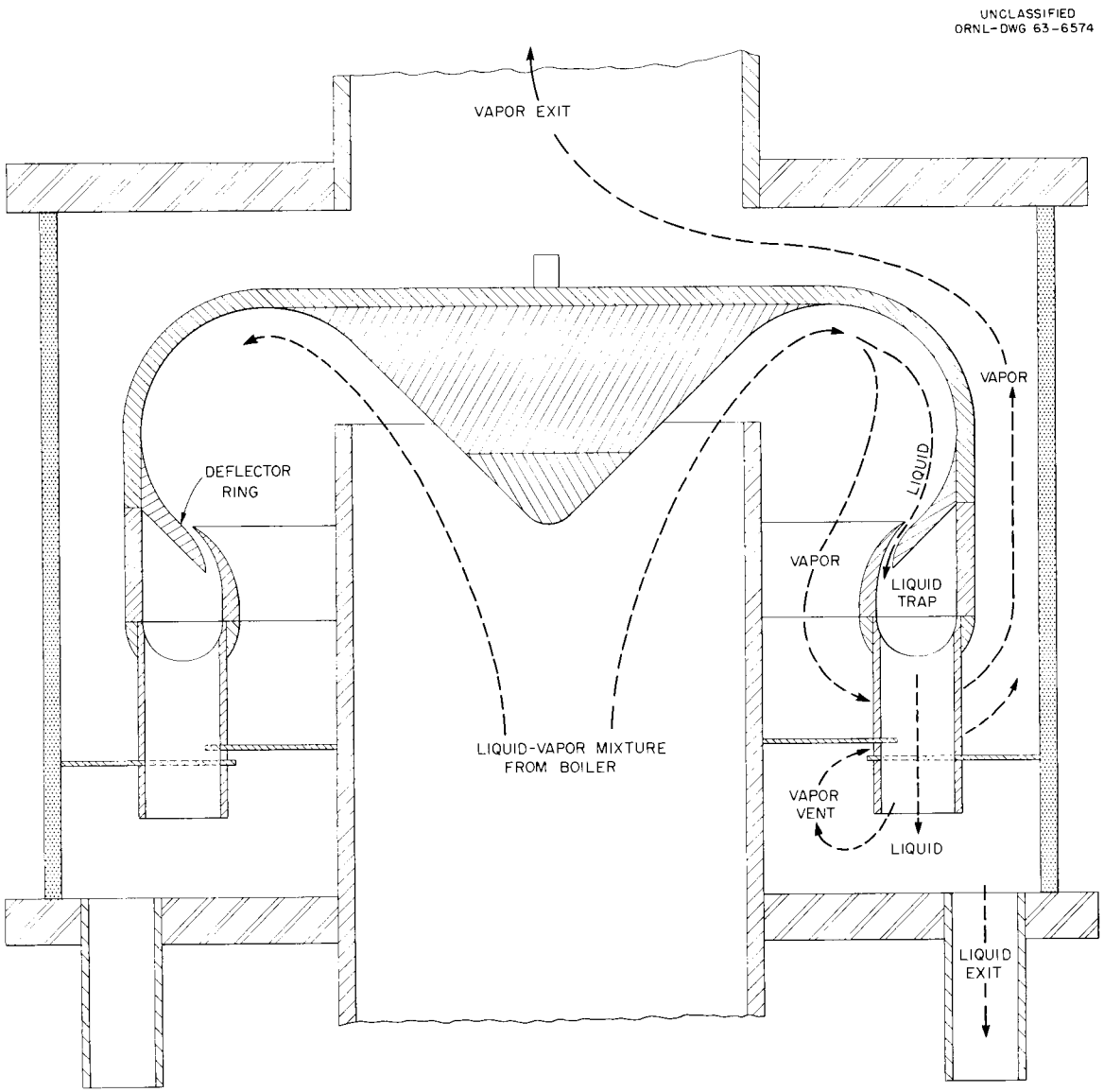

Fig. 3.6. Plastic Vapor-Separator Test Assembly.

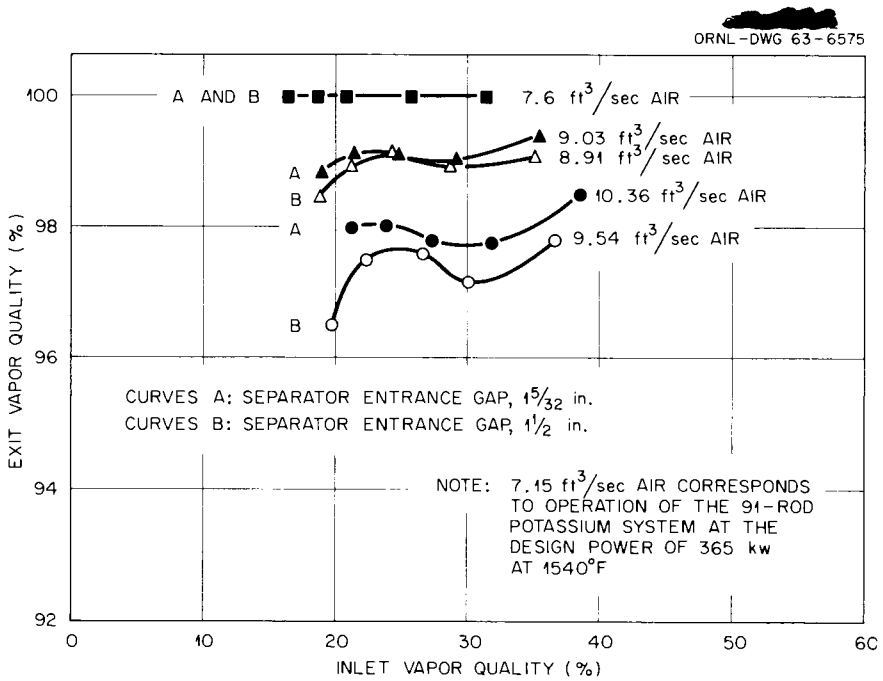

Fig. 3.7. Performance of Plastic Prototype for 91-Rod Potassium System Vapor Separator.

system, presently being refitted for Phase II operation with the tapered tube condenser and a turbine-driven pump, runs at temperatures too high for use of the Lucite vapor separators, a spare, glass vapor-separator assembly for the 91-rod boiling-water system was cut in half in the horizontal plane and fitted with an aluminum deflector ring, as shown in Fig. 3.8. Air-water tests were then carried out with a number of ring widths and ring positions. Although this adaptation of the spare, glass vapor-separator assembly did not perform quite as well as the plastic unit of the revised design, performance improvement was substantial, and the modified glass assembly will be used for the Phase II operation of the 91-rod boiling-water test system. The performance of the glass separator is indicated in Fig. 3.9. This assembly was delivered for installation in the 91-rod boiling-water test system for Phase II operation.

Further tests are being conducted on the air-water test stand using the plastic separator assembly shown in Fig. 3.6. These tests will include the determination of the effects of dimensional perturbations, means for inducing swirl in the expansion tank to stabilize the free-liquid

[redacted]

UNCLASSIFIED
ORNL-DWG 63-6576

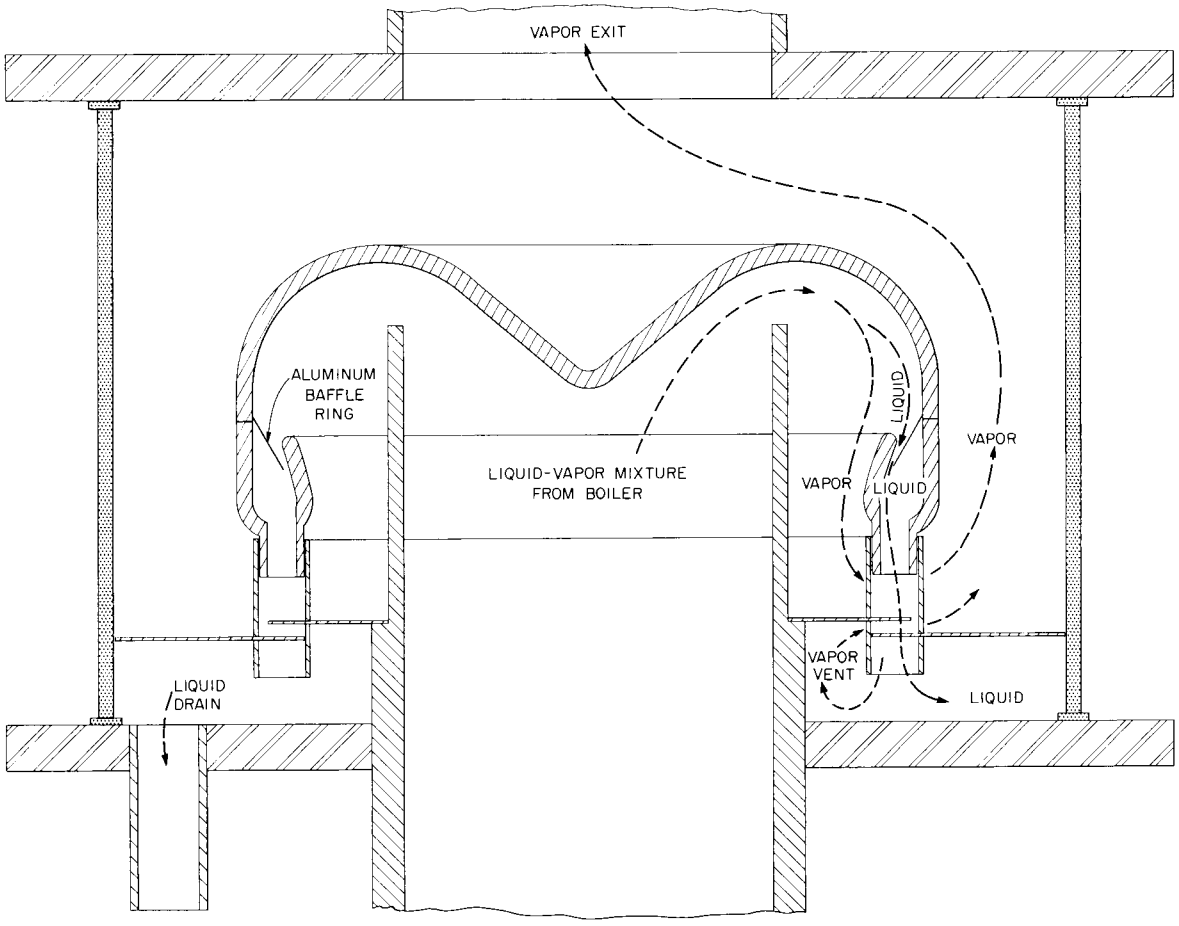

Fig. 3.8. Glass Vapor Separator for 91-Rod Boiling-Water Test System.

surface under 0-g conditions, and the effects of modifications to the shape of the top of the boiler barrel (e.g., hexagon vs round, etc.).

Single-Rod Capsule Tests with Water

J. K. T. Jung

Experiments with several different types of nucleation site were performed in the single-rod glass mockup of the boiling-potassium system. The boiling was observed visually to determine how each type of nucleation site functioned as a nucleator to promote boiling stability. In each case, a 1/2-in.-long stainless steel sleeve was fabricated and

[redacted]
ORNL-DWG 63-6577

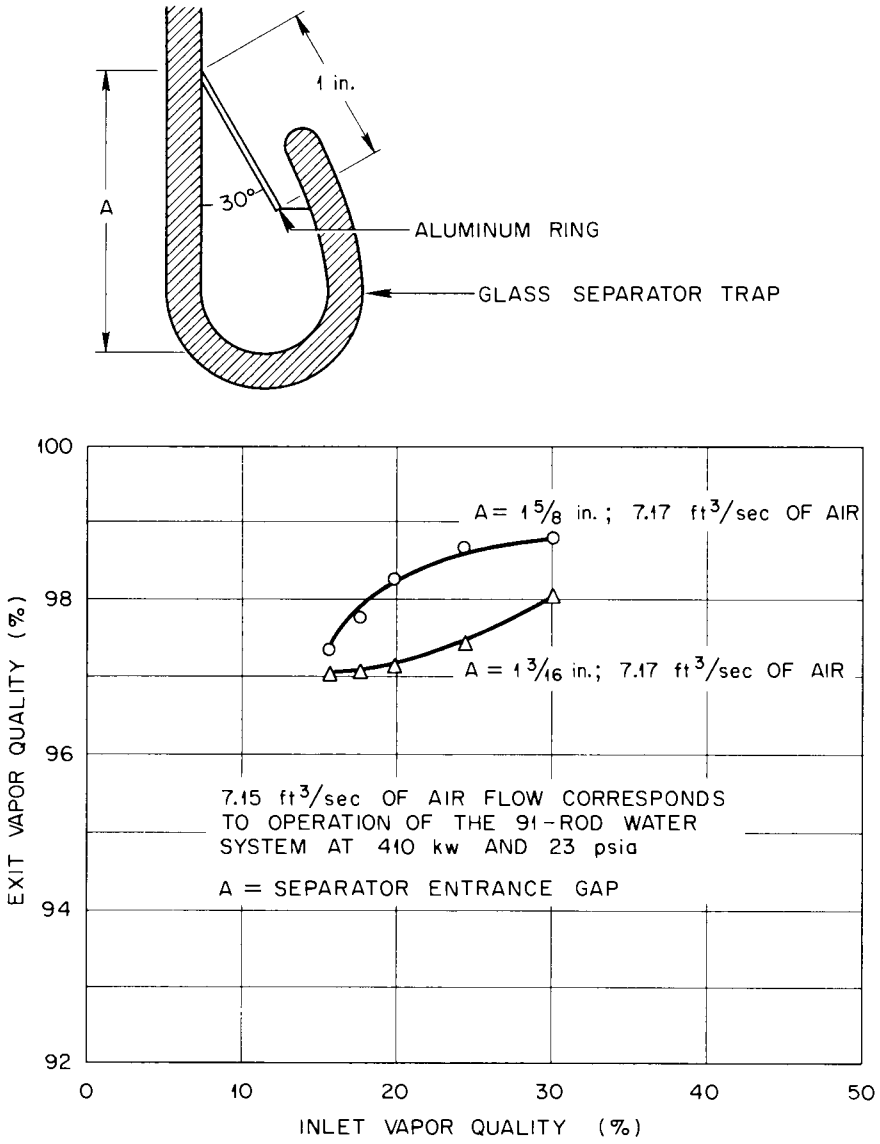

Fig. 3.9. Performance of Glass Vapor Separator with Aluminum Deflector Ring.

attached tightly to the surface of the heater rod. The samples tested are shown in Fig. 3.10. Specimen A is a 28%-void, sintered, stainless steel-powder sleeve made of a pellet similar to item B. Specimen C is a 1/16-in.-wall type 304 stainless steel sheath, which was attached to the rod by carefully filling the outer portion of the slot with a weld bead in such a way that the collar was shrunk on the rod. A fairly large gap remained between the weld filler material and the rod surface. Specimen D

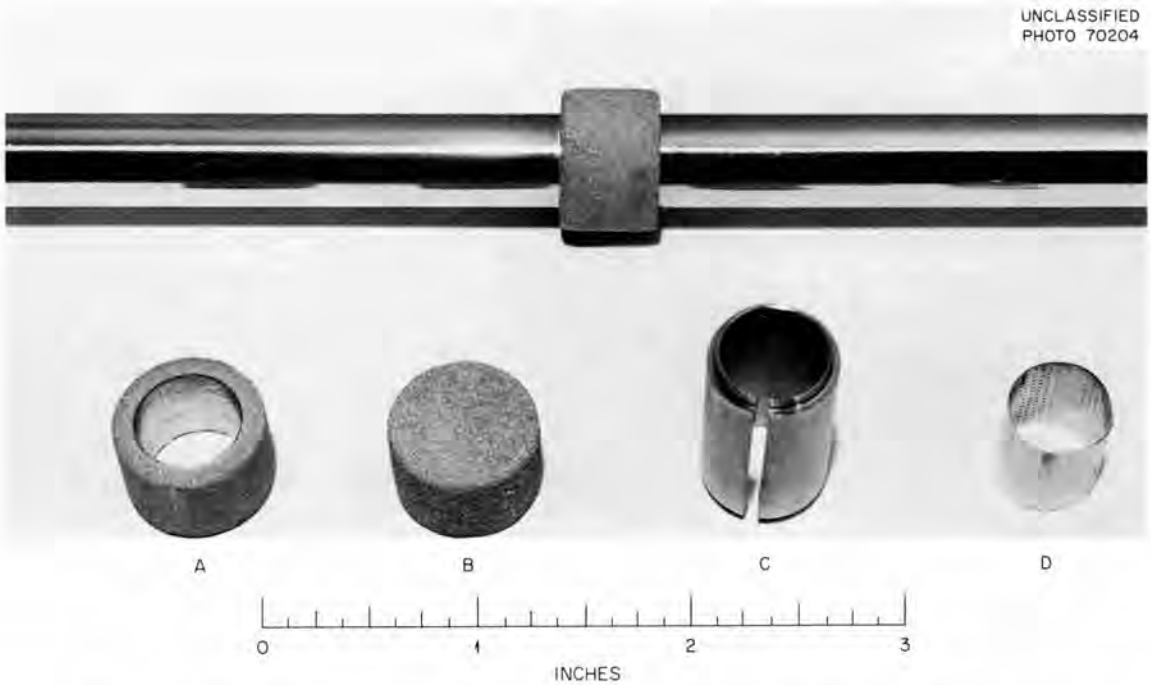

Fig. 3.10. Nucleation Site Specimens Used in Single-Rod Capsule Tests with Water.

is a 3/32-in.-wall cylinder perforated with 1-mil slits. All test pieces were attached to the rod in the lower 1 in. of the heated length, that is, approximately 10 in. from the top of the heater rod.

Tests were run by varying both the heat flux and the boiling temperature of filtered distilled water. In no case was liquid superheat observed once the sites became activated. Superheat (10 to 15°F) could be achieved only at very low pressures and power inputs (i.e., about 1 psia and 200 w). When the temperature and pressure were raised to a level of 130 to 135°F and 3 psia with a heat flux of approximately 20,000 Btu/ft^2·hr, steady stable boiling prevailed. A further increase or decrease in the heat flux increased the turbulence induced by boiling or decreased the nucleation site activity, respectively. High heat fluxes (50,000 Btu/ft^2·hr) at a pressure of 3 psia resulted in burnout conditions. One interesting observation was that irrespective of which test specimen was used, the best nucleation site was the small gap between the rod surface and inner wall of the collar. This site was usually the first to become active and the

last to become inactive. The gap existing between the weld filler and rod surface (specimen B) was not a good nucleation site.

With respect to each specimen, and under comparable conditions, the best set of nucleation sites appeared to be the slits in the perforated collar, and the next best nucleation site was provided by the plain stainless steel collar. No active sites were observed on the surface of the sintered collar.

A more effective set of nucleation sites might be provided by a collar whose perforations were as large as 1/8 to 3/16 in. A test is planned to determine whether this type of collar will permit operation at low pressures to higher fluxes without burnout. High-speed movies were taken of operation with each type of nucleation site, and frames from these will be incorporated in the next report.

Single-Rod Capsule Tests with Potassium

L. W. Evers N. H. Briggs
A. G. Grindell

Tests were continued to find satisfactory nucleation sites for promoting smooth boiling with potassium, to provide satisfactory protective devices against damage to rod sheaths during test operation, and to define the limits of potassium temperature and rod power for the electrically heated rods to be used in the 7-rod and 91-rod boiling-potassium systems. A satisfactory solution to the nucleation site problems was found, and several endurance tests with rod heaters having various nucleation sites were started. An endurance test of 2500 hr with sheathed-type thermocouples was completed. Some experience was obtained with the operation of sheathed thermocouples located inside the rod heater and with measuring the ground current between rod heater element and sheath to provide an indication of incipient failure.

Nucleation Sites

Additional tests were run in the boiling-potassium reflux capsules to find satisfactory means for providing nucleation sites to promote reasonably smooth boiling in the 7-rod and 91-rod potassium boiling systems.

The results are summarized in Table 3.1. The sites considered most satisfactory consisted of five solid collars 1/4 in. long and 1/16 in. in radial thickness, spaced 1/16 in. apart, and mounted on the 1/2-in.-diam heater rod by shrink-welding. This process entails welding the outer edge of a slit in the ring to attach the collar firmly to the rod without risk of damage to the metal sheath.

Table 3.1. Results of Nucleation Site Tests in Boiling-Potassium Reflux Capsules with Single-Rod Heaters

Nucleation Sites	Test Results
Bare rod	Unstable boiling
Sintered-nickel spacers	Unstable boiling
Solid collar with shrink fit open and covered channel closed	Stable boiling up to 5 kw[a] with potassium temperatures ranging from 1300 to 1400°F
Sintered-nickel rings (1/8 in. thick, 1/8 in. long)	Stable boiling up to 5 kw[a] with potassium temperatures ranging from 1400 to 1550°F
Solid spacer with covered channels	Unstable
Solid collar with covered channels open and shrink fit closed	Stable boiling up to 5 kw[a] with potassium temperatures ranging from 1300 to 1400°F
Multicollars (5 collars, 1/16 in. thick, 1/4 in. long, spaced 1/16 in. apart)	Stable boiling up to 4.7 kw[a] with potassium temperatures ranging from 1050 to 1525°F
Sintered-nickel collars (1/8 in. thick, 1 in. long)	Stable boiling up to 4.2 kw[a] with potassium temperatures ranging from 1250 to 1500°F

[a]The maximum power used in the test.

Endurance Tests

Endurance tests were started with rods having multicollar nucleation sites and with one rod having sintered-nickel nucleation sites. The results of these tests are summarized in Table 3.2. Based on these tests the operating conditions for the seven-rod boiling-potassium system were tentatively selected as 3 kw per rod and 1540°F.

Table 3.2. Results of Endurance Tests of Single-Rod Heaters

Test System	Rod Power (kw)	Sheath Temperature (°F)	Nucleation Sites	Operating Time (hr)	Remarks	Starting Date
Boiling-potassium capsules	4.7	1525	Multicollars	120	Failed[a]	
	4.2	1500	Sintered-nickel collars	1900	Failed[b]	
	3.75	1475	Multicollars	2060	Continuing	6-24-63
	2.5	1400	Multicollars and internal thermo-couples	2180	Continuing	6-19-63
Air-cooled systems with bare rods	1.6	1820		2540	Continuing	
	1.6	1820		2540	Continuing	

[a]Failure was believed to be due to the breakdown of the MgO electrical insulation in the rod.

[b]Failure was due to an arc between the power leads just outside the rod.

Protective Devices for Rod Heaters

It is desirable to protect the rod heater sheaths in the boiling-potassium systems against damage caused by film boiling (burnout) or by breakdown of resistance of the electrical insulation in the rod. Tests were therefore made of sheathed thermocouples located inside the heater rod to measure the internal temperature as a function of the power input. The ground current between the electrical resistance wire and the sheath was also measured at several different power levels in the boiling-potassium reflux capsules. The results of these tests indicated the advisability of using both the ground-current measurements and the internal thermocouple signals to protect rod sheaths from damage during elevated temperature operation with potassium.

A life test of sheathed thermocouples for measuring the rod internal temperature was completed after 2500 hr operation in air with the test temperature maintained between 1940 and 1985°F. The individual thermocouples have a stainless steel sheath 0.031 in. in diameter and Chromel-P versus Alumel wires approximately 0.003 in. in diameter. The test results are listed in Table 3.3. The indicated temperature drifted downward relative to the actual temperature, with the bulk of the drift taking place in the first 1000 hr. The drift decreased until the temperature reading

Table 3.3. Drift of the Indicated Temperature for 0.031-in.-OD Sheathed Chromel-P vs Alumel Thermocouples Tested at 1950°F

Thermocouple Number	Error in °F at			
	Start[a]	1000 hr	2000 hr	2500 hr
14532[b]	-20	-137	-206	-215[c]
14535[b]	-14	-104	-138	-153
14521[d]	-16	-98	-114	-115
14533[d]	-17	-98	-123	-126
14562[d]	-22	-94	-98	-91

[a]Initial offset due to prior operation between 1250 and 1850°F.

[b]Normally handled thermocouple.

[c]Thermocouple drifted to -240°F between 2000 and 2500 hr and then recovered.

[d]Specially processed thermocouple.

became almost asymptotic after 2000 hr. Further testing of thermocouple longevity is planned at 2100°F. The three 0.063-in.-OD stainless steel sheath thermocouples, described previously,[2] exhibited the following average temperature drift: at start, -8°F; at 1000 hr, 45°F; at 2000 hr, -63°F; and at 2500 hr, -67°F. The drift values for the three thermocouples were within ±3°F of the above values. The temperature difference from the sheath surface to the interior of the heater rod measured in a boiling-potassium reflux capsule at various rod powers and 1400°F is shown in Fig. 3.11, which indicates an internal temperature of approximately 2100°F at 3 kw per rod and 1540°F.

The measurements of the ground current were not started until the capsules had been operating for as much as six weeks. The ground currents are presented in Fig. 3.12 as a function of operating time at three different test conditions for heater rods in boiling-potassium reflux

[2]L. W. Evers, N. H. Briggs, and C. H. Gabbard, Single-Firerod Capsule Tests with Potassium, pp. 57–65, "Space Power Program Semiann. Prog. Rep. June 30, 1963," USAEC Report ORNL-3489, Oak Ridge National Laboratory.

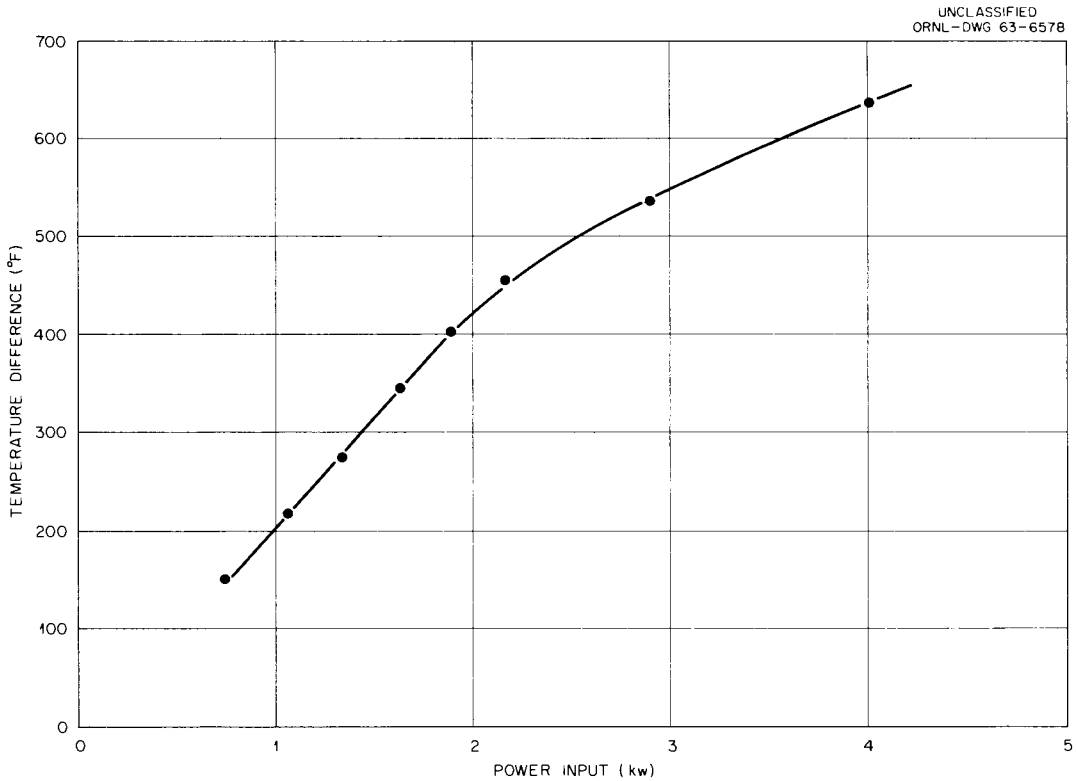

Fig. 3.11. Temperature Difference Between Potassium Pool and Internal Rod Thermocouple as a Function of Power at 1400°F.

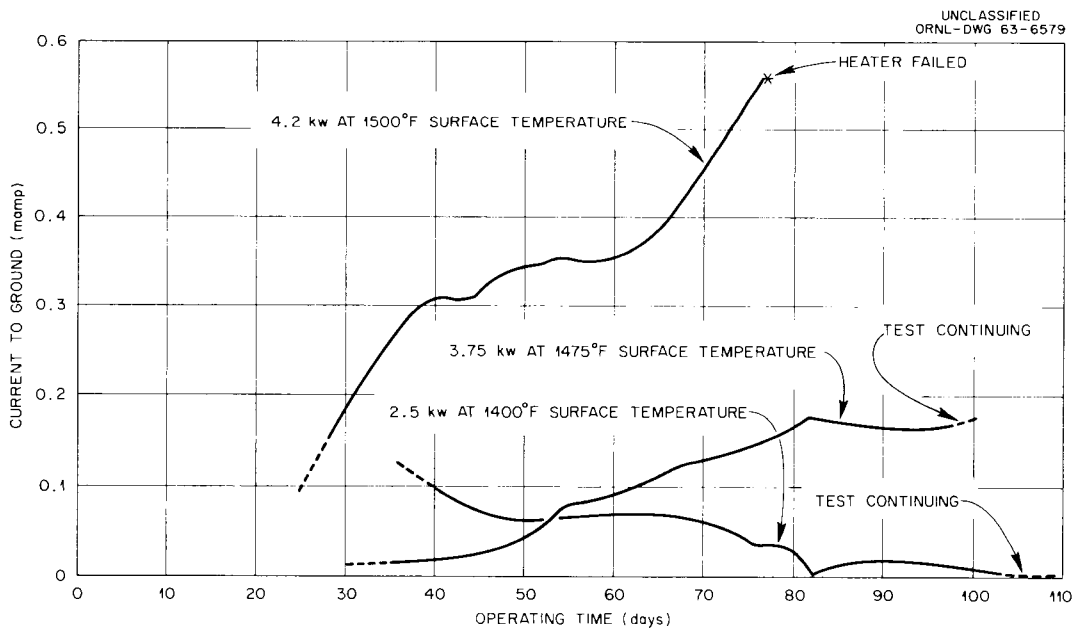

Fig. 3.12. Ground Current Variation with Time for Single-Rod Heaters in Boiling-Potassium Reflux Capsules.

capsules. An increase in the ground current preceded the one failure that occurred.

Seven-Rod Boiler System Tests with Water

H. C. Young A. G. Grindell

Tests were made with the seven-rod boiling-water system modified to conform closely to the configuration of the seven-rod boiling-potassium system, and stable operation was obtained. Several attempts were made to run an unattended 100-hr endurance test with the system. Although minor difficulties, such as leaks and electrical system problems, interfered each time, continuous stable operation for several periods of about 40 hr indicated the feasibility of controlling the distribution of system inventory by cavitation in the free-turbine feed pump.

The modifications made to the system included the installation of a boiler matrix in which the spacing between rods was increased to 1/8 in. (from 9/16 in.), reduction in the passage length between the heated length of the rod and the vapor, installation of a vapor separator having an increased expansion-tank capacity, removal of the capillary screens from the condenser and all valves and flowmeters from the boiler feed line, and installation of the water prototype (Mark II) of the free-turbine-driven feed pump to be used in the seven-rod boiling potassium test. The Mark II free-turbine-driven feed pump provides a greater capacity than the Mark I-a unit.

Tests were run with and without the condenser hot well, the radiator scavenging jet pump, and a U-tube manometer used as a vapor trap. The effects of these devices on system stability were observed. The tests indicated that with the prevailing air inleakage rate, continuous aspiration of noncondensables from the condenser hot well is essential. Although the leaktightness of the glass, metal, and plastic system was considerably improved over that for previous tests, the inleakage of air was sufficient, unless the aspirator was used, to cause the feed pump to lose prime and stop the flow of feed water to the boiler. This led, of course, to a sharp increase in the rod temperatures, and the thermocouples in the rods automatically shut off the power.

The feed-pump discharge pressure was recorded during a 3-hr test in which the boiler power was changed slowly from 25% to full power and back. Above about 50% power the pressure fluctuations had a range of about 5 psi. The fluctuations increased at lower power levels, being about 10 psi at 30% power. The effects of boiler power on the average value of the pump discharge pressure for the run, that is, the pressure required to drive the system, and on the pump discharge pressure that would be available if the pump were not cavitating are shown in Fig. 3.13. The difference between the available and required pump discharge pressures represents the mismatch between the characteristics of the system and those of the turbine-driven pump unit. The reduction in pump performance caused by cavitation accommodates this mismatch. For the larger systems the characteristics of

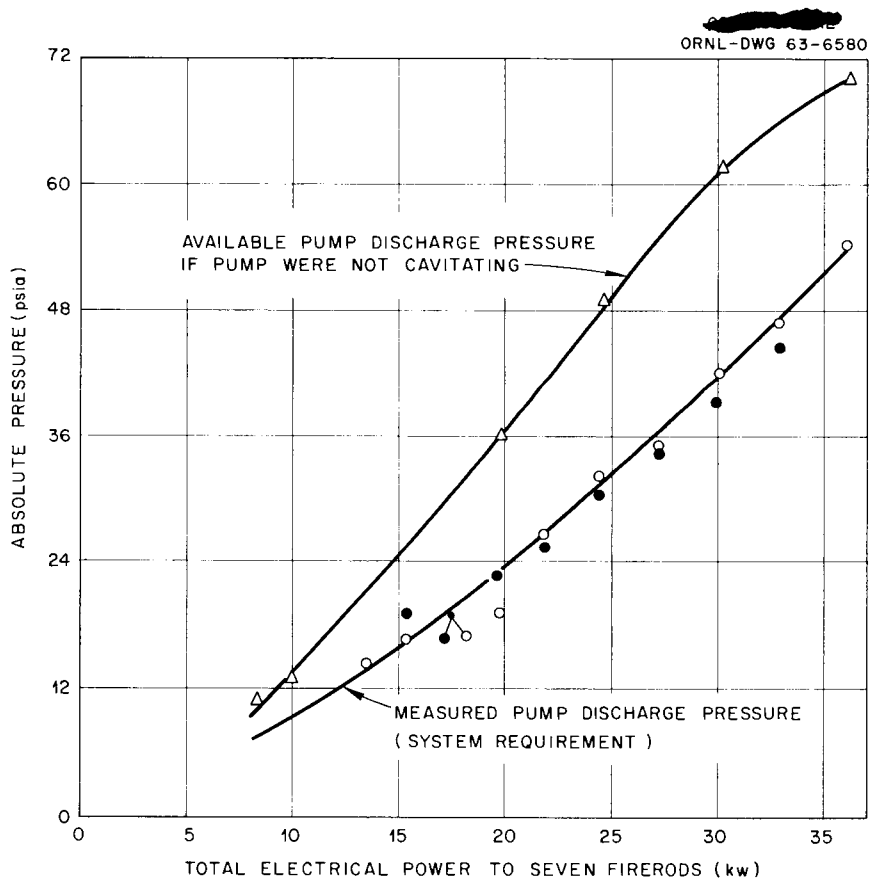

Fig. 3.13. Total Rod Heater Power in Seven-Rod Boiling-Water Test Versus Measured (Cavitating) Feed Pump Discharge Pressure and Pressure Available if Pump Were Not Cavitating.

the turbine-driven pump will be modified so that they will more nearly match the system requirements. It is to be noted that some mismatch is essential; to assure scavenging of the radiator, the pump output should always exceed the system requirements, and hence either the centrifugal feed pump, or the jet pump, or both, must cavitate, as mentioned previously.[3]

A total of 250 hr of operation was accumulated during the attempts to operate the system continuously for 100 hr unattended; the longest unattended run was 44 hr. This run was achieved after making improvements to the boiler scram system and providing boiler-water makeup to replace water lost through the system aspirator. During a test the temperatures of the rod heater sheaths behaved in an increasingly erratic manner until boiler power was scrammed automatically; after flushing the boiler and refilling with clean water having several parts per million of sodium carbonate, the system would again operate satisfactorily for another 40-hr period. It is believed that this behavior was caused by an increase in impurities in the water with time.

A new boiler with a 1/8-in.-rod spacing was then installed. The heater rods were fitted with both internal thermocouples and external nucleation sites indentical to those to be used in the seven-rod boiling potassium system. No important changes in system stability and control were observed. The system is being used to develop detailed startup procedures and to train operators for the seven-rod boiling-potassium system. It is also planned to investigate the effects of boiler exit vapor quality on the boiler power at burnout.

Development of Seven-Rod Boiler System for Tests with Potassium

L. W. Evers R. F. Hyland
H. C. Young A. G. Grindell

The mechanical assembly of the test apparatus was essentially completed, and the instrumentation and controls are being installed. The

[3]H. C. Young and A. G. Grindell, Seven-Rod Boiler System Tests with Water, pp. 65-70 "Space Power Program Semiann. Prog. Rep. June 30, 1963," USAEC Report ORNL-3489, Oak Ridge National Laboratory.

liquid-level indicator for the vapor-separator and expansion-tank region and the speed counter for the turbine shaft were tested and found to be satisfactory. The test loop description and startup procedures are being written. The schedule calls for the installation work to be completed and testing to begin early in November.

System Construction

The stainless steel components for the system were assembled, and the system was leak tested and found to be leaktight. An overall view of the system under construction is shown in Fig. 3.14. A large box with double walls surrounds the radiator so that the radiator can be operated at the desired temperature at any heat load over a fairly wide range. The cooling air does not pass directly over the tubes, but, rather, it passes between the double walls of the box surrounding the radiator so that heat is rejected by thermal radiation from the radiator to the inner walls of the box, and these are cooled by the air blast. Calrod heaters within the inner box permit preheating to as much as 1000°F for system cleaning and startup operations or for the investigation of various startup procedures. A closeup view of the boiler and the major components in its immediate vicinity is shown in Fig. 3.15. The condensate manifold at the outlet of the radiator lies immediately behind the valve that simulates the turbine-generator unit.

The turbine-driven pump unit was designed so that the rotor and bearing support assembly can be removed by cutting a seal weld at the end of the turbine casing. The components used can be seen in Figs. 3.16, 3.17, and 3.18. The three pipes going into the bottom of the turbine casing shown in Fig. 3.18 each terminate in a nozzle so that three nozzles direct vapor into the perimeter of the turbine wheel.

Turbine-Driven Pump Development

The water prototype (Mark II) of the small turbine-driven pump unit to be used in the seven-rod boiling-potassium test rig was operated over 300 hr in the seven-rod boiling-water test rig. The unit was removed for inspection after several days operation, and the thrust bearing and journal bearing surfaces were in good condition. The observed leakage through

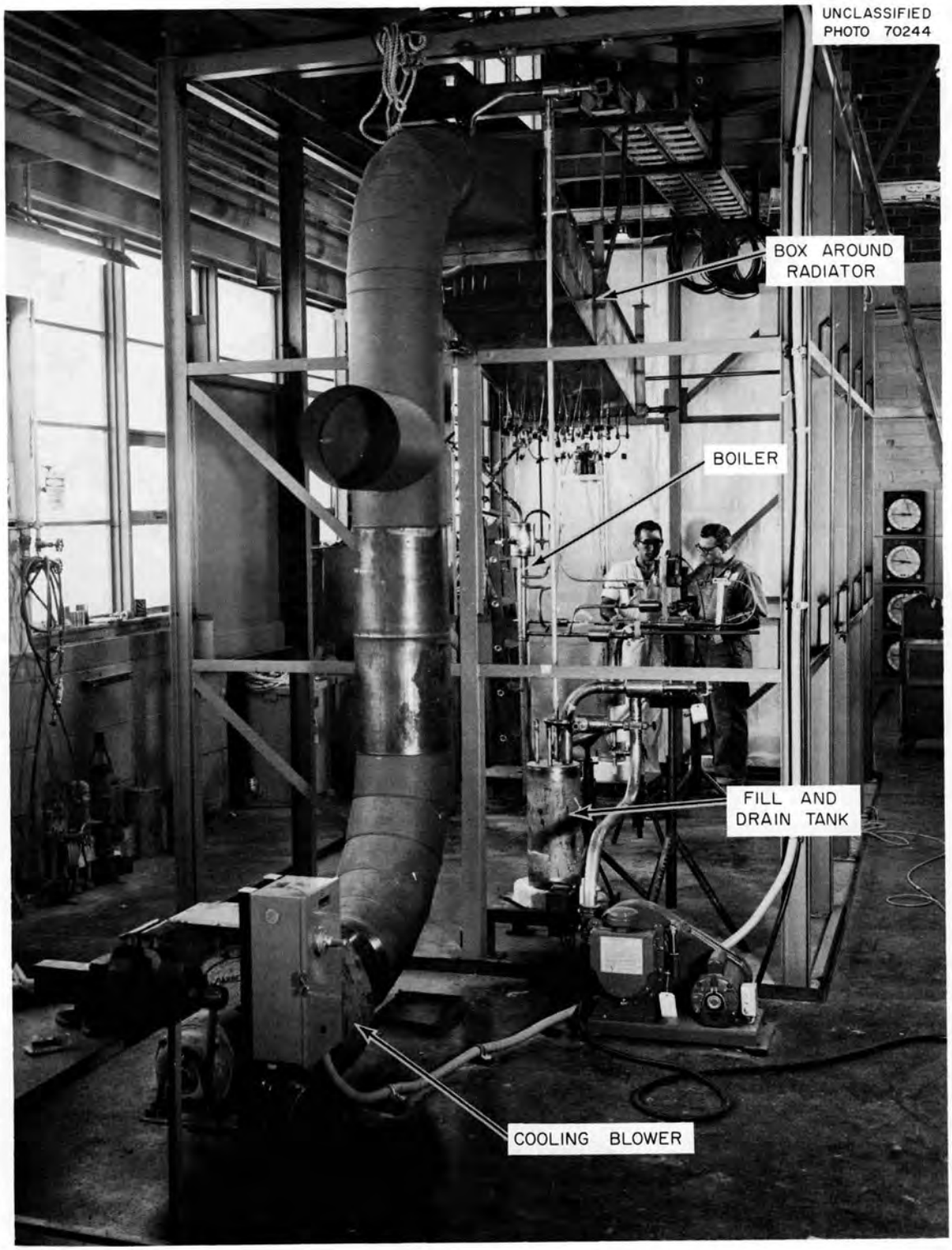

Fig. 3.14. Seven-Rod Boiling-Potassium System Under Construction.

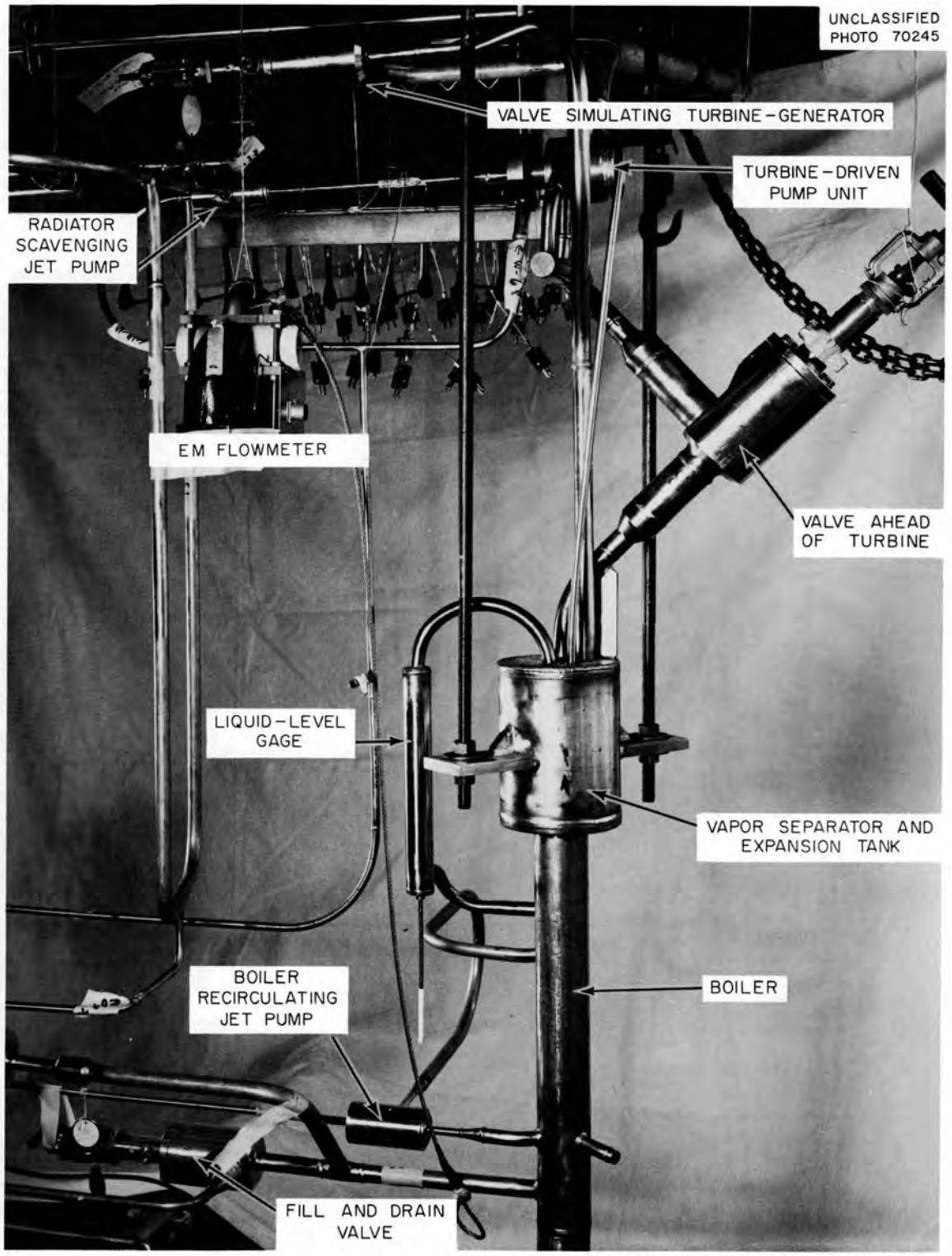

Fig. 3.15. Closeup View of the Components in the Vicinity of the Boiler in the Seven-Rod Boiling-Potassium System.

Fig. 3.16. Turbine-Driven Pump Rotor Assembly and Closure Cap Ready for Installation in the Casing.

the bearings to the turbine housing was not excessive. This indicates that earlier development problems[4] of excessive leakage from the bearing region to the turbine exhaust region and unbalanced thrust forces have been resolved.

Final machining of the turbine-driven pump for use with potassium was held up to evaluate a more efficient turbine wheel in the seven-rod boiling-water rig. The new wheel provided somewhat better matching of pump performance to system requirements but would have required larger thrust bearings and modification of the pump housing, which was already fabricated. It was decided therefore to use the less efficient design

[4]E. Storto, L. W. Evers, H. C. Young, and R. F. Hyland, Apparatus for Seven-Rod Boiler System for Tests with Potassium, pp. 70-77, "Space Power Program Semiann. Prog. Rep. June 30, 1963," USAEC Report ORNL-3489, Oak Ridge National Laboratory.

Fig. 3.17. Pump Impeller and Shaft, Bearing Support Assembly, Turbine Rotor, and Retaining Nut.

for which parts were already on hand. Two rotary assembly units were fabricated and a speed counter, described below, was added to the unit.

Instrumentation

A successful bench test of the high-temperature turbine-speed-measuring system was completed. The test fixture consisted of the shaft with two HIPERCO-35 segments and attached bearings, bearing sleeve, bearing holder, a simulated stainless steel turbine housing, and an air-driven stainless steel turbine wheel. Accurate speed measurements in the range 0 to 24,000 rpm were made. Current tests are aimed at reducing the effect of 60-cycle pickup, which is induced in the pickup coil by Calrod heaters on the turbine housing.

Material for making liquid-metal-level indicators of the swaged construction described previously[3] was procured and representative samples of each of the three sizes obtained were installed in a test vessel for calibration. A 3/16-in.-OD resistance element made from this material was installed in the vapor separator. Additional units will be installed in manometers later in the test program to obtain accurate measurements of the small pressure drops across the boiler and condenser.

Fig. 3.18. Turbine Casing Showing Internal Pad for Mounting the Bearing Support Assembly.

An automatic scram system is being installed to shut down the boiler and the cooling blower for the condenser and to reduce the amount of heat supplied by the pipe heaters. This system is activated by several signals, including high boiler pressure, turbine overspeed, high values of temperature or ground-current signals from the heater rods, and excessive temperatures indicated by selected thermocouples in the system.

Endurance Test Conditions

The endurance test experience with Firerods operated in potassium capsules discussed earlier in this report indicates that the endurance tests on the seven-rod boiler test rigs should be conducted with either the power or the temperature (or both) reduced below the design value. Since there is a strong incentive from the corrosion standpoint to run the test at the full design temperature, it seems best to limit the operating time at high power and temperature to that required to obtain data on the system performance. For the endurance tests the power would be reduced to about 70% of full power while holding the temperature at the design point. This can be done by changing the size of the critical pressure-drop orifice used to simulate the turbine-generator unit. Since this will reduce the boiler feed flow rate required by a small amount, it may also prove necessary to reduce the vapor flow through the free-turbine-driven pump unit. To accomplish this, valves have been provided at these locations to give operating flexibility. Neither of these valves will ordinarily be fully closed; both will operate as variable restrictors.

Tests of a 91-Rod Boiler System with Water

M. M. Yarosh
S. E. Bolt C. H. Gabbard
A. G. Grindell

Measurements taken during the Phase I test program indicate that burnout conditions are likely to occur when the vapor quality at the boiler exit drops below 36% at the design power of 360 kw at a boiler pressure of 17 psia. As the result of an error in operating procedure that made the rod thermocouple protection system only partly effective,

five of the heater rods were seriously damaged at a vapor quality of about 27% and a reduced boiler pressure of 13 psia (the design operating pressure is 22 psia). The boiler was repaired and an improved vapor separator was installed while the system was being modified to incorporate the free-turbine-driven pump unit, the tapered tube radiator, and the jet pumps for the Phase II test program.

Phase I Tests

A total of approximately 200 hr of test work at boiler powers up to 440 kw (5 kw per rod) was completed. The problem of the flow distribution within the vapor-separator region, discussed previously,[5] was solved by revising the separator so that the boiler recirculation jet pumps receive their suction flow from the expansion tank rather than from the collection trough of the vapor separator. This made the recirculation flows independent of flow asymmetries within the separator. The revised design is shown in Fig. 3.19.

During the operation of the system with the original vapor separator, it was necessary to drain the expansion-tank liquid to the condenser because there was a spillage of approximately 0.8 gpm from the separator trough. At a boiler power of approximately 375 kw the normal condensate flow plus the 0.8 gpm of separator overflow would overload the feed pump to the point where there was insufficient pump head to drive the required flow through the boiler jet-pump nozzles. Since the electric-motor-driven feed pump had excess flow capacity but a limited operating head, a jet-pump booster was installed in the feed-pump suction line to raise both the suction and discharge pressures of the feed pump about 25 psi. This modification permitted operation of the system to the design boiler power of 440 kw. It was found that cavitation was effective in reducing the output of this jet pump so that it was not necessary to use the automatic hot-well level-control valve to match the boiler-feed flow rate to the evaporation rate. The jet pump gave very smooth control over a 50-kw range

[5]C. H. Gabbard, Tests of 91-Rod Boiler System with Water, "Space Power Program Semiann. Prog. Rep. June 30, 1963," USAEC Report ORNL-3489, Oak Ridge National Laboratory.

UNCLASSIFIED
ORNL-DWG 63-6581

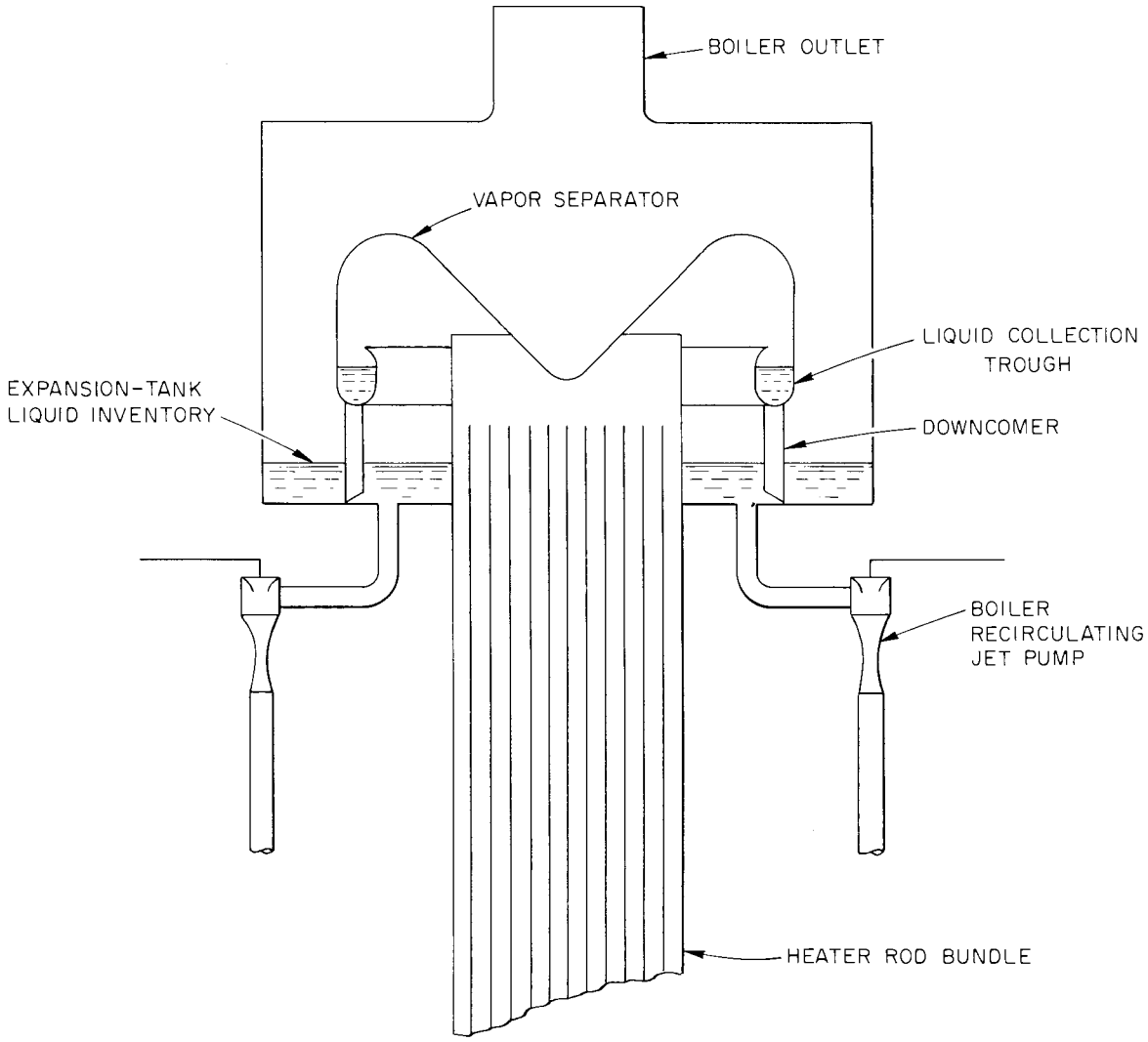

Fig. 3.19. Revised Vapor-Separator Design for Boiling-Water Test Phase I.

of boiler power without the use of valves, thus providing inherent control of the distribution of the system inventory. This control range will be extended greatly by using the jet pump in combination with the Phase II system free-turbine-driven pump. The variable speed of the latter will give characteristics that come much closer to matching the boiler requirements than those of the constant-speed electric-motor-driven pump of the Phase I system.

A series of tests was carried out at a constant boiler pressure of 17 psia to determine the maximum and minimum limits for the boiler exit vapor quality as a function of boiler power. The maximum quality limit was defined by burnout conditions, as evidenced by intermittent abrupt increases in the temperature of a heater rod. The minimum quality limit depended on the capabilities of the boiler recirculating jet pumps and the pressure drop through the boiler system. The results of these tests are shown on Fig. 3.20. Most of the data were taken with the original vapor separator. The minimum quality obtainable at 440 kw with the revised separator was reduced from about 28 to 20%. This increase in the boiler recirculation rate stemmed from the increase in the capacity of the boiler recirculation jet pumps obtained by the improvement in the suction condition to the jet pumps, described above.

Further tests were in progress to determine the effects of the boiler pressure on the burnout limited quality when the sheaths of five of the heater rods were damaged, apparently by high heater temperatures resulting from a burnout condition. The failure occurred during a transient following a power increase from 300 to 350 kw for which the boiler

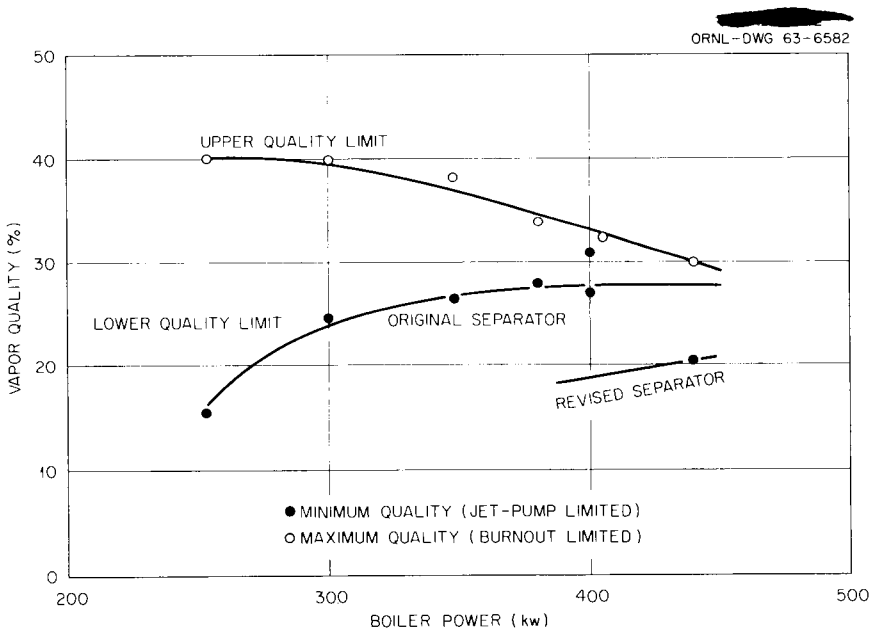

Fig. 3.20. Vapor Quality Limitation Versus Boiler Power in 91-Rod Boiling-Water System Operating at 17 psia.

recirculation loops had been throttled to a condition that would provide a quality of 25% at full power. Examination of the charts from the recording instruments indicated that boiler exit quality was about 27% at the time of failure. The operator noticed some of the heater rods glowing red and shut off the power. None of the 17 heater rods with thermocouples showed any signs of overheating.

In questioning the operator after the accident it was found that, contrary to instructions, he had not been keeping the rods with thermocouples at a power input at least 10% above the rest. This had been felt to be essential because otherwise, statistically, repeated deliberate approaches to burnout would inevitably lead to burnout conditions on rods not equipped with thermocouples, and damage would result in the course of one of the excursions.

There are several other factors that may have contributed to the failure:

1. The boiler was operating at 13 psia rather than 17 psia, and burnout should be expected at a quality lower than the 37% found at a boiler pressure of 17 psia. (The operator did not realize that this was the case.)

2. Leakage of air into the system could have caused errors in the flow measurements and therefore the boiler exit quality may have been higher than indicated.

3. During previous tests to determine burnout limits, some rods may have been distorted sufficiently to interfere with the adequate cooling of these and neighboring rods.

4. Deposits were observed on heater sheaths during disassembly. These may have reduced the wetting forces sufficiently to reduce the burnout limited power. Difficulties with this were experienced repeatedly in the seven-rod boiling-water system.

5. An electrical breakdown could have initiated the failure, but this is not believed to be the case because several scrams had occurred earlier at similar conditions without any indication of rod damage.

The five damaged heaters are shown in Fig. 3.21. When the boiler was disassembled, some 25 additional heaters were found to have been locally overheated. This damage could have occurred in some of the previous

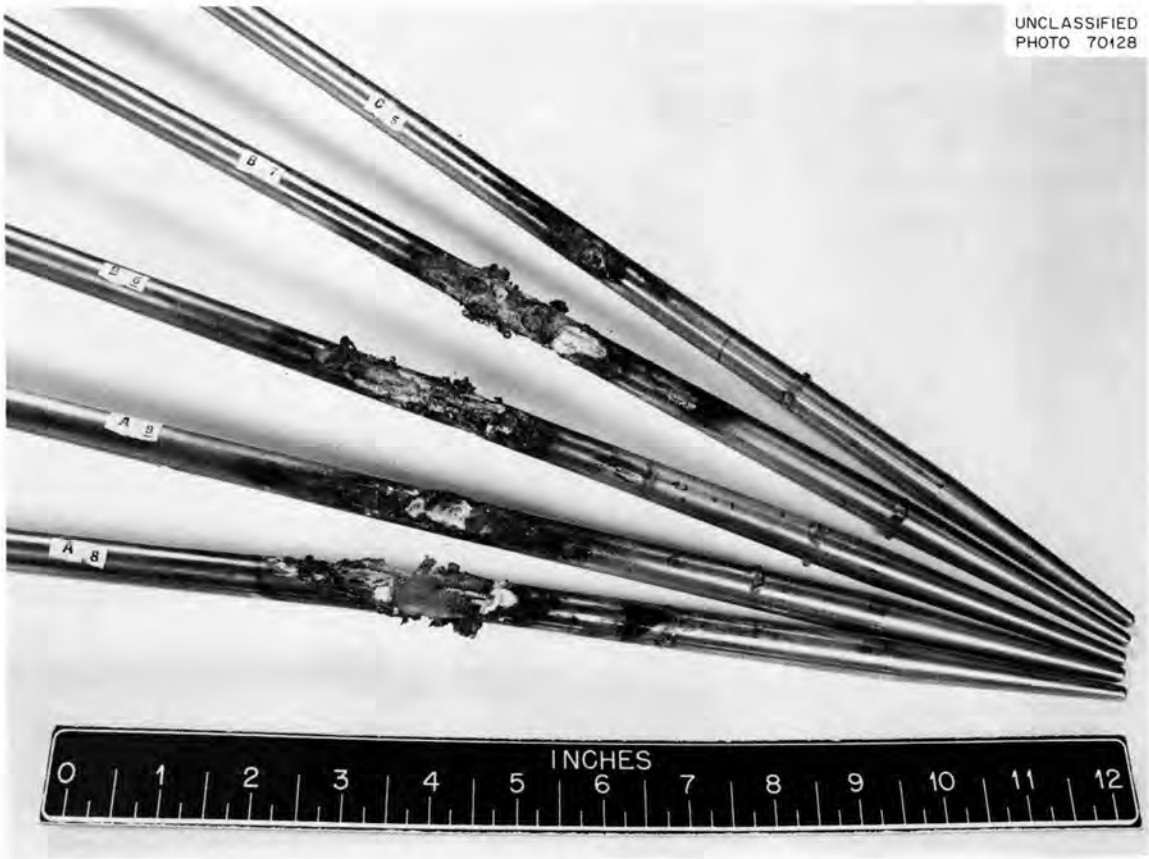

Fig. 3.21. Damaged Heater Rods from the 91-Rod Boiling-Water Test System.

approaches to burnout conditions, since many of these were made with all rods at the same power. The need for keeping the rods with thermocouples at a power at least 10% above the average is now abundantly clear.

Correlation with Literature Data

One of the reasons for initiating the electrically heated mockup test work was the paucity of experimental data in the literature for burnout at fairly high qualities under boiling conditions for axial flow through matrices of heated rods or tubes. A recent paper by Becker[6] shows the effects of both pressure and power output on the quality at which burnout occurs for several heat fluxes. Curves from Becker's data are

[6]K. M. Becker, "Burn-out Conditions for Flow of Boiling Water in Vertical Rod Clusters," AICHE Journal, p. 216, March 1963.

reproduced in Figs. 3.22 and 3.23. It is to be noted, in particular, that the burnout heat flux obtained for flow through the inside of circular tubes (round ducts) is much higher than that obtained in the passages between the rods in a rod bundle. These effects are consistent with the ORNL data that have been obtained in the four-rod slab boiler and the seven-rod cluster tests and with the 91-rod boiler test data presented in Fig. 3.20.

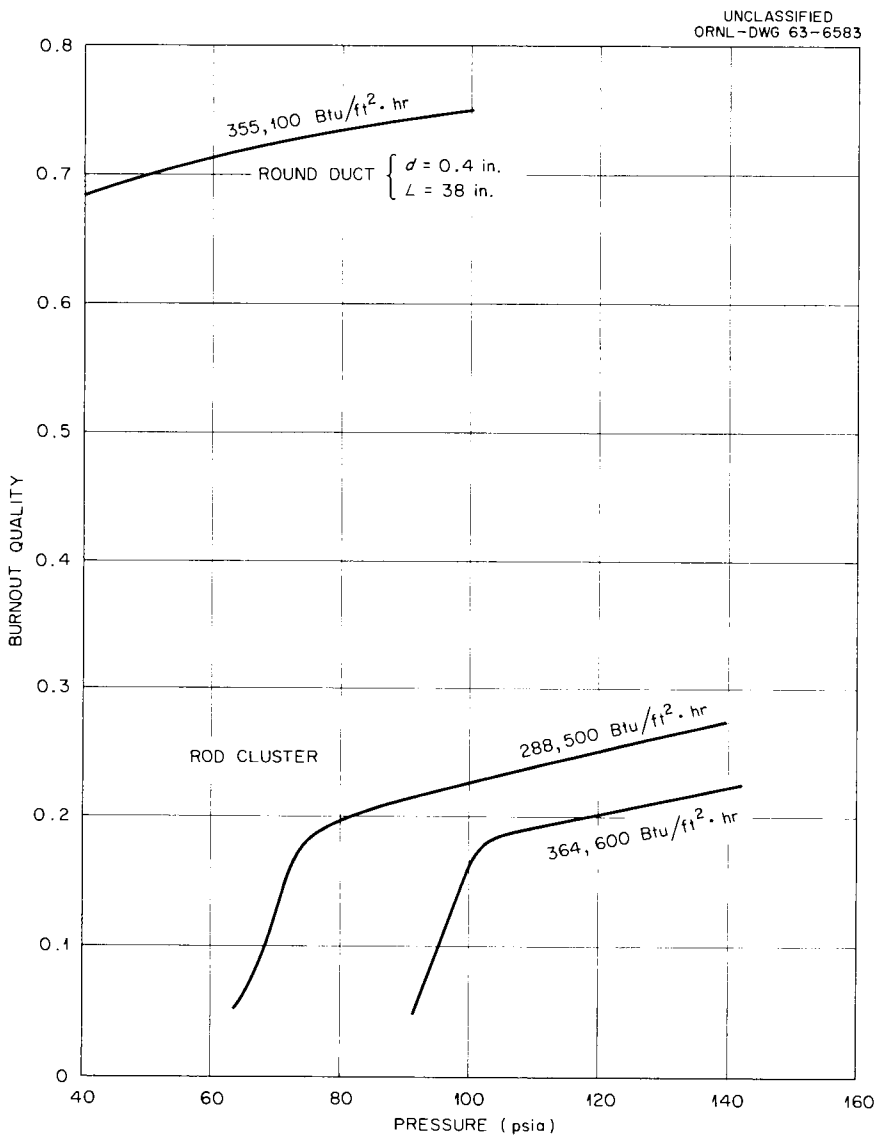

Fig. 3.22. Burnout in a Rod Cluster Compared with Burnout in Round Ducts.

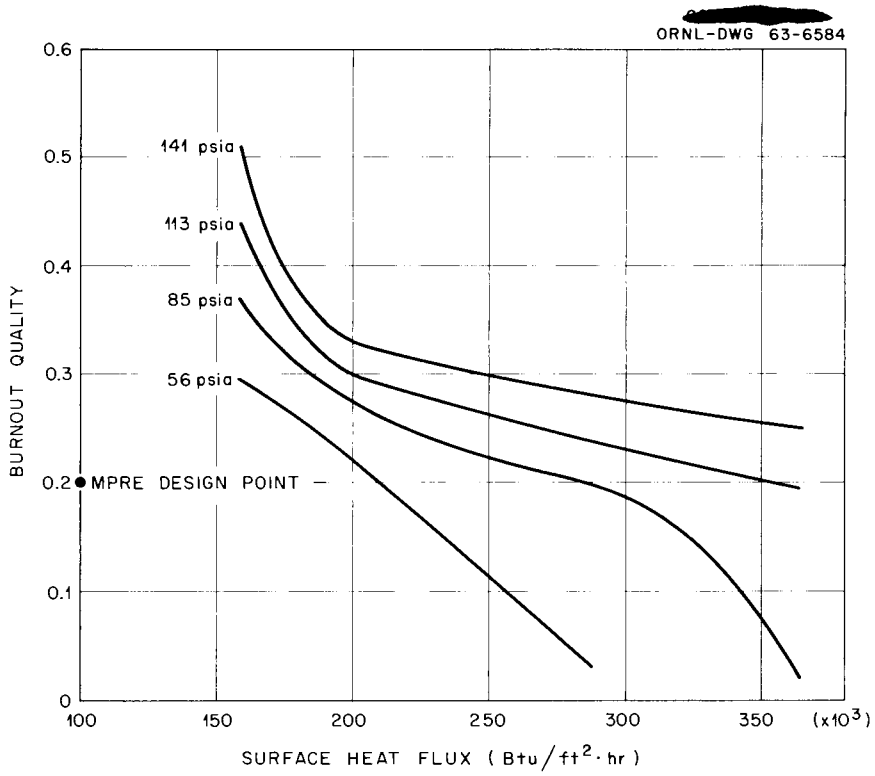

Fig. 3.23. Cross Plot of Burnout Data of Becker (ref. 5) for Water Flowing Axially Through Rod Clusters.

Phase II System

Design, procurement, fabrication of components, and assembly of the Phase II configuration were completed, and shakedown and leak testing are under way. The process flow sheet for the revised system is shown in Fig. 3.24. The prototype space condenser mounted in its cooling-water box is shown in Fig. 3.25, and the condenser water box assembly and the associated piping of its cooling-water system are shown in Fig. 3.26. The 2500-gpm centrifugal pump will be used to circulate water to the box to remove the heat of condensation. The temperature of the bath will be controlled by varying the throughput flow rate of fresh water to the cooling water system. Octadecylamine will be added to the water in the system to maintain a concentration of about 10 ppm in the tank to inhibit corrosion of the carbon steel surfaces.

A revised boiler with the improved vapor-separator and expansion-tank assembly discussed above is shown in Fig. 3.27. The heater rods were

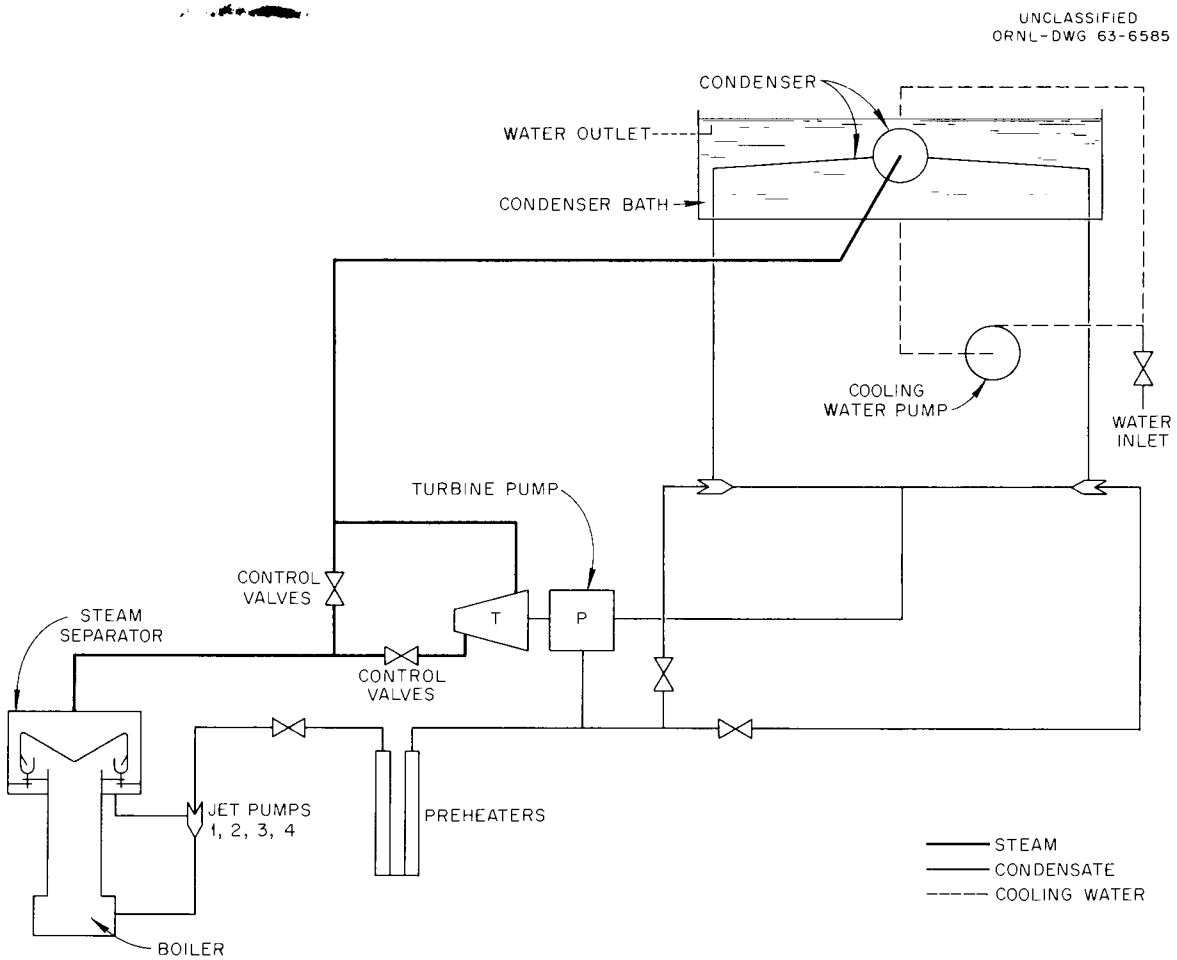

Fig. 3.24. Simplified Process Flow Sheet for Phase II 91-Rod Boiling-Water Test System.

modified to include a more positive arrangement for spacing each heater rod from its neighbor. Three spacing pins penetrate the extension on each rod at three different elevations and at 120° intervals in plan view. Eighteen heater rods in the matrix contain internal thermocouples to provide an indication of incipient burnout conditions.

The instrumentation and controls of the system were modified extensively, as required by the addition of the steam turbine-driven pump and the prototype space condenser. The silicon-controlled-rectifier power-control circuits were modified by replacing the existing amplifiers in each control circuit with matched magnetic-control amplifiers. This change should ensure uniform control of power input to all circuits over the entire power range of the system.

Fig. 3.25. Prototype Space Condenser Mounted in Cooling-Water Box.

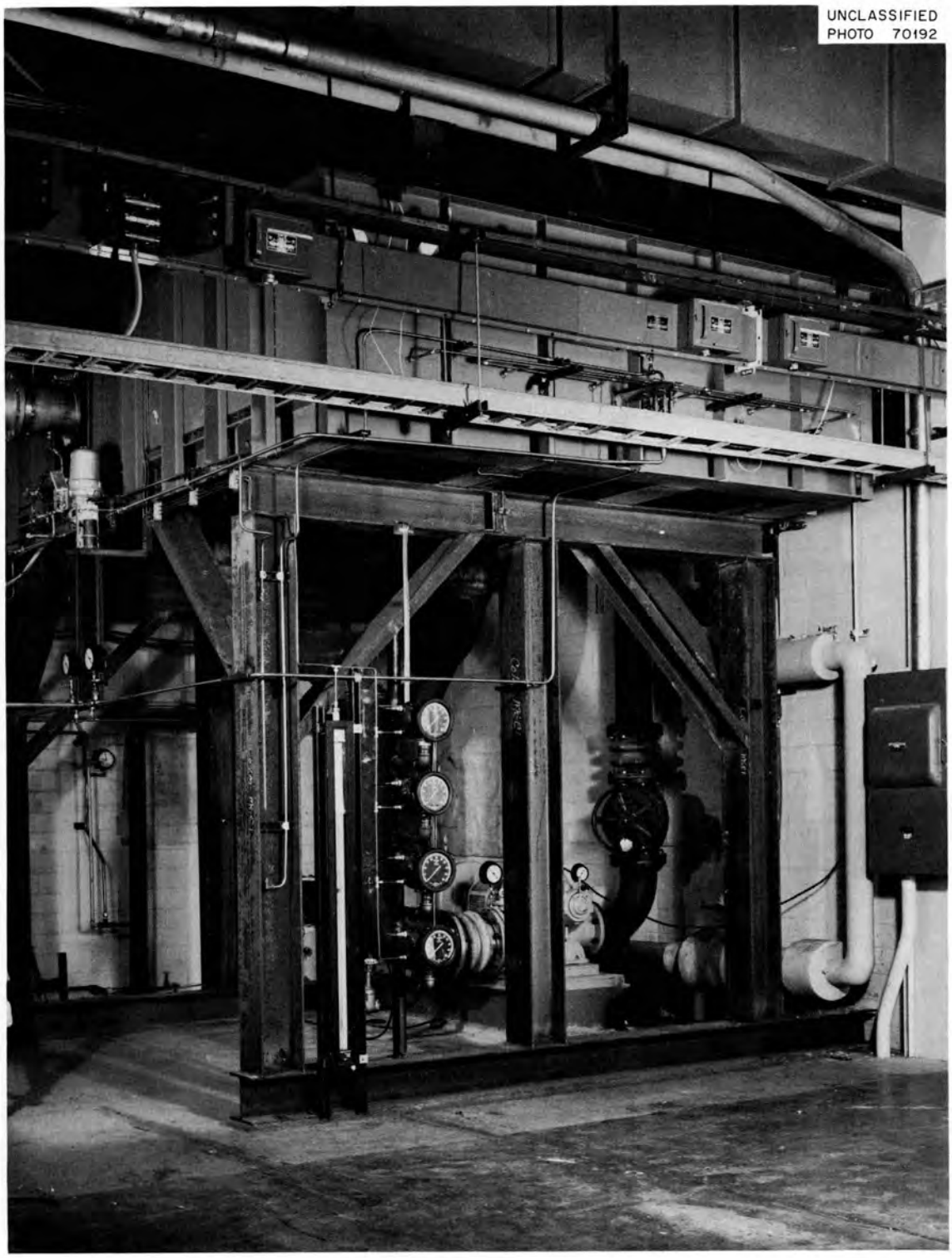

Fig. 3.26. Condenser Water Box Assembly.

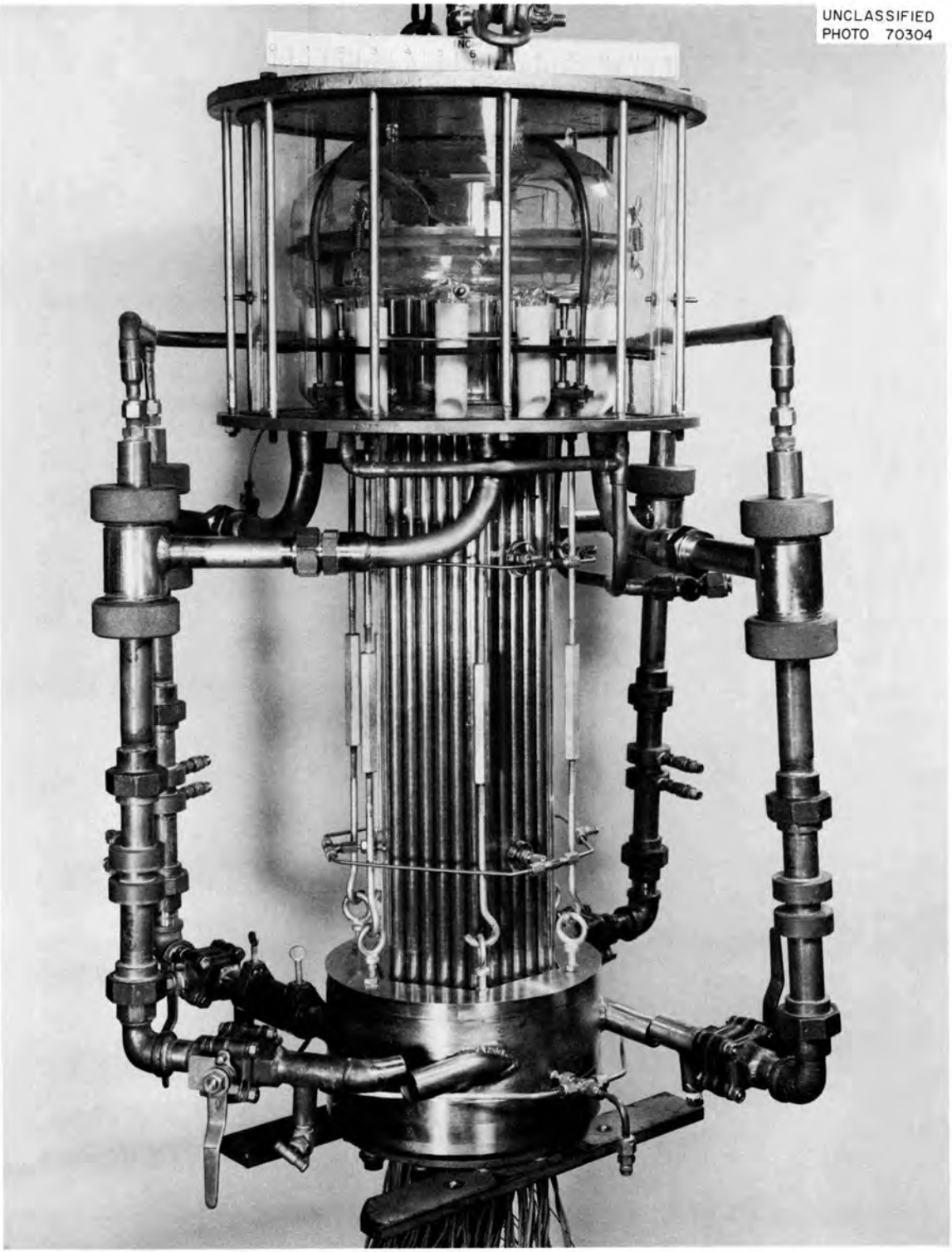

Fig. 3.27. Boiler and Vapor-Separator Assembly.

Design of a 91-Rod Boiler System for Tests with Potassium

M. M. Yarosh J. Zasler
C. J. Claffey

The design work on the 91-rod boiling-potassium system is nearing completion, and procurement is well under way. The free-turbine-driven pump units were received, the design of the radiator was completed, and procurement of the radiator is under way. The detail drawings for the boiler and vapor separator were completed, and procurement of all boiler components was initiated. A cross section through the boiler, vapor-separator, and jet-pump assembly is shown in Fig. 3.28, and an isometric view of the piping and system components is presented in Fig. 3.29.

The radiator for the system is completely enclosed by a double-walled air-cooled box whose temperature can be controlled by regulation of the air flowing through an annulus surrounding the shroud. This will allow operation with a constant radiator temperature at variable power levels or operation with a variable radiator temperature at constant power level.

Calculations were made to determine the cooling air flow required as a function of both the boiler power level and the thickness of the cooling air passages for a fixed radiator temperature, and the results are given in Fig. 3.30. The air flow required to follow the system operating curve anticipated for orbital conditions will be somewhat higher than that required for a constant shroud temperature.

Port holes have been provided in the housing and shroud surrounding the radiator to facilitate the use of an infrared scanner for determining the temperature distribution in the radiator, particularly near the outlet ends of the tubes. This will give an excellent indication of both the flow distribution and any tendency of the tubes to load up with liquid.

Final sizing of the jet pumps for the system will be determined from the results of jet-pump tests currently under way.

[redacted]

[redacted]

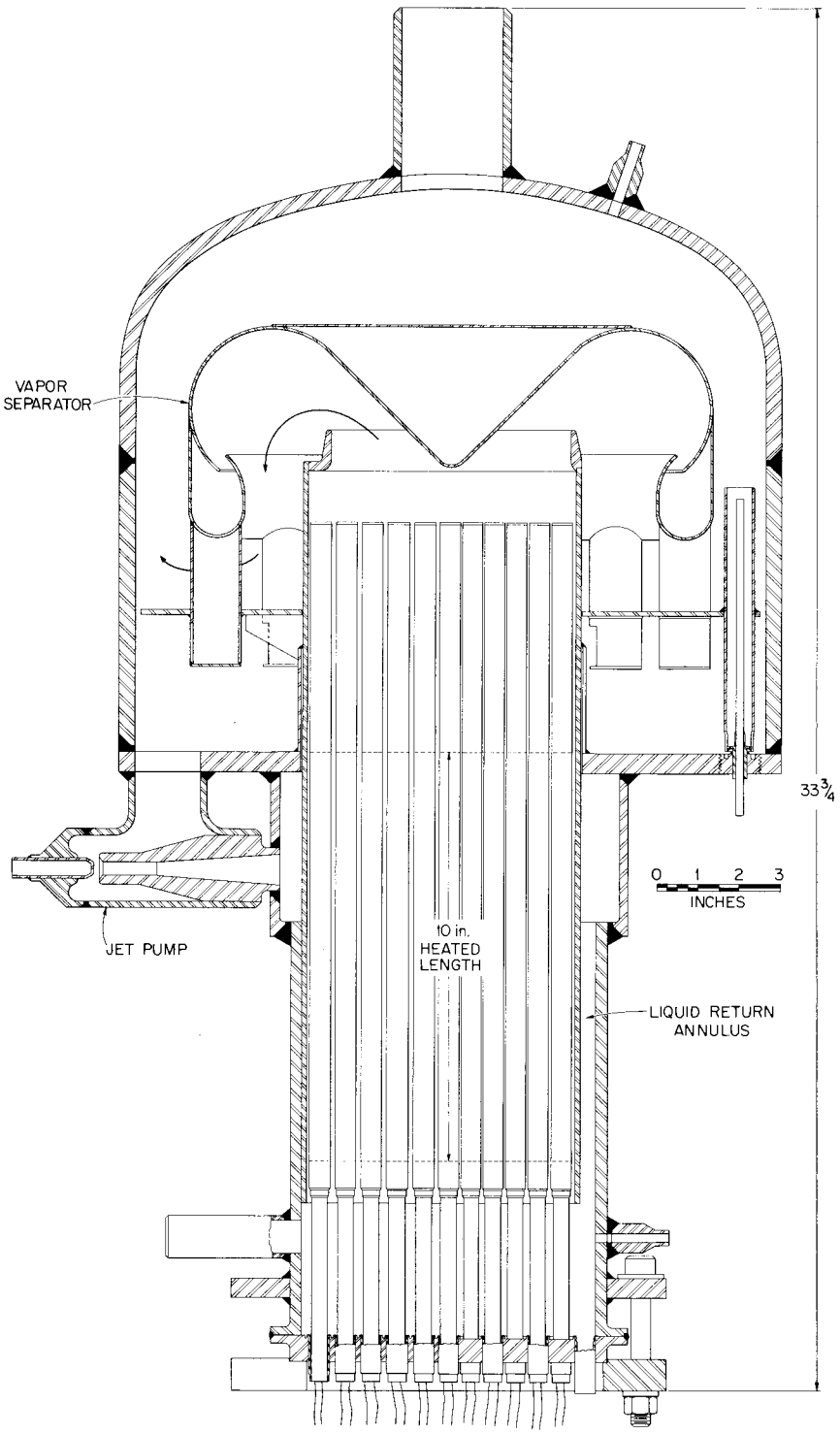

Fig. 3.28. Cross Section Through Boiler, Vapor-Separator, and Jet-Pump Assembly of 91-Rod Boiler System.

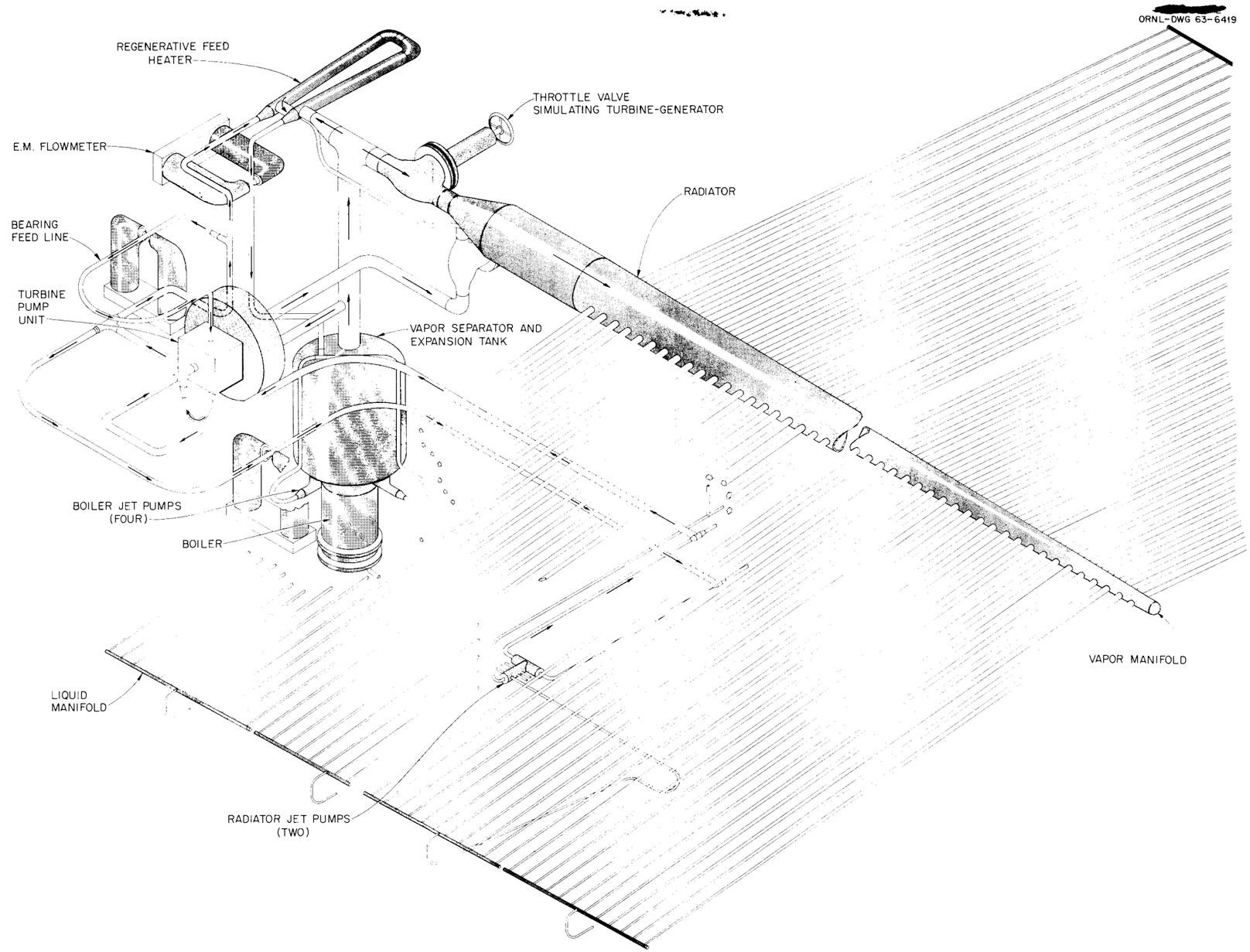

Fig. 3.29. Isometric View of Piping and System Components of 91-Rod Boiler for Tests with Potassium.

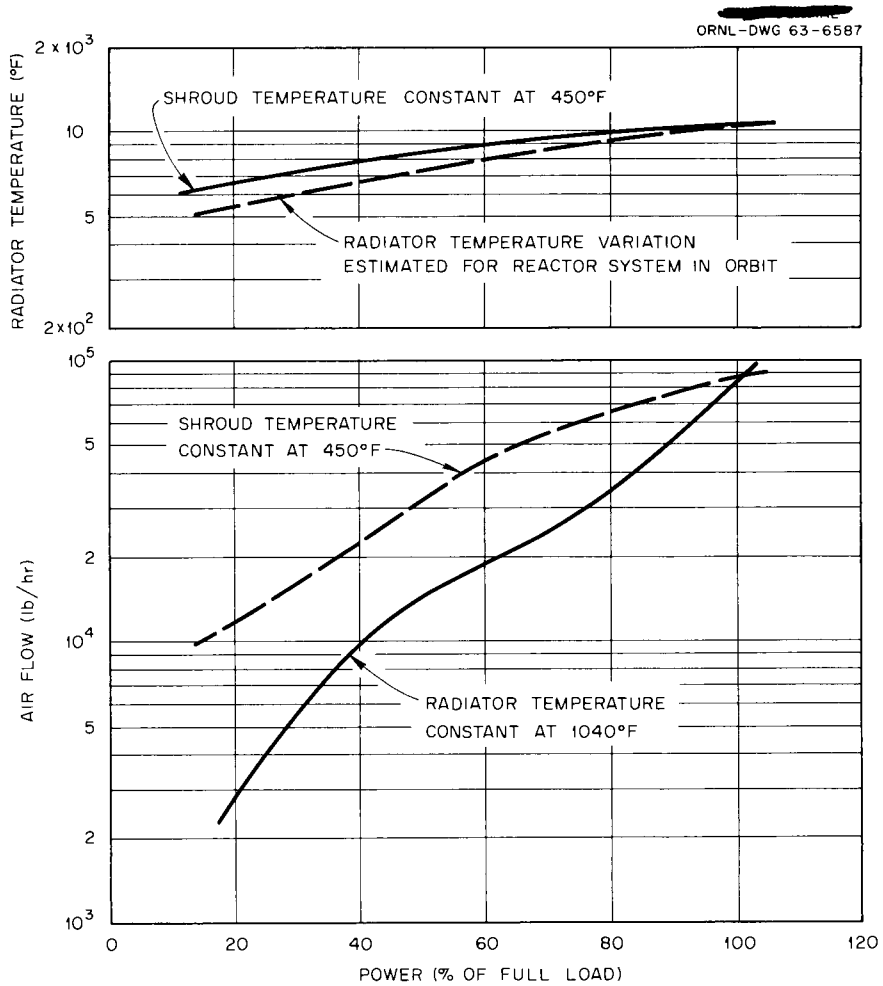

Fig. 3.30. Air Flow Required for 91-Rod Boiler System Radiator as a Function of Power Level for Both a Constant Radiator Temperature and a Constant Shroud Temperature.

Design of a Regenerative Feed Heater

A. P. Fraas

An electric feed heater was considered for the 91-rod system to give additional degrees of freedom in the amount of feed heating employed, but such a unit, if not operated properly, could cause the boiler to be in an unstable condition. Therefore a regenerative feed heater was chosen. The importance of the regenerative feed heater as a means of reducing both thermal stresses in the vicinity of the core inlet and avoiding possible core-flow instabilities associated with the dynamics of the boiling

process, together with the beneficial effects of regenerative feed heating on the thermodynamic cycle and condenser size, was discussed in previous reports.

In designing the regenerative feed heater a number of requirements had to be met. One of these was that the maximum temperature difference between the vapor and the liquid in any given stage be kept to not more than 250°F, even under off-design conditions. Since about half of the total temperature drop occurs in the fluid films on the heat-transfer surfaces and half within the tube wall, this limits the metal temperature drop to less than 125°F, an acceptable figure from the thermal-stress standpoint. This requirement makes it necessary to employ five stages on the vapor side of the regenerative feed heater. The heat flux distribution changes with load at a given system operating temperature, so the maximum heat flux may be as much as twice the average.

While the regenerative feed heater for the MPRE will be supplied with both the exhaust vapor from the free-turbine-driven pump unit and vapor from interstage bleeds in the main turbine, it seemed best in the 91-rod unit to simplify the system by making use of a single vapor bleed-off point and allowing the vapor to expand through a series of critical pressure-drop orifices in the baffles between stages. This led to the layout shown in Fig. 3.31.

The general design requirements to be met by the feed heater are summarized in Table 3.4, and the results of calculations for establishing the detailed design of the heater and of the orificing between stages are presented in Table 3.5. Two sections are included in Table 3.5, one for the design conditions and one for an off-design condition corresponding to operation at design temperature but at half power, that is, a typical endurance test condition at the full design temperature of 1540°F but at a reduced power to increase the life of the Firerod heaters. The temperature distribution through the regenerative feed heater for both of these conditions is shown in Fig. 3.32. The baffle window area between stages was chosen to give the bulk of the regenerative feed heating in the upper stages at full design power. These proportions turn out to give the bulk of the feed heating in the lower stages at the off-design condition of

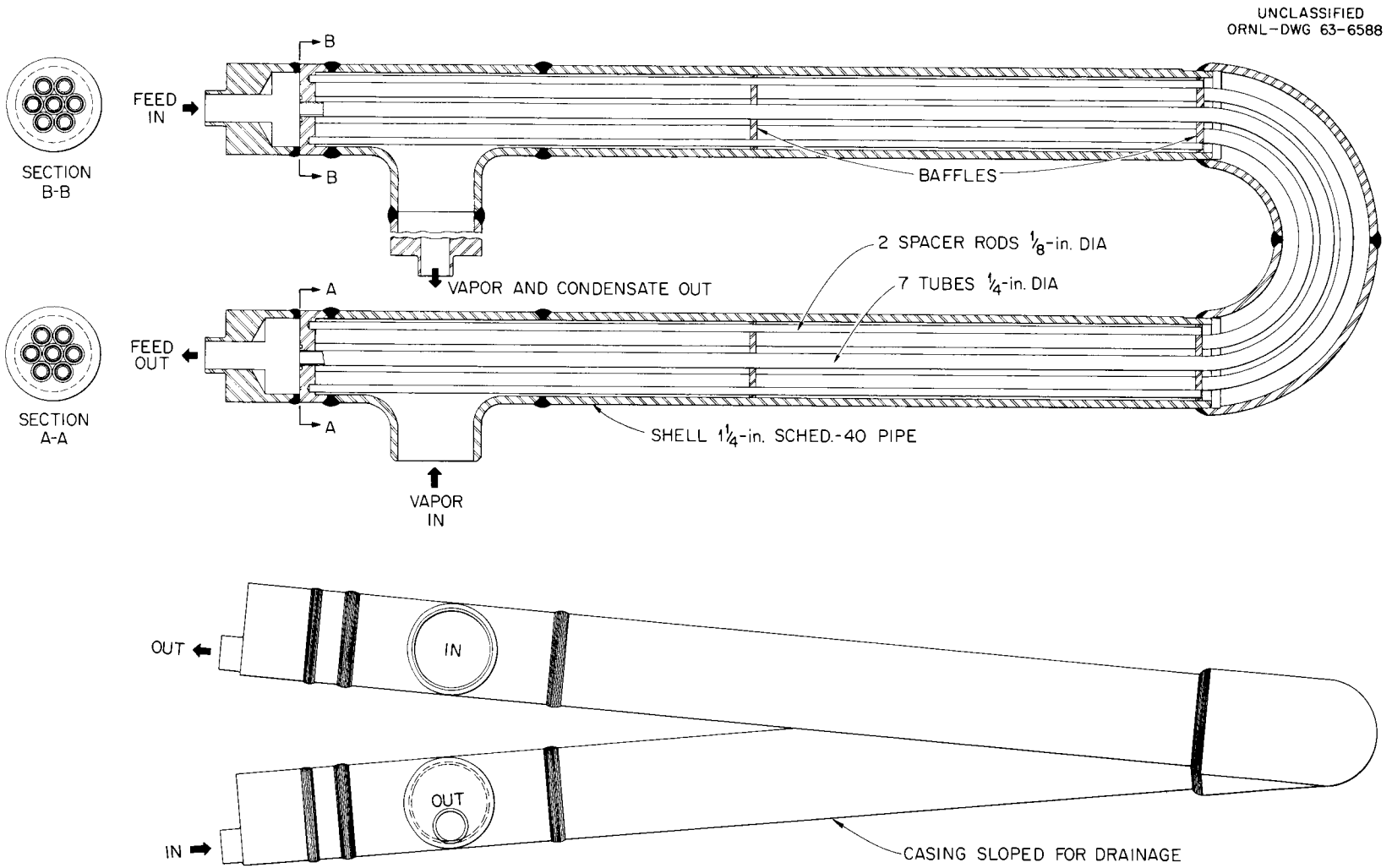

Fig. 3.31. Regenerative Feed Heater for 91-Rod Boiler System for Tests with Potassium.

Table 3.4. Design Requirements for the Regenerative Feed Heater for the 91-Rod Potassium Boiler System

Boiler	
Design power output, kw	376
Outlet temperature, °F	1540
Boiler feed flow	
lb/sec	0.406
ft^3/sec	0.0095
lb/hr	1460
Regenerative feed heater	
Feed temperatures, °F	
Inlet	930
Outlet	1480
Feed enthalpy rise	
Btu/sec	42
Btu/lb	102
Feed density, lb/ft^3	43
Vapor temperatures, °F	
Inlet	1520
Exit	1060
Vapor enthalpy drop, Btu/lb	915
Vapor flow, lb/sec	0.045
Total heat load, Btu/hr	159,000
Number of stages	5
Surface area per stage, ft^2	0.262
Overall heat transfer coefficient, Btu/hr·ft^2·°F	1500
Number of tubes	7
Tube outside diameter, in.	0.25
Tube inside diameter, in.	0.194

half power and 1540°F. It can be seen from Fig. 3.32 that the design chosen represents a compromise that gives acceptable temperature distributions for both the full power and the half power 1540°F operating conditions. It should be mentioned that, in making the design calculations, the orifice coefficients were taken from papers giving experimental data

Table 3.5. Results of Calculations of the Temperature and Pressure Distribution Through the Regenerative Feed Heater for the 91-Rod Boiling-Potassium System[a]

Orifice coefficient used for openings in the interstage baffles: 0.85

	Stage 1	Stage 2	Stage 3	Stage 4	Stage 5
Full-Power Operation					
Vapor pressure, psia	1.7	3.2	6.5	11.5	28
Vapor temperature, °F	1050	1143	1247	1341	1520
Feed temperature, °F					
Inlet	930	1022	1114	1215	1310
Outlet	1022	1114	1215	1310	1470
Rise	92	92	101	95	160
Greatest difference (GTD)	120	120	133	126	210
Least difference (LTD)	29	29	32	31	50
Log mean difference (LMTD)	64	64	71	67	111
Vapor inlet velocity, ft/sec	1842	1906	1970	2045	
Vapor density, lb/ft^3	0.0038	0.0077	0.0155	0.029	0.053
Vapor in-flow, lb/sec	0.0083	0.0159	0.0242	0.0320	0.0412
Vapor condensed, lb/sec	0.0076	0.0076	0.0083	0.0078	0.0092
Inlet orifice area, $in.^2$	0.200	0.184	0.133	0.091	
Half-Power Operation					
Vapor pressure, psia	1.7	6.9	10	16	28
Vapor temperature, °F	1050	1243	1334	1430	1520
Feed temperature, °F					
Inlet	930	1043	1230	1328	1424
Outlet	1943	1230	1328	1424	1515
Rise	113	197	98	96	91
Greatest difference (GTD)	120	200	106	102	96
Least difference (LTD)	7	13	6	6	6
Log mean difference (LMTD)	40	69	34	33	32
Vapor inlet velocity, ft/sec	1908	1925	1940	2045	
Vapor density, lb/ft^3	0.0038	0.014	0.023	0.035	0.053
Vapor in-flow, lb/sec	0.016	0.0241	0.0278	0.0320	0.358
Vapor condensed, lb/sec	0.0047	0.0081	0.0037	0.0042	0.0038
Inlet orifice area, $in.^2$	0.200	0.184	0.133	0.091	

[a]Physical property data from W. D. Weatherford, Jr., et al., "Properties of Inorganic Energy-Conversion and Heat Transfer Fluids for Space Applications," WADD Technical Report 61-96, November 1961.

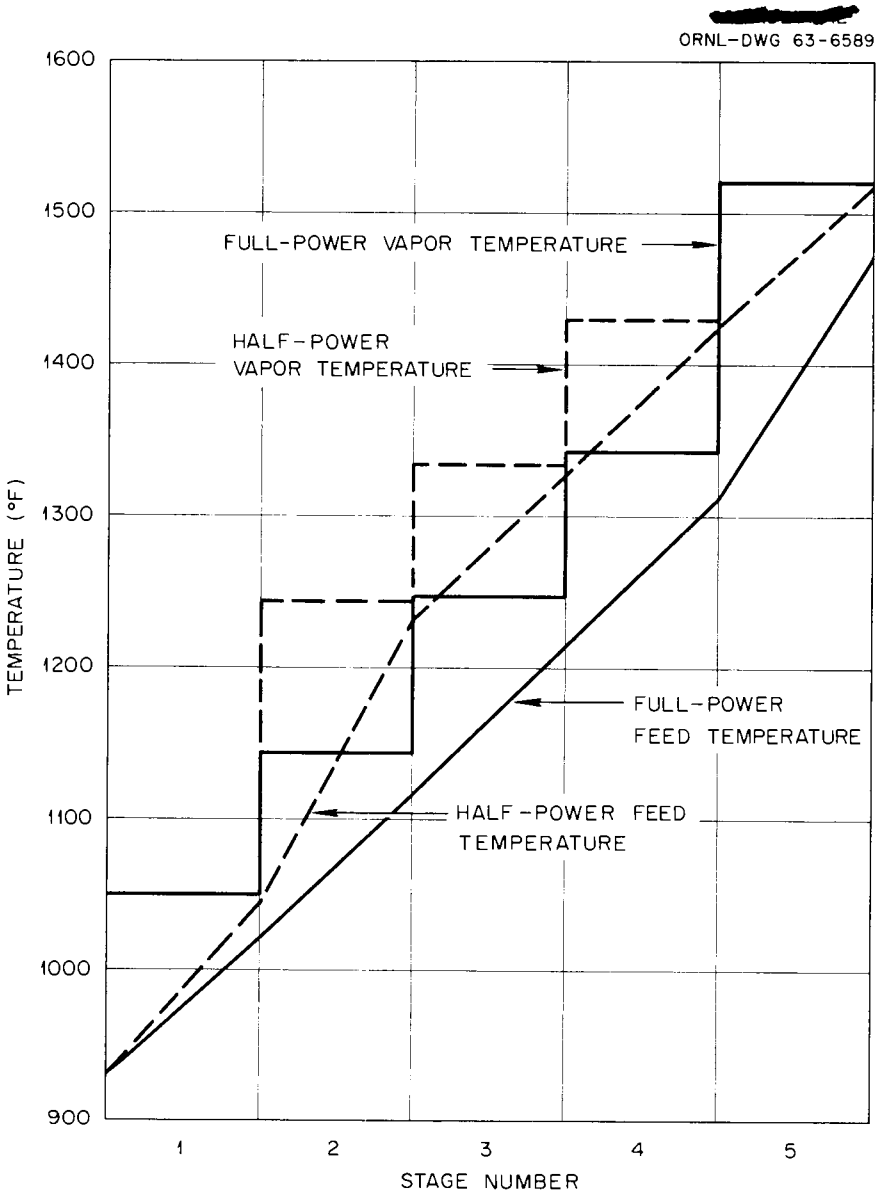

Fig. 3.32. Vapor and Feed Temperatures as Functions of Axial Position in the Regenerative Feed Heater for the 91-Rod Boiling Potassium-System.

on discharge coefficients for sharp-edged orifices in the transonic region.[7,8]

---

[7]A. Weir, Jr., et al., "Two- and Three-Dimensional Flow of Air Through Square-Edged Sonic Orifices," ASME Trans., 78: 481 (1956).

[8]R. G. Folsom, "Nozzle Characteristics in High-Vacuum Flows-Rarified Gas Dynamics," Trans. ASME, 74: 915 (1952).

Preparations for Tests of a Small Vapor Separator with an Air-Water Mixture Under Zero-Gravity Conditions

R. B. Korsmeyer

The small zero-gravity test loop described in the previous progress report[9] was built, and arrangements are being made for bench tests. The principal problem is concerned with making connections between the 400-cycle fan motor and an existing motor-generator set.

---

[9]R. B. Korsmeyer, Zero-Gravity System Tests, "Space Power Program Semiann. Prog. Rep. June 30, 1963," USAEC Report ORNL-3489, Oak Ridge National Laboratory.

ORNL-3534

C-93a — Advanced Concepts for Future Application — Reactor Experiments
M-3679 (31st ed., Rev.)

Internal Distribution

1. S. E. Beall
2. M. Bender
3. D. S. Billington
4. E. P. Blizard
5. A. L. Boch
6. R. B. Briggs
7. A. D. Callihan
8. W. B. Cottrell
9. F. L. Culler
10. J. H. DeVan
11. J. Foster
12. A. P. Fraas
13. L. C. Fuller
14. W. R. Grimes
15. A. G. Grindell
16. E. Guth
17. W. O. Harms
18. M. R. Hill
19. H. W. Hoffman
20. A. Hollaender
21. L. B. Holland
22. W. H. Jordan
23. J. J. Keyes
24. R. B. Korsmeyer
25. A. I. Krakoviak
26. C. E. Larson (K-25)
27. M. E. LaVerne
28. R. S. Livingston
29. M. Lundin
30. R. N. Lyon
31. H. G. MacPherson
32. R. E. MacPherson
33. F. C. Maienschein
34. W. D. Manly
35. H. C. McCurdy
36. J. T. Michalczo
37. A. J. Miller
38. K. Z. Morgan
39. M. L. Nelson
40. A. M. Perry
41. P. H. Pitkanen
42. A. Rupp
43. H. W. Savage
44. A. W. Savolainen
45. E. D. Shipley
46. O. Sisman
47. M. J. Skinner
48. O. L. Smith
49. A. H. Snell
50. I. Spiewak
51. R. L. Stephenson
52. C. D. Susano
53. J. A. Swartout
54. W. C. Thurber
55. D. B. Trauger
56. A. M. Weinberg
57. M. M. Yarosh
58. J. Zasler

59-61. ORNL-Y-12 Technical Library Document Reference Section
62-64. Central Research Library
65-84. Laboratory Records Department
85. Laboratory Records, LRD-RC

External Distribution

86. Aerojet-General Corporation (NASA)
87. Aerojet-General Nucleonics
88-93. Aeronautical Systems Division
94. Aerospace Corporation
95-96. Air Force Weapons Laboratory
97. AiResearch Manufacturing Company, Phoenix

98. Albuquerque Operations Office
99. Allison Division-GMC
100. Argonne National Laboratory
101. Army Ballistic Research Laboratories
102. Army Combat Developments Command
103. ARO, Inc.
104-107. Atomic Energy Commission, Washington
108. Atomics International
109. Battelle Memorial Institute
110. Brookhaven National Laboratory
111-112. Bureau of Naval Weapons
113-114. Bureau of Ships
115. California Patent Group
116-117. Canoga Park Area Office
118. Chicago Patent Group
119. Cincinnati Area Office
120. Director of Defense Research and Engineering (OAP)
121. DuPont Company, Aiken
122. Electro-Optical Systems, Inc.
123. Foreign Technology Division (AFSC)
124. General Atomic Division
125. General Dynamics/Astronautics (AF)
126. General Dynamics/Fort Worth
127-130. General Electric Company, Cincinnati
131-133. General Electric Company, Richland
134-135. Jet Propulsion Laboratory
136. Johns Hopkins University (APL)
137-138. Knolls Atomic Power Laboratory
139. Ling Temco Vought, Inc.
140. Lockheed-Georgia Company
141. Lockheed Missiles and Space Company (NASA)
142. Los Alamos Scientific Laboratory
143. Mound Laboratory
144. Marquardt Corporation
145-146. Martin-Marietta Corporation
147. Martin-Marietta Corporation, Denver
148. NASA Langley Research Center
149-153. NASA Lewis Research Center
154. NASA Manned Spacecraft Center
155-157. NASA Scientific and Technical Information Facility
158-159. National Aeronautics and Space Administration, Washington
160. Naval Air Development Center
161. Naval Air Engineering Center
162. Naval Ordnance Laboratory
163. Naval Postgraduate School
164. Naval Radiological Defense Laboratory
165. New York Operations Office
166. New York Operations Office, CANAL Project Office
167. North American Aviation, Inc., Downey
168. Oak Ridge Operations Office
169-170. Office of Naval Research

171. Office of the Assistant General Council for Patents (AEC)
172. Office of the Chief of Naval Operations
173-174. Phillips Petroleum Company (NRTS)
175-178. Pratt and Whitney Aircraft Division
179. Pratt and Whitney Aircraft Division (NASA)
180. Rand Corporation
181. Sandia Corporation
182. San Francisco Operations Office
183. School of Aerospace Medicine
184. Tennessee Valley Authority
185. United Nuclear Corporation (NDA)
186. USAF Headquarters
187-188. University of California, Livermore
189. Walter Reed Army Medical Center
190-192. Westinghouse Bettis Atomic Power Laboratory
193. Westinghouse Electric Corporation, LIMA
194. Westinghouse Electric Corporation (NASA)
195-234. Division of Technical Information Extension
235. Division of Research and Development, AEC, ORO
236-237. Reactor Division, AEC, ORO